Fernando Jorge Neiva Ferreira Nunes

Licenciatura em Química Aplicada

Molecular properties of VOC's sensing materials

Dissertação para obtenção do Grau de Mestre em
Química Bio-Orgânica

Orientador: Arménio Barbosa, Ph.D.,
Faculdade Ciências e Tecnologias - NOVA

Co- Orienta-dora: A. Cecília Roque, Associate professor,
Faculdade Ciências e Tecnologias - NOVA

Júri:

Presidente: Prof Doutor Paula Branco

Arguente: Doutor Manuel de Melo

Vogal: Doutor Arménio Barbosa

07 de Outubro, 2019

FACULDADE DE CIÊNCIAS E TECNOLOGIA
UNIVERSIDADE NOVA DE LISBOA

Molecular properties of VOC sensing material

Copyright © Fernando Jorge Neiva Ferreira Nunes, Faculdade de Ciências e Tecnologia, Universidade Nova de Lisboa.

A Faculdade de Ciências e Tecnologia e a Universidade Nova de Lisboa têm o direito, perpétuo e sem limites geográficos, de arquivar e publicar esta dissertação através de exemplares impressos reproduzidos em papel ou de forma digital, ou por qualquer outro meio conhecido ou que venha a ser inventado, e de a divulgar através de repositórios científicos e de admitir a sua cópia e distribuição com objetivos educacionais ou de investigação, não comerciais, desde que seja dado crédito ao autor e editor.

À minha avó Teresa

Firstly, I would like to acknowledge my supervisor Ph.D. Arménio Barbosa for the unrestful support he provided, in the long hours of Python scripts exploration and the quest for the analysis of the various results obtained. Despite of the constant presence in my work, always allowed me to make the decisions concerning the path that was to be taken, helping me improve not only in a scientific level but in a personal level as well.

To all my lab co-workers that always worked together in order to have a healthy work environment.

To my family that had always been the most supportive people in my life.

And to all my friends that have accompanied me in life.

Abstract

Liquid crystals (LCs) have been studied for over 100 years and are part of our daily lives. They are mostly used in emulsions or dispersed along a polymeric matrix. However, the interface resulting from the binary mixture of amphiphilic molecules and LCs, or the use of surfactants in the PDLC, have various applications like in gas-sensors, thermometers, etc. Currently, computational approaches can be used in order to rationalize the physical-chemical properties of the interface and the main interactions between an amphiphilic molecule and a LC.

Molecular Dynamics simulations were used to study at an atomic level the interface between an ionic liquid (IL) and a LC. Through these simulations it was possible to replicate the bulk of the nematic phase of LCs 5CB and 8CB, and the bulk of the IL [BMIM][DCA]. The mixture of 5CB and water was successfully simulated as well.

This work allowed to conclude that the main interactions acting in the LC - IL interface are π-π stacking, hydrophobic interactions and electrostatic interactions between dipoles, however all these have different impacts, and all depend on the ratio between the various components of the interface. In this mixture, the most relevant interaction to obtain a planar arrangement are π-π interactions or dipole interactions with the imidazolium rings and cyano moieties of 5CB. And that water plays a crucial role in the anchoring forces of the LC to the IL and in the ordering of 5CB. The obtained results will allow to rationalize responses of the LC-IL system to various VOC's and transfer this knowledge to other binary LC – amphiphilic/surfactant systems.

Keywords: Molecular dynamics, Liquid Crystals, Interface, Amphiphilic molecules, Ionic Liquids.

Resumo

Cristais líquidos têm sido estudados por mais de 100 anos e hoje fazem parte da nossa vida quotidiana. São usados maioritariamente em emulsões ou dispersos numa matriz polimérica. Porém a interface resultante da mistura binária de cristais líquidos e líquidos iónicos, ou então do uso de surfactantes em PDLC têm várias aplicações, como por exemplo em sensores de gases, termómetros, etc. Atualmente métodos computacionais são utilizados de forma a racionalizar as características físico-químicas da interface e as principais interações entre uma molécula anfifílica e um cristal líquido.

Dinâmicas moleculares foram utilizadas de modo a estudar a interface a um nível atómico a interface entre um Cristal Líquido e um Líquido Iónico. Através dessas simulações foi possível o estudo do *bulk* da fase nemática do 5CB e 8CB, as simulações permitiram imitar o *bulk* do [BMIM][DCA]. E a mistura de 5CB com água foi simulada com sucesso também.

Este trabalho permitiu conclui que a principal interação que age na interface entre cristais líquidos e líquidos iónicos são acoplamentos π-π, interações hidrofóbicas e atrações electroestáticas, contudo todas têm diferentes impactos e tudo depende da razão existente entre os vários componentes da interface. Na mistura de LC-IL, a interação mais relevante para obter um arranjo planar são as interações π-π ou as interações existentes entre os dipolos na ligação ciano do 5CB com os anéis de imidazole do IL. E que a água apresenta um papel crucial no desenrolar da organização molecular. Com estes resultados é possível racionalizar resposta aos vários VOC's e transportar este conhecimento para outros sistemas binários de cristais líquidos e moléculas anfifílicas/surfactantes.

Palavras-chaves: Dinâmicas moleculares, Cristais Líquidos, interface, moléculas anfifílicas, líquidos iónicos.

Content

Figure and Table list

1

Introduction

1.1- Liquid Crystals

Matter has three classic states: solid, liquid and gas [1]. The solid state is defined by having a regular stack of molecules or group of molecules periodic in all directions, where the intermolecular forces are strong enough to hold them steady in place. However, when the temperature rises or the pressure falls, the vibration of the molecules (that arose from the energy being transferred from heating or lowering the pressure of the system), eventually becomes stronger than the forces holding the molecules in place, leading to a disruption of the forces and turning the solid into a liquid [2]. If the system continues heating, ultimately a gaseous phase will be achieved following the same set of changes.

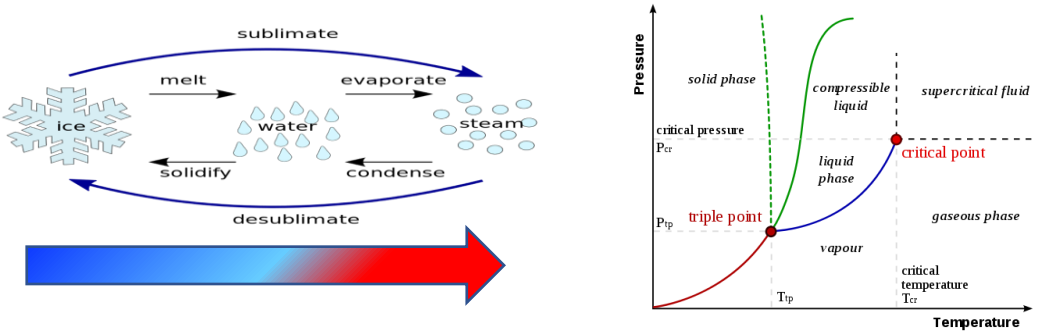

Figure 1 A typical phase diagram on the right [3 a] and the three typical phases of matter and on the left three classical phases of matter, displayed as water[3 b].

Nonetheless, in 1888 Friedrich Reinitzer, while examining physico-chemical properties of various cholesterol derivatives in *"Beitr ge zur Kenntniss des Gholesterins"* [4], noted that cholesteryl acetate and cholesteryl benzoate exhibited two melting points and displayed a broad array of colors [4]. Struck by the discovery he made, he sought advice in one of the most remarkable scientists in crystallography, that had developed the polarization microscope, Otto Lehmann. He then confirmed the phenomena registered by Reinitzer, in August 1889 he wrote that: "*It is of high interest for the physicist that crystals can exist with a softness, being so considerable that one could call them nearly liquid*". Later that year the term liquid crystals was used for the first time [5], little did Reinitzer knew the impact that the

double melting point phenomenon in cholesterol derivatives had for the study of soft matter in the future.

Liquid crystals nowadays are defined as a state of matter which has characteristics both from solids, like orientational and/or positional ordering, and from liquids, as molecular mobility and fluidity [6].

But why do liquid crystals instead of having a clear transition between solid and liquid, have a cascade of phase changes? Due to having some intermolecular forces which are stronger than others intermolecular forces (and these weaker intermolecular forces are the first to break, creating an anisotropic medium, this is the molecules are not randomly oriented), when temperature rises, this leads to the total or partial loss of positional order, and orientational ordering is still retained [7]. Liquid crystals can be distinguished in two major classes: lyotropic and thermotropic [2]

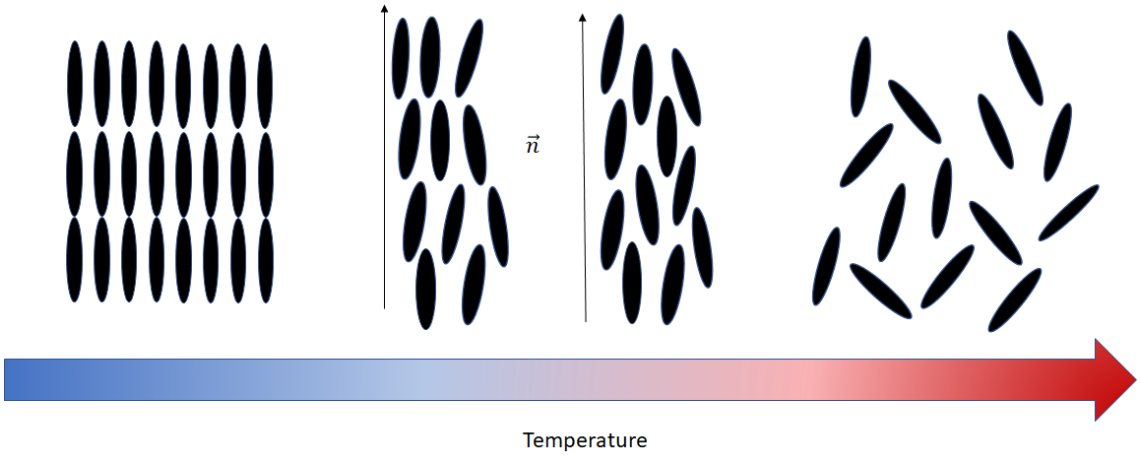

Figure 2 Phase transition in Liquid Crystals with increasing temperature

Lyotropic phases are observed as a function of concentration of amphiphilic molecules in isotropic solvents [8]. These molecules have a critical micelle concentration in which above that concentration of solute, the molecules tend to aggregate in micelles. These mesogenic molecules are very sensitive to temperatures changes. Due to its instability, this eliminates the possibility to have a thermally induced phase change [9]. The main reason for the phase appearing is the interactions between the solute and the solvent [8]. Normally lyotropic

mesomorphs are composed of two main components inside the molecule: a polar and a nonpolar moiety [9].

Thermotropic phases, when the mesophases appearance are triggered by temperature changes, instead of the concentration of the solute, in this type of materials interactions between solute is what contributes most to the demonstrated phase [8].

Thermotropic mesomorphs are composed of elongated organic molecules, called calamitic thermotropic mesomorphs, for example 5CB [7].

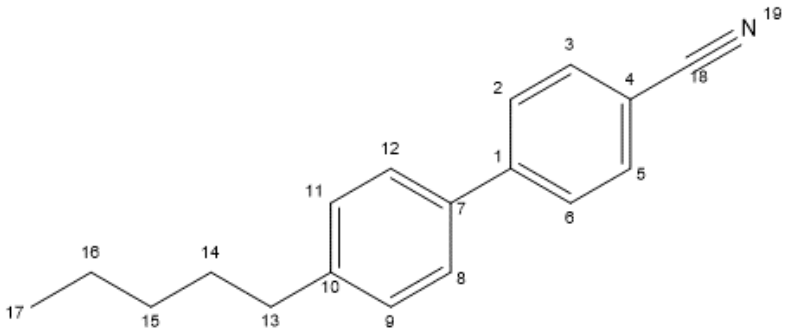

Figure 3 Typical structure of a calamitic mesomorph, in this case the structure depicted is 5CB with an arbitrary atoms' numeration.

1.1.1 - Main thermotropic Mesophases

Various mesophases exist, however the focus of this thesis will turn to the calamitic phases that can be divided in three distinct phases: nematic, smectic and cholesteric phases. Although different between them, all have the existence anisotropy in common.

Different phases have different behavior under the inspection of Polarized Optical Microscope (POM), where different Schliren-textures lead to the classification of the different phases. Since each phase has specific features, this is

because of different order levels and/or packing of the molecules in the mesomorphic phase, interacting then differently with the polarized light probed by the microscope [10].

Nematic

The nematic phase is the least ordered phase since it only presents one dimensional orientational order virtue of correlations of the long molecular axis roughly parallelly aligned. According to a vector $\vec{n}$, this director has no polarity in uniaxial nematics, therefore $\vec{n}$ and $-\vec{n}$ are equivalent [11].

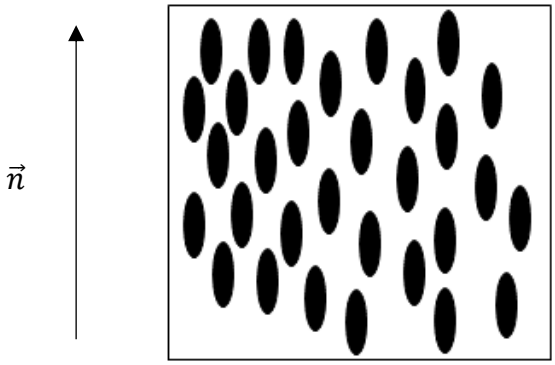

Figure 4 Representation of the nematic phase, where $\vec{n}$ is the phase director.

Though, as seen in Figure 4, the molecules are not all perfectly aligned to the director, and the angle between a molecule and the director, is given by θ, as represented in Figure 5.

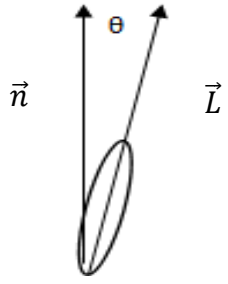

Figure 5 Representation of Θ referred in the Equation 1 where $\vec{n}$ is the system's director and $\vec{L}$ is the molecular long axis and θ is the angle between both the vectors.

The nematic order parameter of the system is calculated by doing the mean average of the second-degree Legendre polynomial which can be calculated using Equation 1 [11,12].

$$P2 = \langle \frac{3}{2} * cos^2(\theta) - \frac{1}{2} \rangle$$ Equation 1

P2 represents the nematic order parameter and θ is the angle between the long molecular axis and the director.

P2 varies between 0 and 1, where 0 is a fully isotropic system and 1 is a fully nematic state, where all the molecules are perfectly aligned to the director. A typical nematic has a P2 ranging from 0,4 to 0,7 [13], for example 5CB presents a typical nematic value of 0,54 [14,15].

Nematic LCs' most important application in the modern world is in displays. The first LC displays where twisted nematic liquid crystals or super-twisted nematics as their base, since by manipulating the twist the birefringence can be manipulated in order to obtain the desired application [16], nevertheless nematic LCs are not only used in displays as described next.

Due to the absence of positional ordering of the molecules' center of mass, nematic liquid crystals present high fluidity. This leads to interesting applications in Liquid-Gas Chromatography as stationary phases, due to its ability in distinguishing isomers [17].

Given the orientational properties of the nematic phase, they present birefringence. This means that the material will present two refractive indices, according to the plane where the light is probed: if the light is probed parallel to the director a refractive index will be obtained; if the light passes perpendicular to the director another refractive index is obtained [17]. Some sensors use birefringence as a basis for its working [18,19,20].

Nematic phase observation through POM, has typical textures according to the director nonetheless this subject will be approached more in-depth in the following sub-chapter.

Cholesteric

Cholesteric phase consist of nematogenic molecules containing a chiral center [21], and this existence of chirality, this phase can also be given the name chiral nematic. This phase doesn't occur only in pure chiral compounds as sometimes, an achiral component is mixed with a chiral, mesogenic or not, dopant [21, 22].

This phase is characterized by the presence of various nematic layers that due to the presence of chirality, there is a helical torsion along an axis, as in Figure 6. Where h is the axis of rotation is periodic and at every 2π degrees of rotation is designed the pitch of the system, this pitch is related to the amount chirality present in the system, the shorter the pitch the more chiral the system is [23].

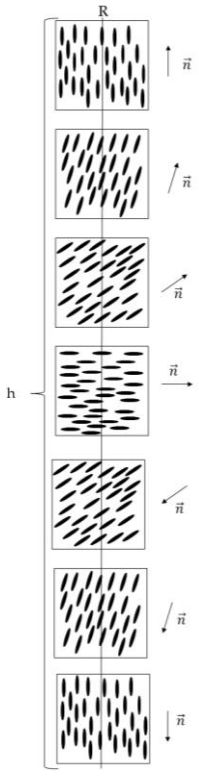

Figure 6 Representation of the cholesteric phase, where $\vec{n}$ corresponds to the various directors in each layer, R is the axis of rotation of each layer and h is the pitch of the cholesteric phase

As in nematic liquid crystals, a second-degree Legendre Polynomial is used to measure the order parameter, however in this case, since the director is constantly changing, the P2 values are local for each layer.

Cholesteric liquid crystals are used as thermometers by exploiting the critical temperature dependence of the selective reflection of this phase, this is a consequence of the pitch of the system that according to the temperature, with the change of the pitch different colors are emitted by the phase, allowing to monitor the temperature of a system [24] .

However, since the cholesteric phase, presents the twist present in the twisted nematics, they can be used in displays as well [25].

Given the chiral properties of cholesterics, interesting applications in NMR arise when an anisotropic, optically active and fluid material is used as a solvent, since a way of calculating enantiomeric purity is achieved without having the downside of the price of shift reagents but achieving the same results [26]. These properties are interesting in chemical synthesis, since a chiral, anisotropic and fluid solvent can alter the course of a reaction by controlling the orientation of the solute and impart constraints to the solute mobility, removing in part the randomness inherent isotropic solvents, favoring the desired reaction in obtaining a higher enantiomeric purity for example [27].

Smectic

The smectic phase is more ordered then the nematic phase since it presents orientational order and the molecules' center of mass has positional order [28] as presented in Figure 7.

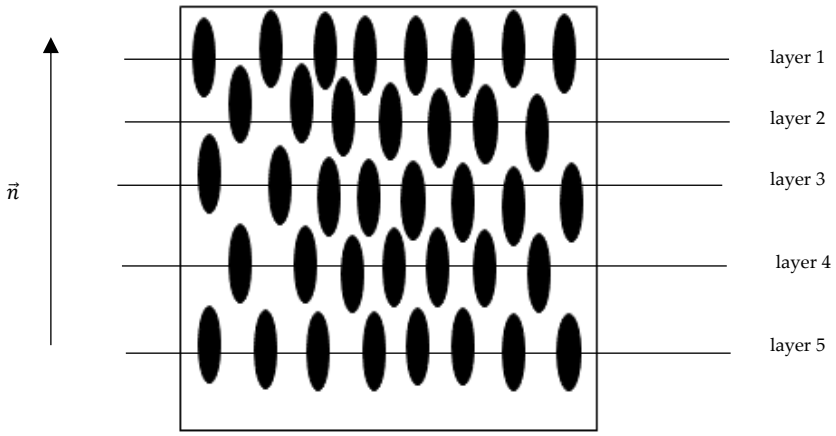

Figure 7 Representation of a smectic liquid phase, where $\vec{n}$ is the phase director

As seen in Figure 7, smectic phases are characterized by having well-defined layers of mesogens and interlayer spacing. The molecules present orientational order between their long axis, having the same definition of director as in nematic phases, however various smectic phases exist, according to how the director is set according to layer plane or how the molecules are packed together in each layer [28].

Smectic-A phase is defined by having the molecules' director perpendicular to the layer stacking axis, Smectic-C phase presents the molecules' director tilted about the layers stacking axis [29]. as seen in Figure 8.

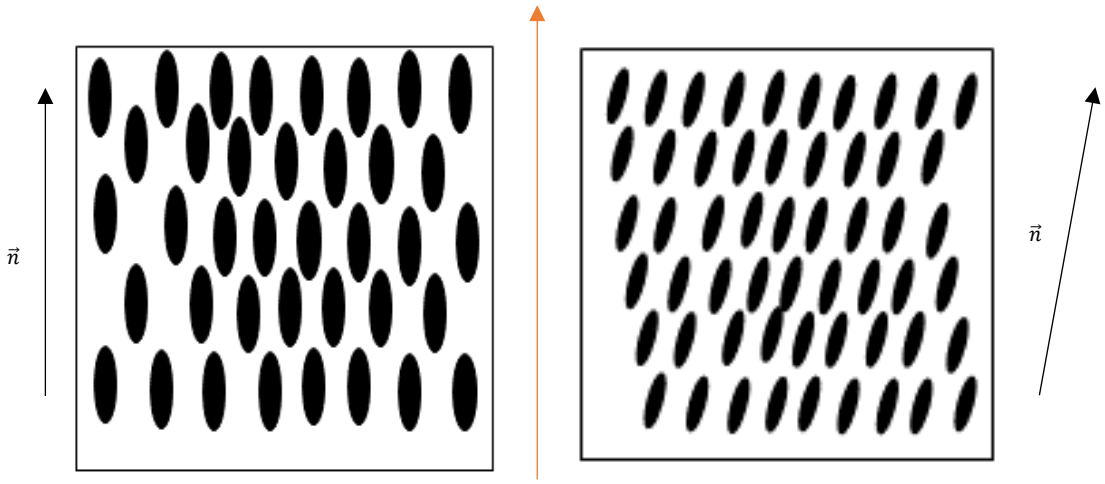

Figure 8 Smectic-A phase vs Smectic-C phase where $\vec{n}$ is the phases director and the orange vector represents the layer stacking vector

Nonetheless other variations of smectic phases exists, some have a strict packing as in Smectic-B where the molecules in each layer have an hexagonal packing and the director is perpendicular to the layers' plane and variations of this phase when the director is either tilted towards the apex of the hexagon (Smectic-J) or to the side of the hexagon (Smectic-G) or if the molecules packing is orthorhombic or monoclinic a different smectic phase is obtained [29].

1.2– Polymer Dispersed Liquid Crystals

Polymer Dispersed Liquid crystals consist in microscopic nematic droplets, usually of hundreds of microns, dispersed in a solid polymeric matrix [30].

This confinement of the molecules inside the cavities leads to elastic deformations of the nematic director, this leads to the appearing of point defects in the droplets. And according to the director alignment, or not, to the polymeric matrix leads to various kinds of droplet morphologies [30].

When the director is homeotropically aligned to the polymeric matrix, the director is perpendicular to the polymeric matrix in each point, occurring a droplet with a radial texture. If the director assumes a parallel alignment to the polymeric matrix, then a planar alignment is attained, reaching then a bipolar texture, however various droplet configurations can be obtained when the director positions in between the radial and homeotropic alignments [31].

The most interesting for the development of this work are the bipolar and radial arrangement, as seen in Figure 9.

a) b)

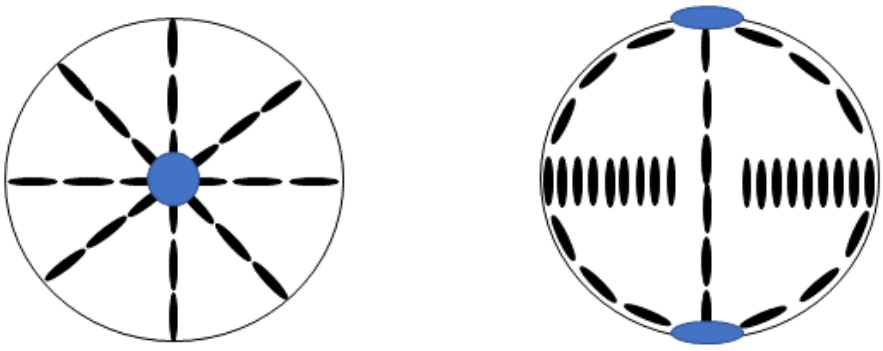

Figure 9 Radial arrangement inside a droplet **(a)** Bipolar arrangement inside a droplet **(b)** with the defect points highlighted in blue.

They have varied applications since the orientation of the nematic liquid crystal can be modulated by applying an electrical or magnetic field. Thermometers, as the liquid crystals properties are greatly related to the temperature [32]. Biosensors given that liquid crystals can change their configuration in the presence of other molecules [33] and by monitoring optical changes [34] in the system molecules can be sensed or in "smart-glass" that consist of a window that can be switched from opaque to transparent by applying an electric field [35].

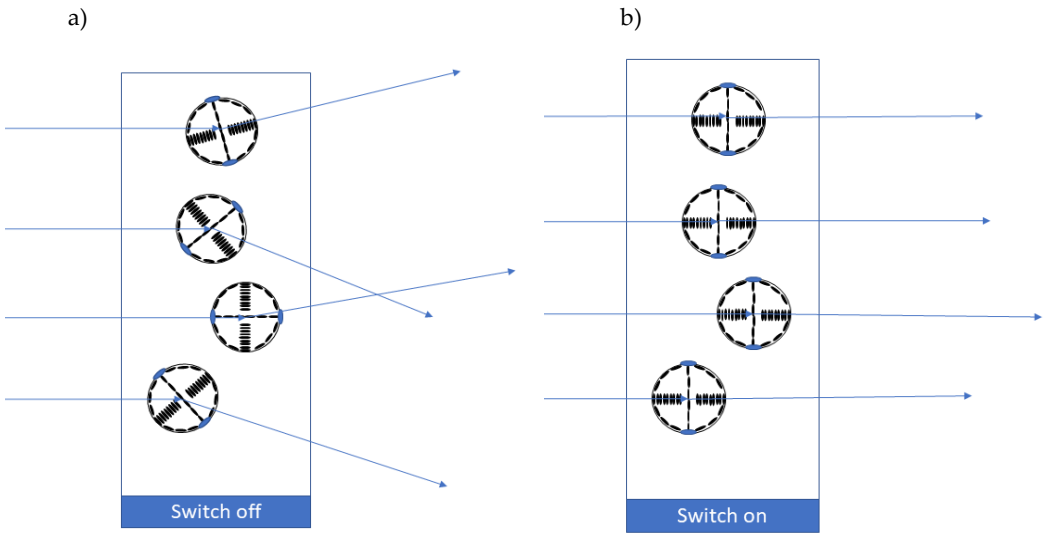

Figure 10 Typical "smart-glass" layout, where when the switch is off the light passing (blue vectors) is scattered by the disordered droplets of LC creating an opaque glass **(a)** whilst if the switch is on, the droplets will align to the electrical field and the light passing will not be scattered leading to transparent glass **(b)**.

In the "off-state" the molecules are randomly oriented leading to the light to be dispersed creating an opaque glass, however when an electric filed is applied to the glass, the liquid crystal inside the droplets will all align to the electric field, with this alignment the light will not be dispersed creating then a transparent glass.

The alignment of liquid crystals to the electric field or other kind of external stimulation depends on the anchoring force of the liquid crystal to the polymer matrix [36]. But it may be useful to diminish the anchoring forces of the liquid crystals to the polymeric material. A surfactant is therefore needed to achieve

such an alignment [37]. However not only surfactants can be used to achieve such a goal, an amphiphilic molecule [38].

An amphiphilic molecule consists in a molecule that has a polar both hydrophobic and hydrophilic characteristic in the same molecule. For example, triacyclglycerols are amphiphilic as they are composed by a non-polar, hydrophobic long carbon tail and a polar, hydrophilic glycerol and ester moieties.

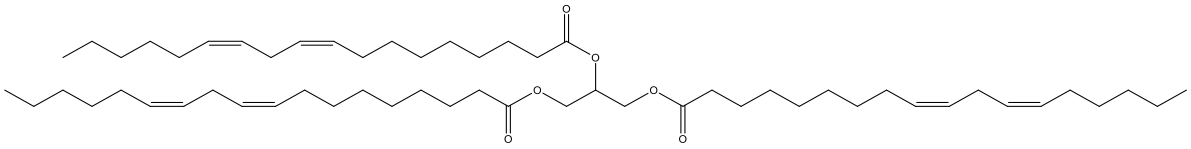

Figure 11 A triacylglycerol molecule as a representation of an amphiphilic molecule

Other molecules that present amphiphilic properties, as they are typically composed of a carbon tail, hydrophobic part, and charged atoms that are highly polar, are for example, Ionic Liquids represented in Figure 13.

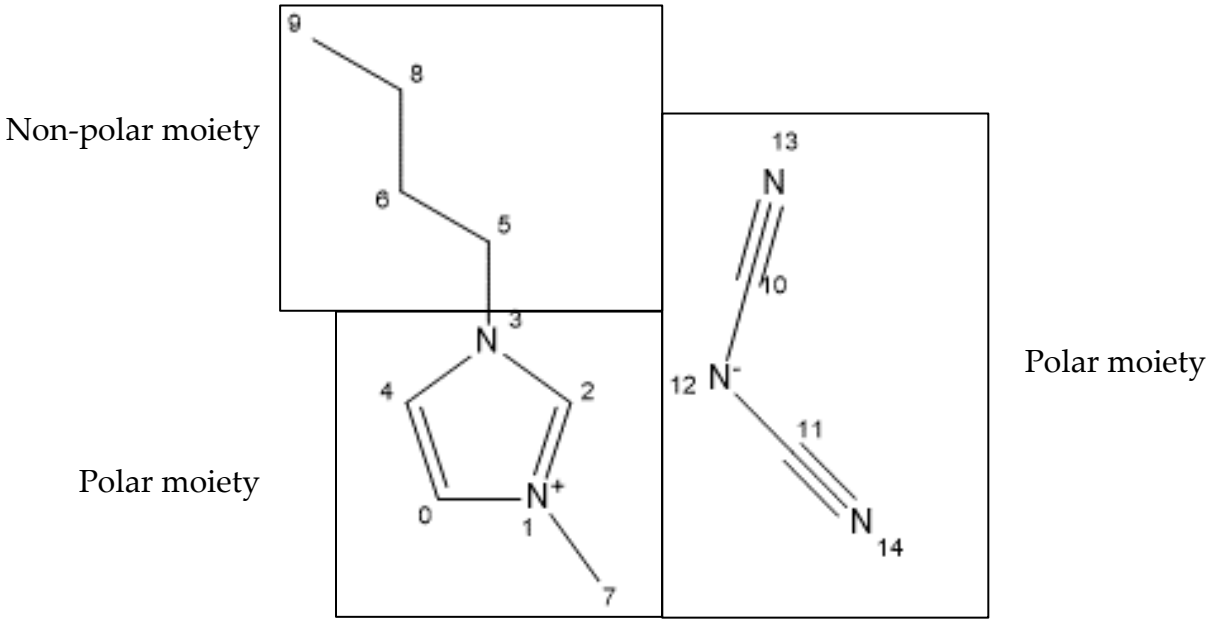

Figure 12 Representation of [BMIM][DCA] ionic liquid, where the grey beads are carbon atoms, white beads are hydrogen atoms, blue beads are nitrogen atoms.

As seen in the former Figure 13, the ionic liquid is comprised of a cation, that has a non-polar carbon chain of 4 carbons and 7 hydrogens and a polar imidazolium ring with the positive charge distributed by imidazolium ring.

The presence of an amphiphilic molecule or surfactant leads to the transition of a parallel anchoring to an homeotropic anchoring, since the nematic liquid when in the presence of water tends to have an parallel anchoring, when the surfactant is added in the PDLC, it tends to intercalate itself between the LC and the water medium [38].

Since Ionic Liquids are the molecules used in the original protocol of the electronic nose, then it will be further discussed [20].

Ionic Liquids in PDLC's

Ionic Liquids are, as the name suggests, liquids comprised entirely of ions, and in the last decades have been a major research subject with thousands of articles being released every year [39].

This ionic liquid "fever" is given to its very interesting chemical and physical properties, since it presents a negligible vapor pressure, it is considered as a green solvent [40]. Given it is comprised entirely of ions it presents high conductivity and a wide electrochemical window, i.e. the voltage range between oxidation and reduction of the material [41]. They can also form gel and polymerize [42].

This last property is very interesting in the scope of this work, since a PDLC can be assembled in the presence of an ionic liquid, and two important occurrences exist, the LC anchoring force is going to be diminished leading to less energy for the liquid crystal to undergo phase transitioning, this is important where this phase transition is used to sense any event, and the large electrochemical window and high conductivity allows for the IL to more easily transport electrical charges compared to water and this electrical charge is not enough to make changes in the chemical properties of the ionic liquid.

IL/LC gas sensing gel

Having the previous properties in mind, a LC gas-sensor based on a gel, is being developed by the biomolecular engineering group, where a mixture of a liquid crystal, as the optical sensor, an IL, used as a surfactant to diminish the anchoring force of the LC, and gelatin, as matrix support for the droplets, is used. The way this gas sensor works is in the presence of VOC's is that the nematic phase turns isotropic, and when the VOC's disappear the nematic phase arises again [20].

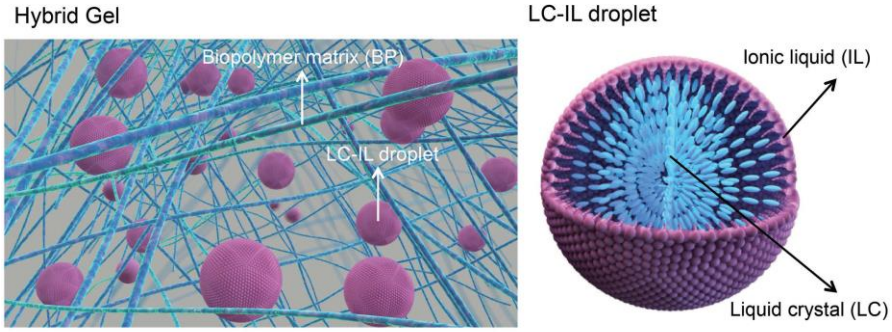

Figure 13 Gas sensing hybrid gel, where it is depicted the system in which the droplets (right side of picture) are deposited in a polymeric matrix (left side of picture) and it is possible to note the possible arrangement of the LC molecules along the droplet and the arrangement of the IL to the LC molecules [20].

Nonetheless, a lot is still to be unveiled in how this sensor works, since this is one of the first ionic liquid/liquid crystal gel [20, 43] made there isn't much knowledge about, the questions leading to this work are the following.

- What is the orientation and stacking of the liquid crystal inside the droplet?
- How are the LC and IL molecules interact in the interface?
- What is the effect of the water in the orientation and ordering of the LC inside the droplet?
- What is the preferred orientation of the IL in the interface?
- What is the preferred orientation of the LC in the interface?

To obtain such answers an atomistic knowledge is needed, and in order to obtain such knowledge computational aid is required, and this is the subject of the following chapter.

1.3 Molecular Modelling

Molecular modelling is way of mimicking molecular behavior either in a system containing various molecules or of a single molecule [44]. This mimicking is important because it allows for the rationalizing of matter's behavior and predict new matter behaviors.

The two most common ways of realizing chemical modelling are:

- Quantum mechanics
- Classical mechanics

Quantum Mechanics

Quantum mechanics calculations try to mimic molecular behavior by trying to solve the Schrodinger equation.

$$H\Psi = E\Psi \qquad \text{Equation 2}$$

In equation 2, H corresponds to the Hamiltonian operator, Ψ is the wave-function created by all the atoms present in the system and E is the total energy of the system [45].

The Hamiltonian operator depicts all the factors interesting to calculate the systems energy, as kinetic energies both from nuclei and electrons and all the potential energy coming from the interactions between electrons themselves, nuclei and between nuclei and electrons [45].

However, solving this equation completely is impossible since the system has electronic correlation, this is all the electrons depend on themselves to calculate the system's energy [45].

So, all the energies obtained through *ab-initio* calculations are approximations of the Schrodinger's equation, and the following approximation are transversal to all the equation-basis used in *ab-initio*:

- Born-Oppenheimer Approximation

In this approximation states that due to the difference between the masses of the nuclei and electrons, the movement of the nuclei can be neglected as it is very slow compared to electrons, this leads to the nuclei kinetic contribution to the system energy to be considered always zero, allowing for a more fast calculation [46].

Other approximations are used in *ab-initio* however those depend on the equation basis to be used, and that is outside the scope of the present work.

Major uses for *ab-initio* calculations is the calculation of various physical properties (absorbance of the molecule in study [47], bond vibrations [48] between others) and chemical properties (Molecular orbitals energy [49], transition state of a reaction [50], various acid or basic constants [51]).

Classical Mechanics

In molecular dynamics system properties are recreated using only classical mechanics, where only nuclear positions are considered in calculations [52].

For example, to describe the stretching potential of a bond, Hooke's law where atoms are considered as an assemblage of weights in springs [53], as shown in Equation 3.

$$E_{bond} = k_s(r - r_0)^2 \qquad \text{Equation 3}$$

Where E_{bond} is the energy of stretching of a bond, k_s is the stretching constant of that particular bond, r is the length of a bond and r_0 is the bond length at an equilibrium state.

In order to calculate k_s it is necessary to *a-priori* the frequency of the bond, the mass of the atoms present in the bond, and the equilibrium bond length. Because k_s can be extrapolated by the following equation.

$$\nu = \frac{1}{2\pi} * \sqrt{\frac{k_s}{\frac{m_1 m_2}{m_1 + m_2}}}$$

Equation 4

As it possible to understand just for this example, using molecular dynamics needs a parametrization for every kind of energy contributor to the system, intermolecular forces (electrostatic interactions), and intramolecular forces (bond strength, bond angles, proper dihedral angles and improper dihedral angles).

Yet, this is a smaller problem when a system is made of only a restricted type of atoms, as for example proteins, that are constituted mostly out of amino acids (only in special cases other types of molecules are included in a protein constitution), this closed spectra of molecules leads to a defined amount of parameters to be defined.

However, the same does not apply to other organic molecules, as millions of combinations are possible. And the same moiety can assume very different behavior depending on the neighboring moieties.

For example, a carbonyl bond in an amide is different from a carbonyl bond in a ketone. This variability of characteristics of the same bond depending on the neighboring atoms, leads to a very difficult task of parameterizing small organic molecules.

There are three ways for parametrizing a molecule:

- **Doing it all parametrization in the lab**

Depending on the molecule it is being parametrized it either is a very complicated procedure due to the scarcity of information or the molecule has a large

amount of information available making the parametrization easier. Another option is too use *ab-initio* simulations in order to parametrize all the things needed

- **Using online parametrization tools**

This method allows the use of online descriptors in order to have full parametrization to the desired forcefield, this method vary from online descriptors using classical mechanics as a way of doing energy minimization (where the atoms are parametrized in a data base) to having *ab-initio* calculations of the molecule to be parametrized.

- **Retrieving a full parametrization from the literature**

If a molecule has been a target of molecular dynamics simulations, it is possible to find full parametrization and even custom forcefields, that were put available for academic or personal use.

The next step after doing the parametrization is to choose the appropriate forcefield in which the simulations undergo. Since forcefields have different contributions to calculate, this can be seen in Equation 5 as 6, where in Equation 5 is depicted the functional form for Assisted Model Building with Energy Refinement (AMBER) [54] and in Equation 6 it is show the Optimized Potential for Liquid Simulations (OPLS) [55].

$$V\left(\{\vec{r}_N\}\right) = \sum_{bonds} \frac{1}{2} k_b (r - r_0)^2 + \sum_{angles} k_\theta (\theta - \theta)^2 + \sum_{torsions} \frac{1}{2} V_N [1 + \cos(n\omega - \gamma))] + \sum_{i=1}^{N-1} \sum_{j+i=1}^{N} \{4\varepsilon_{ij} * [(\frac{\sigma_{ij}}{r_{ij}})^{12} - (\frac{\sigma_{ij}}{r_{ij}})^{6}] + \frac{q_i q_j}{\varepsilon r_{ij}}$$

Equation 5

$$V\left(\{\vec{r}_N\}\right) = \sum_{bonds} \frac{1}{2} k_b (r - r_0)^2 + \sum_{angles} k_\theta (\theta - \theta)^2 + \sum_{torsions,N=1}^{4} [\frac{V_N}{2} [1 + (-1)^{N+1} * \cos(N\phi)] + \sum_{i=1}^{N-1} \sum_{j+i=1}^{N} \{4\varepsilon_{ij} * [(\frac{\sigma_{ij}}{r_{ij}})^{12} + (\frac{\sigma_{ij}}{r_{ij}})^{6}] + \frac{q_i q_j e^2}{r_{ij}}\} f_{ij}$$

Equation 6

As can be noted by the analysis of both the functional forms it is possible to see differences in the contributions to the energy of both the forcefields.

After choosing the correct forcefield pre-simulation steps are needed to be performed, first the desired system needs to be constructed, where the number of molecules is defined, the size and shape of the simulation box is decided and

if the system contains water or Ions (in order to make sure the system is truthfully represented as normally, for every charge there is an ion countering it).

The first step in the Molecular Dynamics protocol is Energy Minimization (EM), to minimize the energy of the system created, this allows for the system to have the most stable configuration possible [56]. EM deletes incoherencies made by the system construction (overlapping bonds or atoms that are too close together).

Normally two algorithms are performed to obtain EM:

- **Steepest Descent algorithm (SD)**

SD consists in of a multidimensional function for all coordinates 3N, and this algorithm trough a various number of iterations calculates the minimum of this function in order to have all the atoms in their lower energy states. Through the calculation of the gradient of the function, that gives the direction in which the function increases the most, so if steps are made in the opposite direction a decrease in energy is always guaranteed, and at iteration, potential energy and maximum force is calculated and new atom positions give rise to new functions and the cycle repeats, however there is a downside to this algorithm as both the gradient and the direction of successive steps are necessarily perpendicular one to another, leading to a zig zag movement of the decrease in energy. This algorithm is faster in the initial stage of EM, since the first corrections are the one that lead to biggest descents in energy [56].

- **Conjugate Gradient algorithm (CG)**

CG is used to eliminate the downside of the SD method, because in each step gradients are orthogonal, however the direction of each step in conjugate on to another, leading to the elimination of the zig-zag pattern created by the SD algorithm. However, it is only used after the major EM step is performed by the SD algorithm as it slower, in the initial stages [57].

The next step in the simulation is the Equilibration step, in order to apply heat and pressure to the system until these parameters are stable. The way the energy of the system is calculated is by solving Newton's motion equation.

$$m_i \frac{\delta^2 \vec{r}_i}{\delta t^2} = \vec{F}_i \qquad \text{Equation 7}$$

Where $\vec{r}_i$, $\vec{F}_i$ and m_i are the coordinates, forces acting on it and mass of the particle i respectively.

The algorithm used to iterate over the Equation 7 it is the leapfrog iterator. That calculates velocities at half integer steps and positions are calculated at integer steps [58]. As depicted in Figure 14.

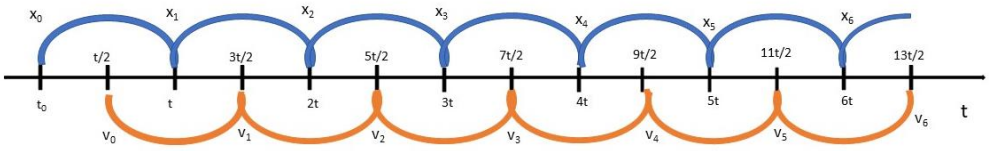

Figure 14 Leap Frog integrator depiction where t is the time of simulation, v is the velocity calculated and x are the positions calculated

So, at the integer time steps, the forces and positions are calculated and at half-integers time steps velocities are calculated that are used to calculate the new positions at the integer time steps [58].

The Molecular Dynamics simulation start after the equilibration (using various algorithms, however all solve the same equation differing only in the iterator used).

However, MD simulations have various levels of detail regarding the parametrization and Forcefield used:

- **Fully Atomistic Simulation**
    - **All atoms (AA)**

In these simulations, all the atoms of the molecule are considered in the system's energy calculation.

    - **United Atom (UA) Simulation**

In these simulations the non-polar hydrogens are withdrawn from the structure to be calculated, however are implicit in the parametrization of the molecules. This leads to faster calculation times, since less atoms are contributing to the system's energy.

- **Coarse Grained (CG) simulations**

In CG, atoms are not considered individually, instead super-atoms are created having inside the parametrization all the features of atom groups that constitute the super-atom.

As stated before in this sub-chapter, the major work developed in MD simulations revolve around proteins.

- Unveiling the structure of a protein [59]
- Binding assays with a ligand [60]
- Catalysic studies of proteins (mixed MD - Quantum mechanics) [61]

Nevertheless, MD simulations are used in various fields of organic chemistry, however only the studies of LC and IL are going to be described in the present work.

Molecular Dynamics in Liquid Crystals and Ionic Liquids

With the possibility of studying longer simulation times with somewhat cheap hardware, LC became an extensively studied field, where suddenly order diffusion became a possible study opening the gates to most of the MD studies performed today. As for example:

- **Calculate order parameters and Molecular stacking of LC**

Zhang *et. al "An Atomistic Simulation for 4-Cyano-4'-pentylbiphenyl and Its Homologue with a Reoptimized Force Field"* [12] reoptimized "Transferable Potentials for Phase Equilibria" forcefield to simulate 5CB bulk phase, in order to calculate P2 order values and how the molecules are packed in the bulk, having obtained a convergency at 25 ns of the system to have a P2 order value of 0,51 and noted that the molecules tend to align trough the cyano heads and by π -π stacking, as simulated in Figure 15.

Figure 15 Various stackings of 5CB possible, in the left π-π stacking and on the right trough the cyano heads

- **Calculate elastic constants of nematic LC**

Sidky et. al in " *In Silico Measurement of Elastic Moduli of Nematic Liquid Crystals* " [62] demonstrated that all nematic elastic constants could be calculated directly from atomistic molecular dynamics.

- **Interfacial studies of 5CB and water**

Ramezani-Dakhel *et. al* in " *Understanding Atomic-Scale Behavior of Liquid Crystals at Aqueous Interfaces* " [63] studied the interface between 5CB and water and between 5CB and vacuum, calculating tilt angles, order parameter along the 5CB layer. And the type of anchoring of the LC in the water interface, noting that it was planar. As simulated in Figure 16.

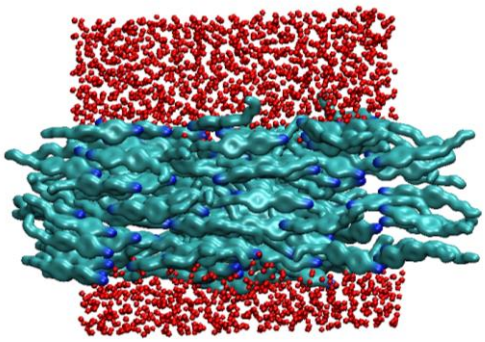

Figure 16 5CB and water anchoring, with water depicted as red beads and 5CB shown as the cyan and blue beads

The author calculated the tilt angle of the 5CB molecules with the interface along an axis. Where the molecules' long axis orientation varies with the distance to the interface, having a variance in the director of the phase, as depicted in Figure 17.

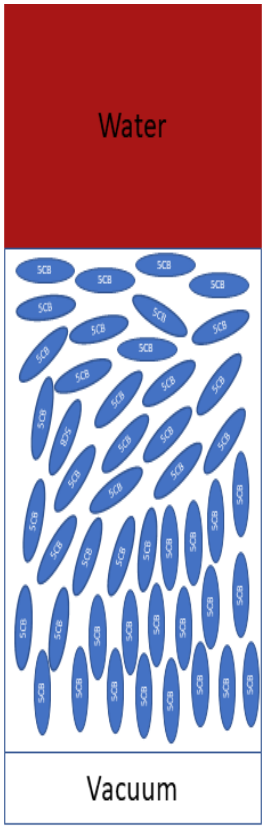

Figure 17 Variance in the director of the nematic phase of 5CB

- **Interfacial studies of LC and amphiphilic molecules**

Abbot et al in " *Amphiphile Induced Phase Transition of Liquid Crystals at Aqueous Interfaces*" [38] studied the effect of an amphiphilic layer in between water the water layer and the LC layer, noting that the amphiphilic layer would induce an homeotropic alignment to the LC phase. An to prove that the amphiphilic would in fact only diminish the anchoring force and not induce a reorientation of the molecules' long axis, a simulation with two water layers, was performed having reached a state where the molecules would have a planar anchoring and an isotropic phase near the amphiphilic monolayer, the simulation is described in Figure 18.

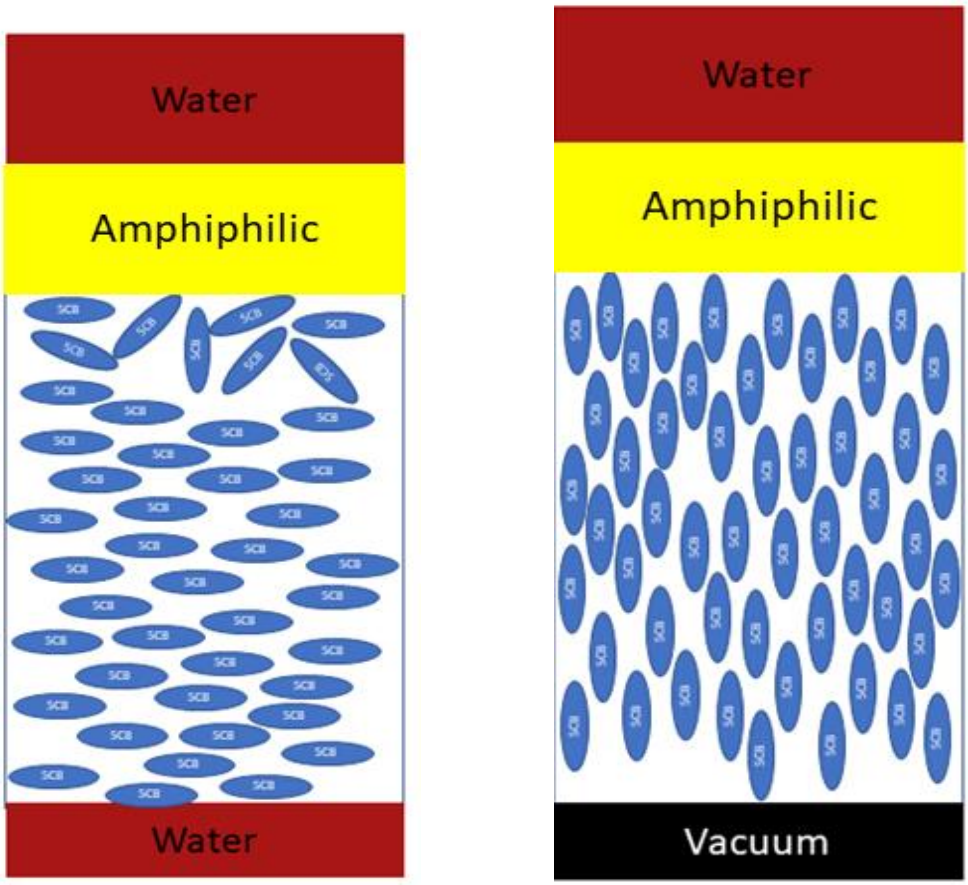

Figure 18 Two simulations done by Abbot with the amphiphilic layers

2

Methods

All simulations undergone the same protocol in order to uniformize systematic errors present in each simulation present in the software used two Gromacs [64] versions (Gromacs 5.1.4 and Gromacs 2018.4), the procedure followed 4 steps.

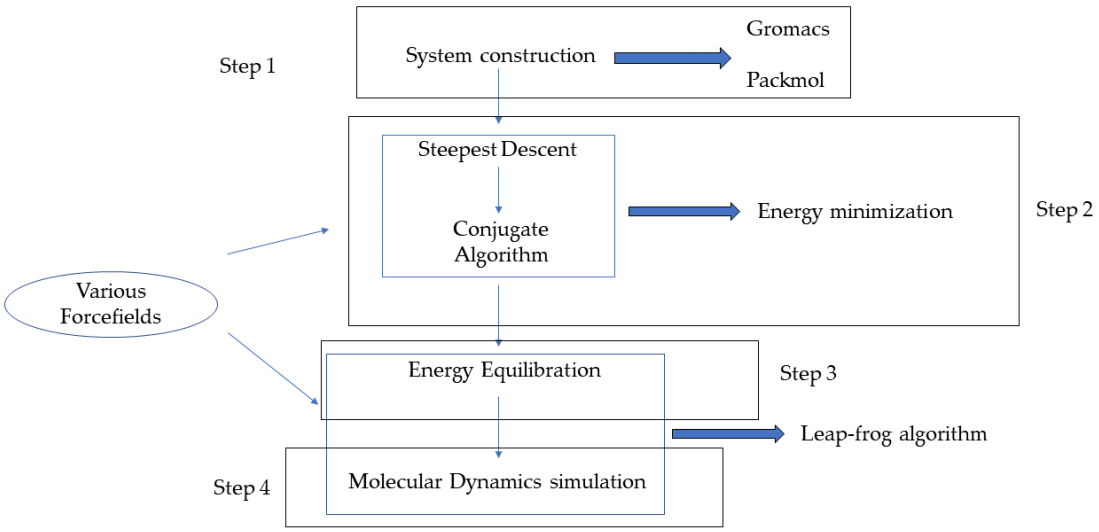

Figure 19 Simulations Workflow

System assembly consisted in using PackMol [65] in order to randomly place molecules throughout the system's box. The user defines the size of the box, the shape of the box and the number of molecules inside the box.

Regarding the hardware used in this work, energy minimizations were all carried out in a computer with a i5-3470 processor without GPU support. The MD simulations of 5CB, 8CB and IL were carried in a computer containing an intel xeon gold e-35 with 24 cores and 4 Nvidia Tesla M2900 with CUDA 8 GPU support, using gromacs 5.1.4. A new computer, with an AMD Ryzen 2700X octa-core CPU and a Nvidia RTX 2070 GPU with CUDA 10 support arrived to the lab mid-project with higher performance, the MD simulations of bigger systems, containing the mixture of 5CB, IL and water, were carried out in it and a newer version of gromacs was used, gromacs 2018.4.

The first forcefield used was gromos53a6 [66], as the first approach was to submit 5CB to Automated Topology Builder (ATB) [67] and retrieve the custom forcefield and parametrization from it. Molecular parameters from PRDRG [68] were also retrieved based on gromos53a6 forcefield. However, the Optimized Potentials for Liquid Simulations (OPLS) forcefield [69] and parametrization was the one chosen since it represented better the characteristics of 5CB, all parametrization for it was retrieved from Ligand Parameter Generator (LigParGen) [70]. For the Ionic Liquid a fully detailed forcefield and parametrization, based on OPLS forcefields was found in the literature [71].

All the simulations were performed at 300 K controlled with a Berendsen thermostat, with 1,03 bar of pressure controlled with a Berendsen barometer employed with a relaxation time of 1.0 and 0.1 ps, a grid neighbor search with a cut-off radius of 1,0 nm was used, and cubic periodic boundary conditions were used, under NPT conditions, Van der Walls interactions were truncated to 1,0 nm in the MD simulations of PRDRG and ATB. For OPLS MD simulations, parameters were retrieved from an article [72], maintaining every parameter equal except for the Van der Walls truncation distance that was raised to 1,4 nm in order to force more interactions between the 5CB molecules, the default and modified parameters are displayed in the Supplementary Information (SI 1 ; SI2).

All performed simulations, were at an atomistic level using all-atoms molecular parameters.

Various analysis were made using gromacs analysis tools, gmx energy was used to calculate the bulk density, gmx density was used to calculate the partial densities along an axis, gmx rdf was used to perform all the RDF's. MDtraj [73] was used to calculate the P2 order parameter with used script in the Supplementary Information (SI 3), and MDanalysis [74] was used to calculate order parameter along an axis with the used script displayed in the Supplementary Information (SI 4).

3

Results and Discussion

In this chapter the various results will be presented, and further discussion will take place.

The chapter is divided in three major sub-chapters:

- The work concerning 5CB
- The work developed in IL
- Finally, the work related to all the components mixed

3.1 - 5CB

The first component that was tackled in this work was the Liquid Crystal, as it was the one that is expected to have the most notable changes in the final system containing, since it is very noticeable the LC phase changes.

Firstly, various forcefields were used to see how the 5CB would be simulated, and in order to evaluate the simulations' success, the properties studied were:

- Density, since it a direct comparison to the experimental data available, being the reported value of 1,02 g/cm^3 [15];

- And the P2 order parameter, since it was known that 5CB had to have a P2 order parameter between 0,4 and 0,6 [12], however it is reported in various cases that simulations tend to overestimate the P2 order value, so it is expected for the order values to be over 0,4 for the phase acquired to be considered as nematic having a nematic order parameter of 0,54 [15].

To facilitate the identification of certain atoms crucial to the development of this chapter, arbitrary numeration of atoms in the molecules is given. 5CB has the following numeration

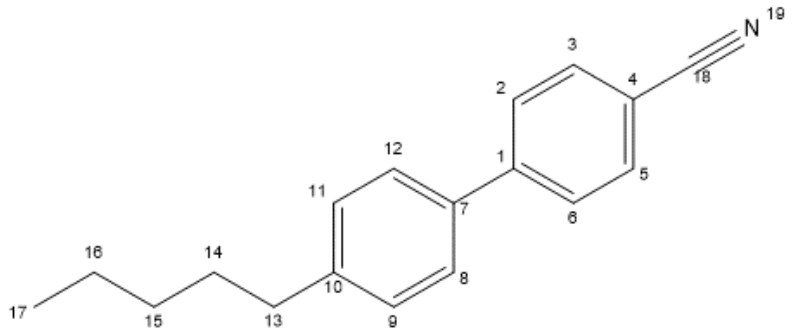

Figure 20 Chemical structure of 5CB with arbitrary numeration

Forcefields

Before any kind of simulation in order to consider a simulation valid the parameters simulated need to have an error inferior to 5% as it was stated in [12], that the average errors of simulations are around 5%.

Another criterion is that all simulations is that they start as isotropic, that is achieved by randomly placing 5CB inside a box using gromacs, insert-molecules command.

Two parametrizations were first used, because they were easy to use. They were PRODRG and ATB, where PRODRG. And, after the literature review seen that gromos53a6 forcefield could be used to simulate the behavior of liquid crystals, ATB was used, since it would output a modified gromos53a6 forcefield. And PRODRG would search for atoms in their database in similar environments outputting the parameters for each atom.

However, the difference between the two parameterizations is that, PRDRG simply outputs a topology file to be used in GROMACS not having any kind of energy minimization, guaranteeing that the input structure is correct, opposingly ATB first would do various stages of energy minimization of the inputted

molecule (starting with molecular mechanics and finishing with density functional theory calculations), giving a more reliable topology file.

Whilst both the topologies retrieved from the servers would give an accurate density simulation, the difference started to be noted at the P2 order value with PRDRG to have difficulties to have reasonable P2 values, achieving only a P2 value of only 0,26, after a simulation of 100 ns with the same inputs as described in the methods.

The evolution of the P2 value can be seen in Plot 1, where the P2 order parameter is Plotted trough time of simulation.

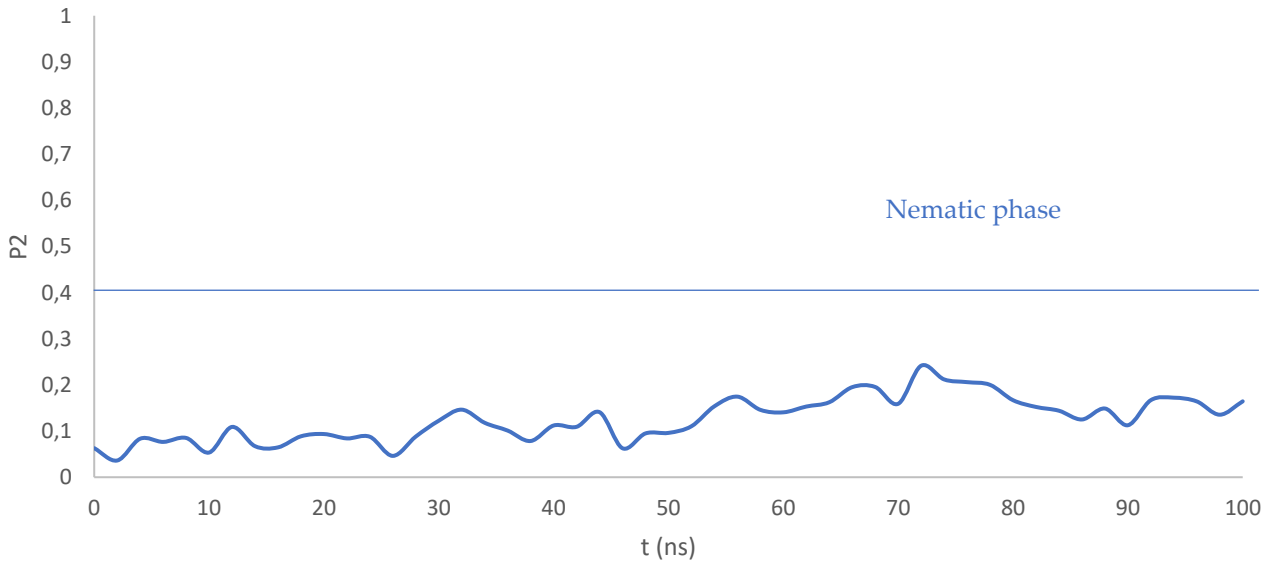

Plot 1 P2 evolution trough time of PRODRG topology, with the phase considered nematic is only above the blue line

As can be seen in the Plot 1 a nematic phase isn't reached, this is due to PRODRG to have flaws simulating charges. And since most of interaction between 5CB are electrostatic and hydrophobic, correct charges are crucial in order to have a plausible simulation of the real system. The lack of order can be assessed in Figure 21 where the last frame of the MD simulation is depicted.

a) b)

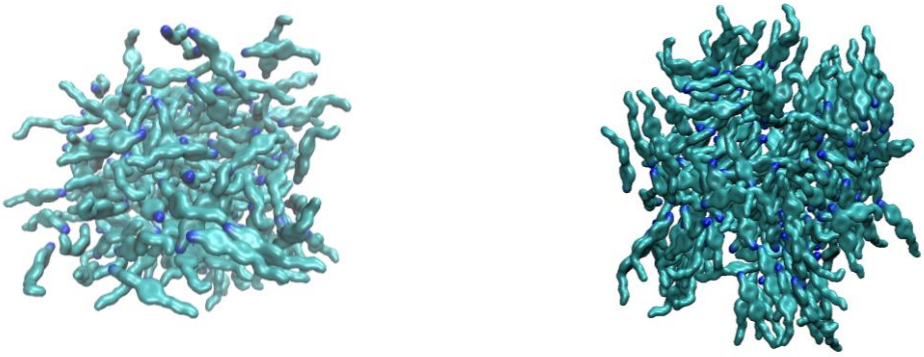

Figure 21 a) Initial configuration of 5CB system containing 165 molecules of 5CB inside a 5nm sided box. **b)** Snapshot of the last frame of the simulation of 100ns, at 300K, at 1 atm.

It is important to note that the molecules don't have a director to which they align to meaning that an isotropic phase was achieved. Although the P2 order parameter isn't simulated in a plausible way, density obtained from the simulations is of 1,031 g/cm^3, having a deviation of 1,07% to the value retrieved from the literature of 1,02 g/cm^3 [15].

Therefore, the next step was to use the ATB parametrization and custom forcefield. The density obtained from the simulations was 0,986 g/cm^3 with a deviation of 2,83% (still a minimal error, given that it is below the stipulated threshold) to the theoretical value, however a P2 order value of 0,47, being significantly higher than the PRODRG topology, however the system obtained was barely nematic phase given the P2 order value being in the lower threshold of what is considered nematic.

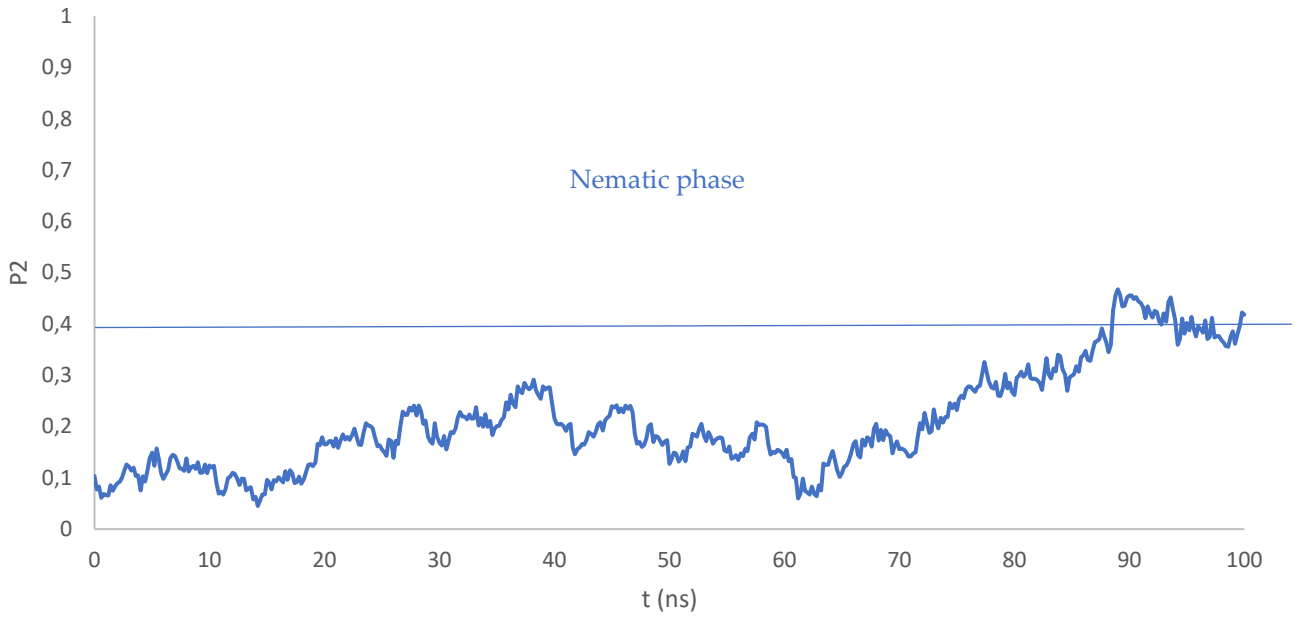

Plot 2 P2 order value over time of 5CB system using ATB topology and modified forcefield, being considered a nematic phase above the blue line

Despite being on the lower end of order values inside the nematic phase, order starts to be noticeably higher than the simulation from PRODRG, as can be seen in Figure 22.

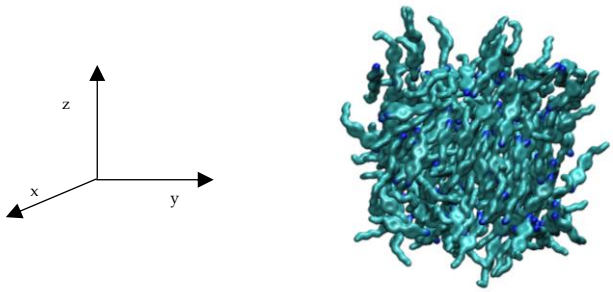

Figure 22 Snapshot of the last frame of simulation using ATB topology as custom forcefield, with a simulation time of 100ns at 300K, with a 5nm cubic box side, and 173 molecules

By the visual analysis of Figure 22, it is possible to note that the molecules tend to align with the Z axis, and the molecules tend to stack by the cyano moieties, being antiparallel each molecule with the partner with the nitrogens being 5,78 Å apart, as depicted in Figure 23 a).

a) b)

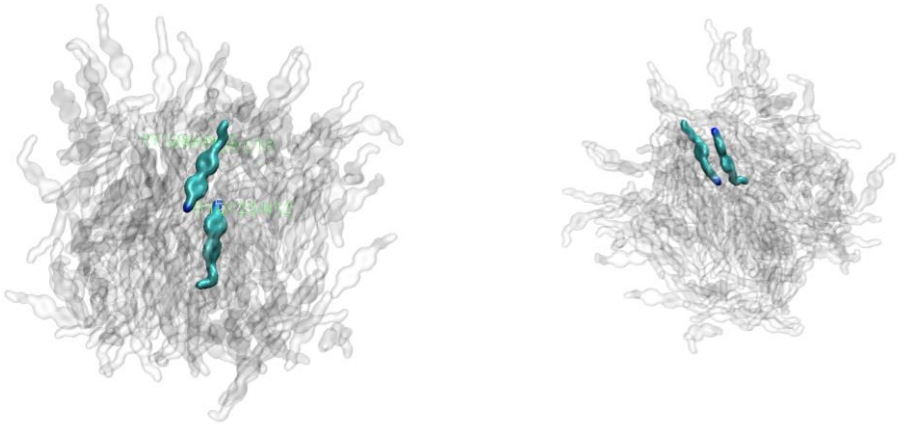

Figure 23 a) Snapshot of a typical cyano head stacking **b)** Snapshot of a typical ***π-π*** stacking

However, this stacking is not the only one happening in the system, π-π stacking may occur as well, having a distance between the nitrogen and the furthest carbon of the biphenyl moiety of 4,88 Å, as shown in Figure 23 b)

These are the most commons stacking options in the nematic phase of 5CB, as confirmed by Zhang et al. in " *An Atomistic Simulation for 4-Cyano-4′-pentylbiphenyl and Its Homologue with a Reoptimized Force Field* " [12], where the author performed Radial Distributions Functions (RDF) between the nitrogens of each molecule in the cyano moiety(atom number 19), and between the nitrogen in the

cyano (atom number 19) and with the furthest carbon atom of the biphenyl moiety (atom number 1). The results of those RDF are displayed in Plot 3.

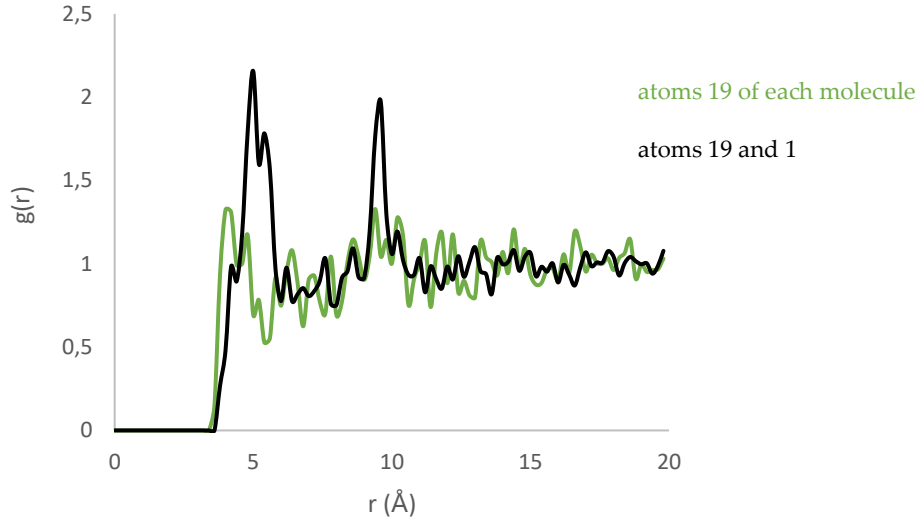

Plot 2 RDF of 5CB with the ATB topology, the green line representing the RDF between atoms 19 of each molecule, the black line between atoms 19 and 1

By scrutinizing Plot 3 the green line, it is possible to conclude that the first peak corresponds to the cyano heads arranged in an antiparallel way as depicted in Figure 23 b). In the black line, it is possible to see two sharp and high peaks, the first peak at about 4 Å corresponds to the π-π stacking as depicted in Figure 23 b) and the second high peak at 9,6 Å corresponds to the distance between atoms 19 and atom 1 in the same molecule (as shown in Figure 24) , the black line has two peaks that corresponds to anti-parallel and parallel arrangement of 5CB molecules, and the values are in accordance with the literature [75], the RDF for the cyano interactions are in accordance with the RDF's obtained in the literature [71]. By analyzing the RDF, the higher peak corresponds to the more likely stacking, that being the π-π stacking.

By reviewing the literature, OPLS was found to be a better option, since various articles were found that used OPLS based forcefields to simulate various LC, either nematic, like 5CB, E7 or smectic like 8CB.

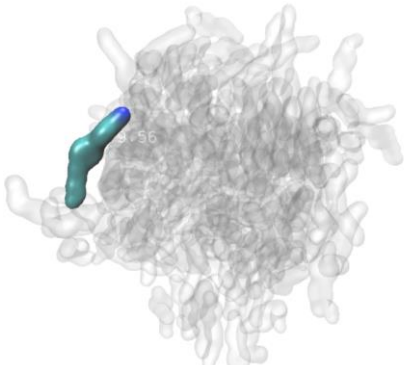

Figure 24 Distance between atom 19 and 1 of a 5CB molecule

LigParGen was used to parametrize 5CB, so the results were very promising since the density value of 1,01 g/cm^3 were in accordance with the previous values found in the literature in MD simulations, inside the same error range, since it had an error of 0,98%. Having a better simulation capability than the PRODRG. However, the real advantage of OPLS forcefield is in the simulation of liquids, since it very accurately represents charges in liquid phases (being the main goal in this forcefield) [75]. So, it is expected for it to excel in representing the nematic phase of 5CB.

And, as excepted it delivered with a P2 order value of 0,65 meaning that the phase obtained was a very clear nematic phase, as portrayed in Figure 25.

By analyzing Figure 25 it is possible to see a clear director inside the phase, where all molecules inside the bulk tend to align to.

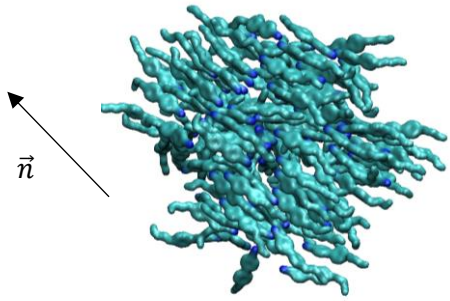

Figure 25 Snapshot of the last frame of the simulation with the LigParGen topology, with a simulation time of 100 ns, at 300K, with a 5nm cubic box side and with 142 molecules, where $\vec{n}$ is the director

Another upside of using OPLS forcefield is the small amount of time needed for the system to present order, as can be seen in Plot 4.

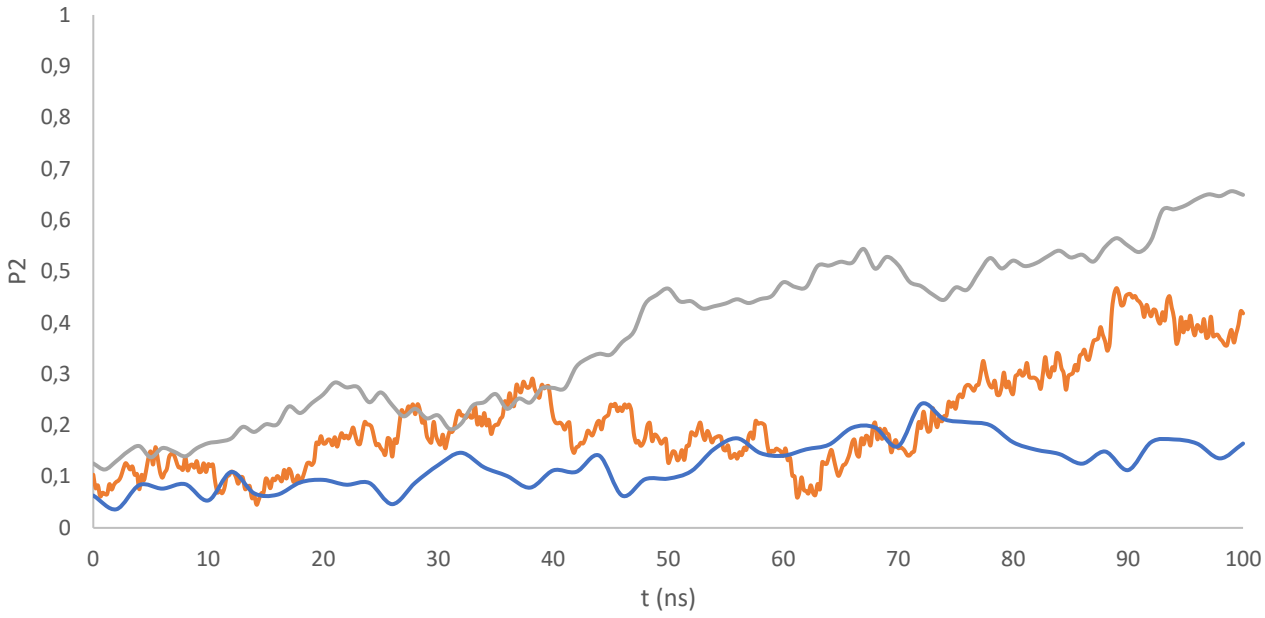

Plot 3 P2 evolution over time of all topologies and forcefields. Blue line represents the PRODRG parametrization, the orange represents the ATB parametrization and the grey line represents the LigParGen parametrization.

The stacking present in the OPLS simulation, is very similar to the stacking in the ATB simulation, having:

- Dipole interaction between the cyano moieties, shown in Figure 26

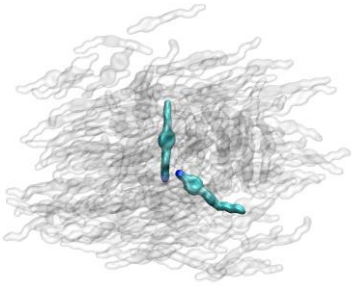

Figure 26 Snapshot of stacking through the cyano moiety

- Stacking through π-π stacking as shown in Figure 27

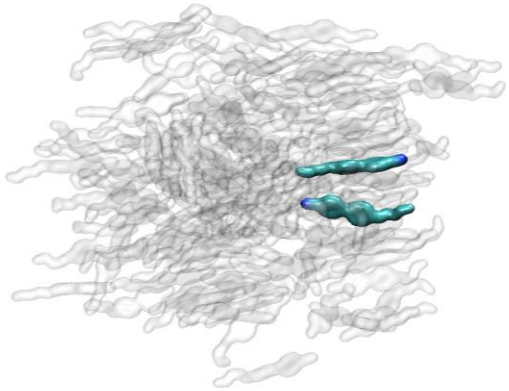

Figure 27 Snapshot of stacking through π-π stacking

To analyze which stacking is more common, an RDF between the same atoms as in Plot 3 was realized, being depicted in Plot 4.

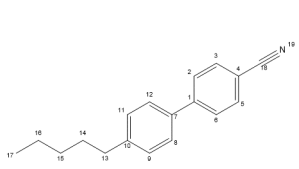

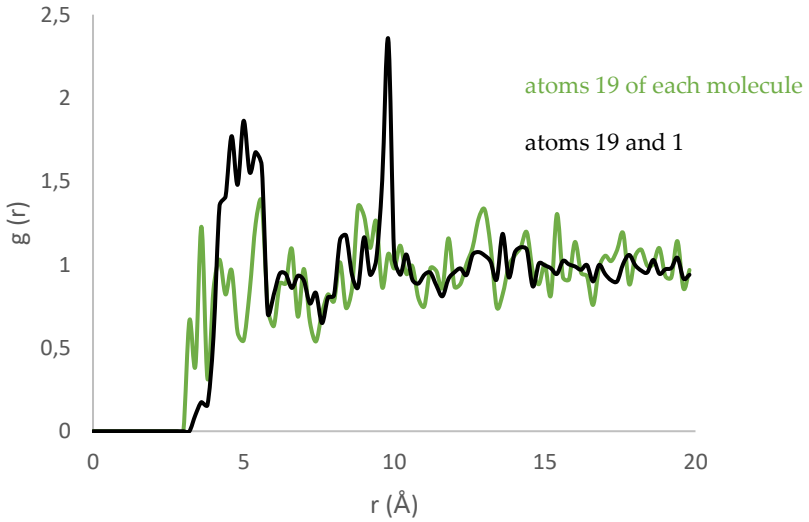

Plot 4 RDF of the 5CB with OPLS forcefield simulation, with the same colour code as Plot 4.

By analysis of Plot 4 is possible to conclude that exist both the stacking in the system, however the stacking coming from the cyano moieties is more recurrent this is given to that OPLS represents better charges in liquid state, promoting therefore the cyano interactions, however the π-π stacking is still predominant,

the values obtained for the distances of π-π stacking are in accordance with the values in the literature [76].

Water Interface studies

Having decided that OPLS was the best forcefield, the next phase is to study the effect of water to the LC. Since in the final system, the goal is to see the differences between the system with and without the Ionic Liquid, and water is present in the system.

It is expected, to have phase separation between 5CB and water, so the protocol to simulate phase separation consisted in:

1. Creating a box and inserting randomly 5CB molecules
2. Through gromacs, insert randomly water molecules in empty spaces
3. Run normal procedure for simulations (Energy minimization, Equilibration and MD run)

So, the initial system of the MDRUN, would look like Figure 28.

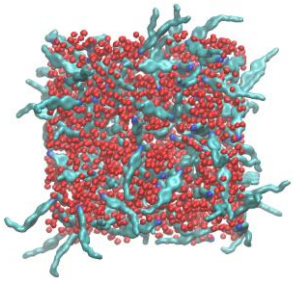

Figure 28 Snapshot of the initial system of the MD run, after the equilibration step, with 5CB coloured blue, and water depicted as the red beads, with a 5nm box and 142 molecules of 5CB

In Figure 28 is possible to observe, the inexistence of two phases, as it was expected, and a random displacement of the 5CB molecules inside the system, translating in a P2 order value of 0,24, and culminating in a P2 value of 0,88 as shown in Plot 5.

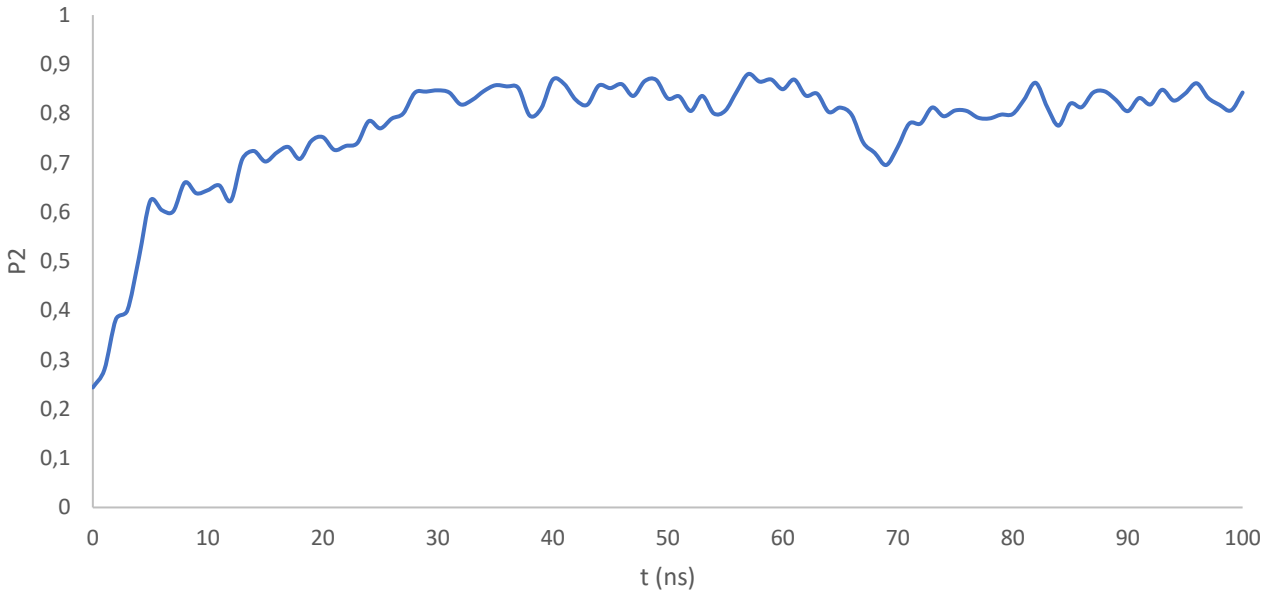

Plot 5 P2 order parameter evolution over time of the simulation containing 5CB and water using OPLS forcefield

By the analysis of Plot 5, can be seen that P2 evolution is steeper than the evolution without water. This is due to water forcing 5CB to order by repulsion of the water molecules by not mixing with it.

The final frame of simulation (100 ns) can be seen in Figure 29.

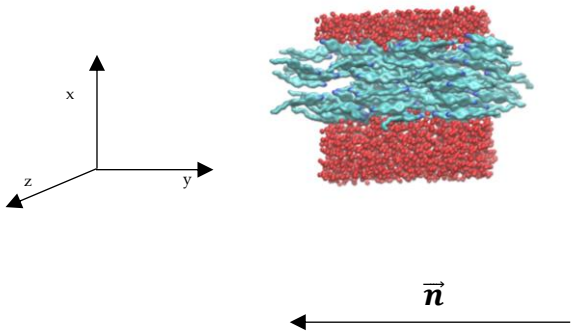

Figure 29 Snapshot of the last frame of simulation of 5CB and water, using OPLS forcefield. Simulation time of 100 ns, at 300K, in a 5nm side cubic box with 142 molecules of 5CB, where $\vec{n}$ is the director of the nematic phase.

Scrutinizing the Figure 30 it is possible to see phase separation of 5CB and water as it was expected, and that can be confirmed when it is calculated the density of 5CB along the X axis (red axis in Figure 30), outputting Plot 6.

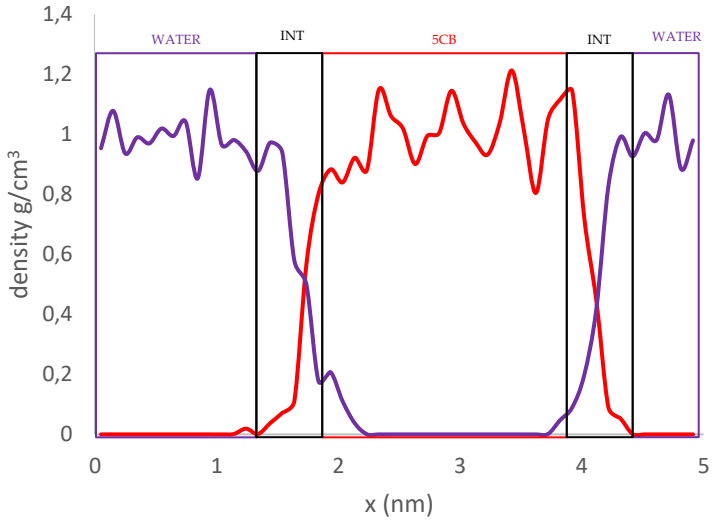

Plot 6 Density of 5CB and water along the X axis; red line: 5CB density; purple line: water density and the black box represents the interface of the system.

By the examination of Plot 6, it is possible to conclude that the average density between 2,1 nm and 3,9 nm (the effective site of 5CB inside the system) is 1,02 g/cm^3 which is in conformity with the experimental density. And the density of water at 300K is of 0,99 g/cm^3 [77] and the average between 0 and 1,6 and 4,2 and 5 nm (the bulk phase of water) is of 0,96 g/cm^3, the rest of the box is not considered to the averages since it is the interface and the density on those sites is influenced by the mixture, so only bulk densities are considered.

The major stacking in water and 5CB simulations consist in π-π stacking like in Figure 30.

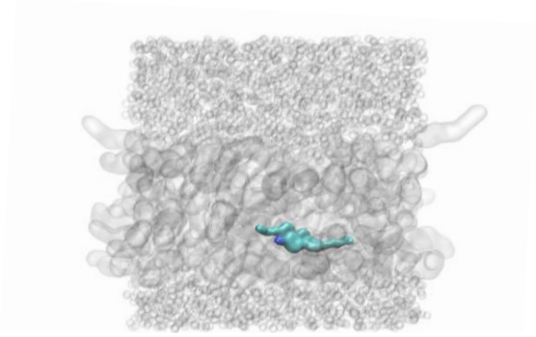

Figure 30 Representation of a π-π stacking

The anchoring in the system, is in accordance with the literature as stated in introduction. 5CB in water environments is planar, the system ended with the 5CB molecules horizontal to the plane defined by the water molecules, to confirm the visual conclusion, the P2 order value to the plane between the molecules' long axis and the YZ plane was calculated. Reaching a value of 0,7 at the interface of 2 nm. This value being lower than the overall P2 where the average of the molecules' long axis produces the director, indicates that the molecules tend to be slightly tilted and not perfectly horizontal.

The stacking of the molecules is assessed the same way as in previous subchapter by performing RDF of atoms 19, between atoms 1 and 19 (following the numbering in Figure 22). The result is displayed in Plot 7.

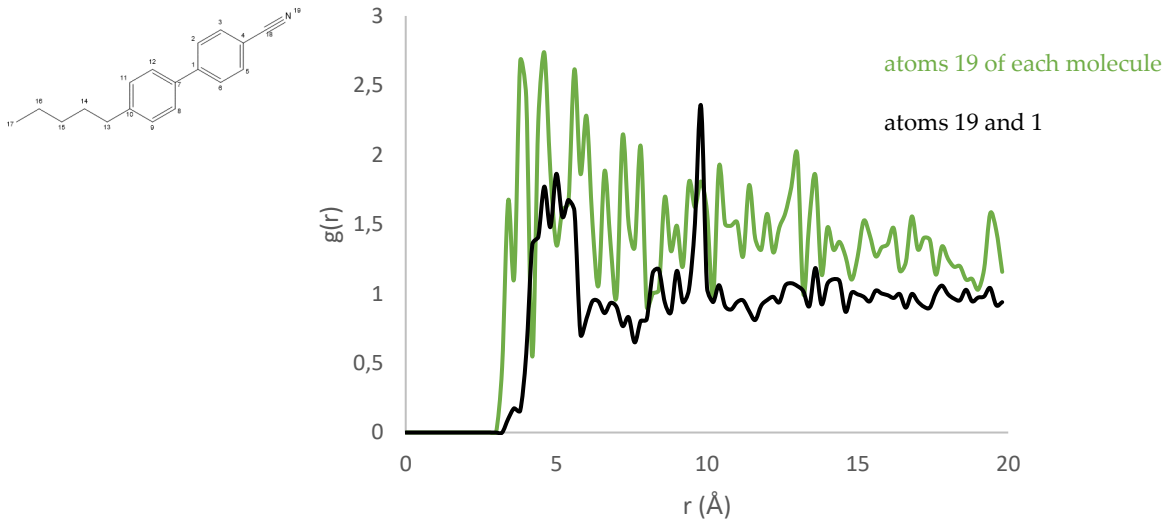

Plot 7 RDF concerning the 5CB and water simulation using the OPLS forcefield following the same colour code as Plot 4

By the analysis of the Plot it is possible to see that the second peak in the blue line is now the sharper and higher than the peaks in the orange line. Indicating that the most common arrangement is through the cyano heads, and the π-π stacking occurs with less frequency. This may indicate that the π-π stacking is present in the arrangement in the layers of 5CB and that the cyano head interaction is present in the bulk of the system.

3.2 [BMIM-DCA]

Herein is reported all the results obtained concerning the studies of the Ionic Liquid BMIM-DCA, it was chosen due to that it was used in the protocol of the sensing gels of the electronic nose reported in "*Tunable Gas Sensing Gels by Cooperative Assembly*" [20]. The only work made was confirming the forcefield used, since it was retrieved from an article [71]

Forcefield Reproduction

As reported in the methods chapter, there were descriptions of OPLS forcefield usage in simulations of a collection of ILs [71], so to make sure the forcefield would have the same results as the article described, a simulation of [BMIM][DCA] at 300 K, with 1000 molecules of IL was performed. The studied parameters were density and RDF (that gives the average distance of the anion and cation and where the cation tends to be).

[BMIM][DCA] has the chemical structure illustrated in Figure 31.

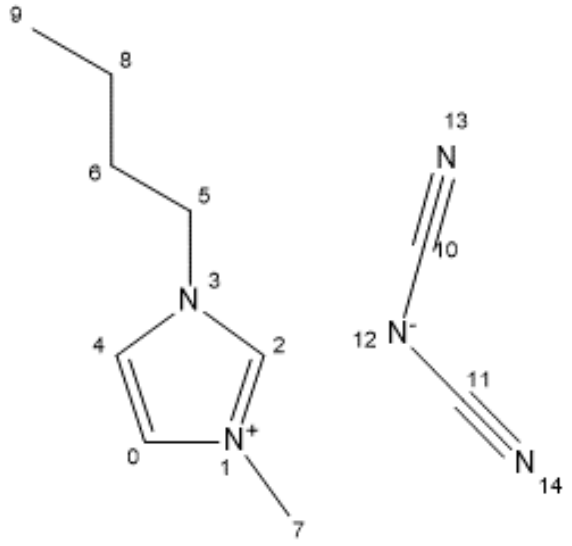

Figure 31 Chemical structure of [BMIM][DCA] with arbitrary numeration

The ions were put in a cubic box with 10 nm of side, using PackMol.

The first frame of the simulation consisted of cations and anions randomly displace inside the box, as depicted in Figure 32.

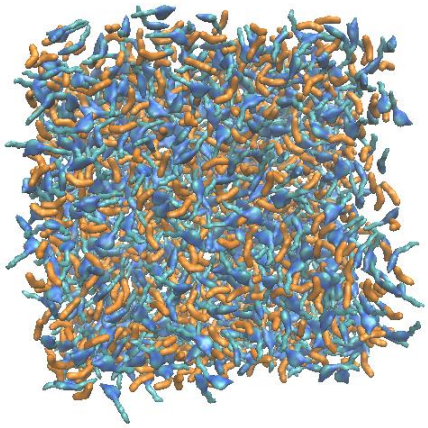

Figure 32 Snapshot of initial stage of simulation with 1000 IL molecules inside a 10 nm sized side cubic box

As seen in the Figure 32 it is possible to confirm that the molecules are randomly displaced and that the cation and anion isn't distributed periodically as it was expected from the literature review.

The simulation undertook 100 ns, outputting the frame depicted in Figure 32.

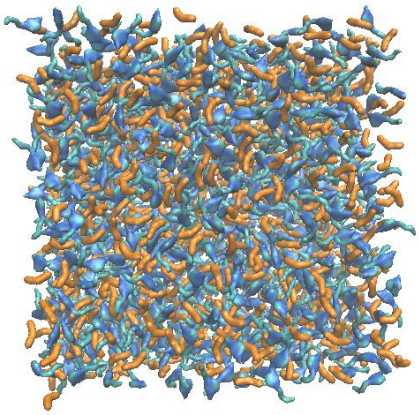

Figure 33 Snapshot of the last frame of the simulation, ran for 100 ns, at 300 K, inside a 10 nm side cubic box with 1000 molecules of [BMIM][DCA]

By examining Figure 33 it is possible to start to note a trend, where the anions tend to be near the nitrogen atoms of the imidazolium moiety.

This can be confirmed by realizing RDF between the hydrogen of the carbon number 2 in the middle in the two nitrogens of the imidazolium ring and between the nitrogens in the cyano of DCA atoms number 13 and 14. The RDF's performed are depicted in Plot 8.

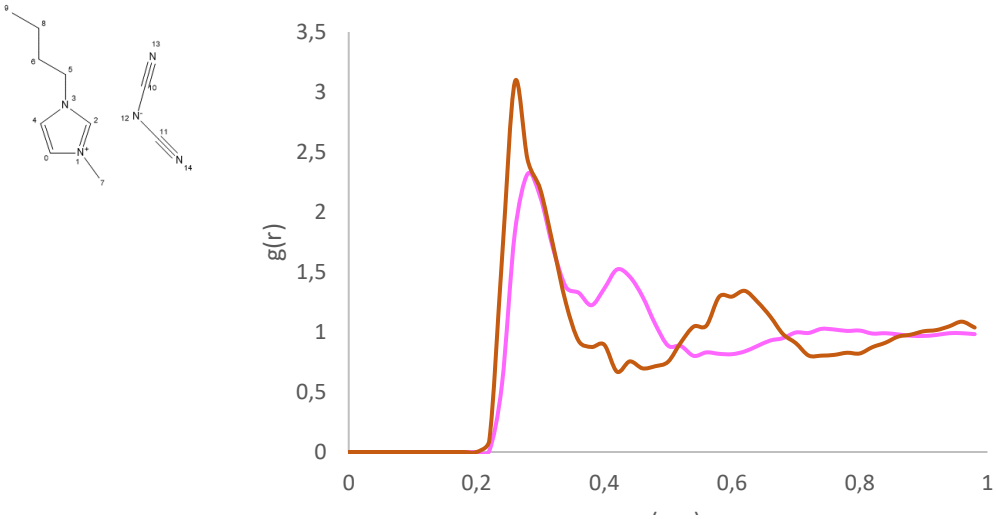

Plot 8 RDF performed in the IL simulation, with the brown line representing the RDF between hydrogen bonded to carbon number 2, and the pink line representing the hydrogens linked to carbon number 7

By the study of Plot 8 it is confirmed that indeed, there is a trend for the anion to stand near the cation's nitrogens and carbon. Given that the blue line and orange line present very sharp peaks, and the tendency is for the anion to be near the cations positive charge.

The second parameter studied in this work was density, having obtained a value of 1,059 g/cm^3, that is in accordance with the experimental values, since it is between 1.057 (value ate 303,15 K) and 1.060 (value at 298,15 K) [78] and as expected the obtained value is smaller than the value at 298,15 K but higher than the 303,15 K value.

3.3– Mixture (5CB; IL; water)

In this last sub-chapter of this chapter, the mixture containing 5CB and Ionic Liquid is going to be reported, starting by a simulation of a box with randomly placed 5CB and IL, to see if phase separation is achieved.

In the first simulation, the initial state of the simulation, is depicted in Figure 34.

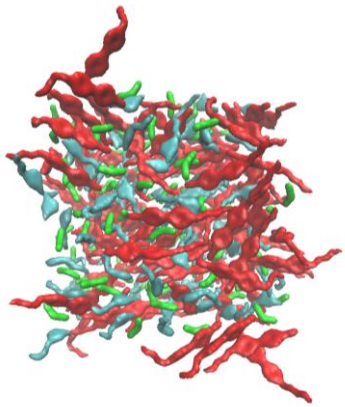

Figure 34 Snapshot of the first frame of the MDRUN, after the equilibration step. With 5CB in red, The cation in cyan and the anion in green

By the scrutiny of Figure 35 it is possible to unveil that indeed the molecules are randomly displaced inside a 5 nm side cubic box, the simulation will be undertaken at 300 K, for 100 ns, at 1 atm of pressure with 100 molecules of both components. The final frame is depicted in Figure 35.

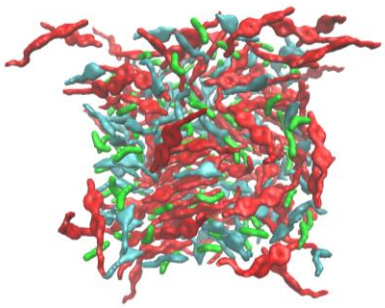

Figure 35 Snapshot of the final frame of the first simulation with 5CB and IL, for 100 ns at 300 K, at 1 atm of pressure, inside a 5 nm side cubic box with 100 molecules of each component, the colour code of the molecules following Figure 35

After inspecting Figure 35 it is possible to conclude that neither there was any kind of phase separation, to confirm density of 5CB and the cation along the X axis is calculated, resulting in Plot 9.

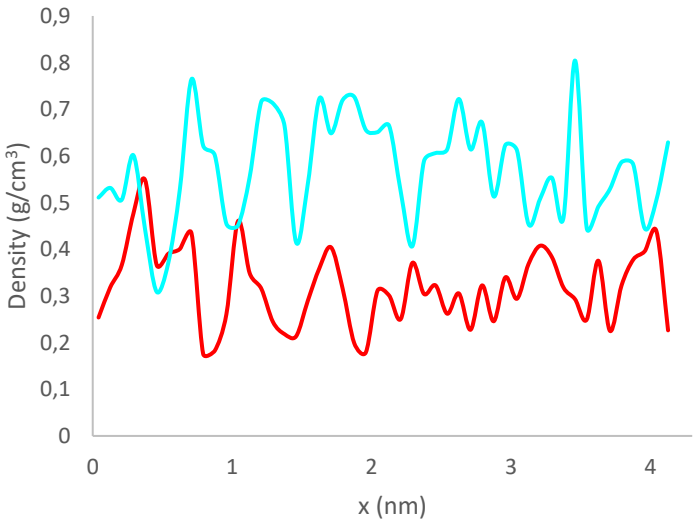

Plot 9 Density along the X axis of 5CB (orange line) and cation (blue line)

By analyzing Plot 9 is possible to conclude that 5CB and the IL had no interface formed by themselves.

Alongside the lack of phase separation, the P2 order parameter was very low, only achieving the maximum value of 0,24. The evolution is represented in Plot 10.

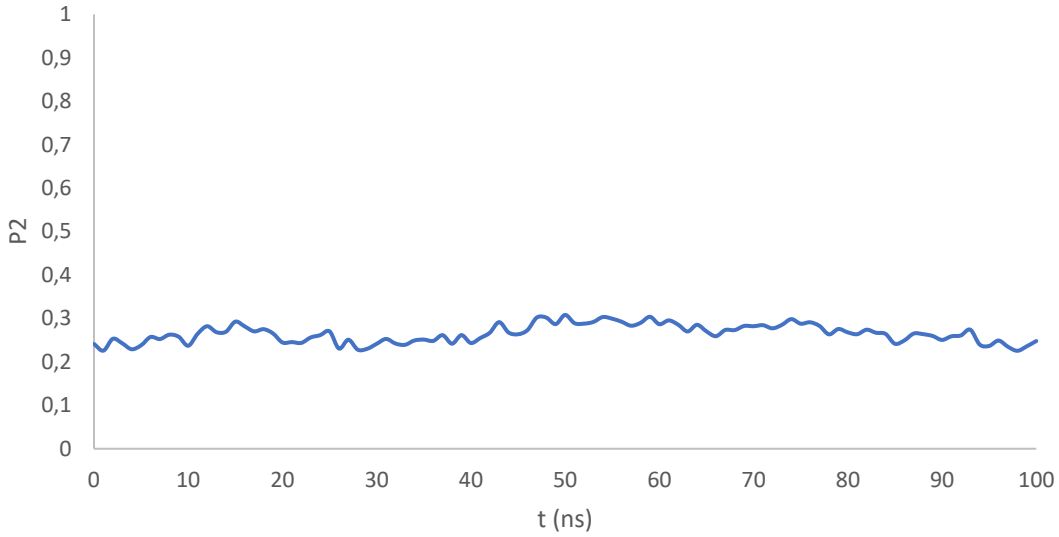

Plot 10 Evolution of P2 with time of the first simulation without any interface

By inspection of Plot 10 it is possible to conclude that the system does not tend to a nematic phase of LC and the changes in the order parameter are negligible.

Since the objective of this work is to study the interface of 5CB and [BMIM][DCA], instead of using cubic boxes, a parallelepipedal box is used where molecules are put in different coordinates, however molecules are put in a random fashion inside their compartments, as in Figure 37.

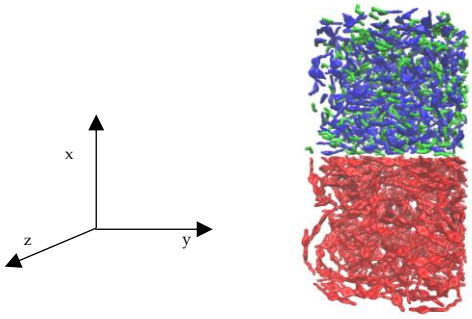

Figure 36 Initial configuration of the forced interface system with 5CB in red, the cation in blue and the anion in green

As seen in Figure 36, the molecules are separated however they are not organized in any kind of way.

However, due to periodic boundary conditions 5CB interacts with the IL both on the top and on the bottom, making 5CB experiencing a bilayer of IL as depicted in Figure 37, where the IL layer is duplicated along the X axis.

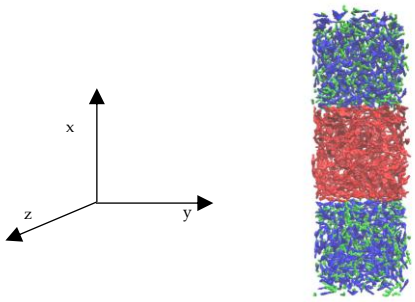

Figure 37 Periodic boundary conditions of the system depicted by replicating the IL layer along the X axis (red axis)

Having this is mind the simulation was undertaken for 100 ns, at 300 K, at 1 atm, on a parallelepipedal box with the following dimensions : x= 10 nm - y= 5nm - z =10, with 312 molecules of 5CB and 386 molecules of IL, those number were calculated in order to have the right density inside each compartment before starting the simulation. The first frame of simulation is depicted in Figure 38 a).

a) b)

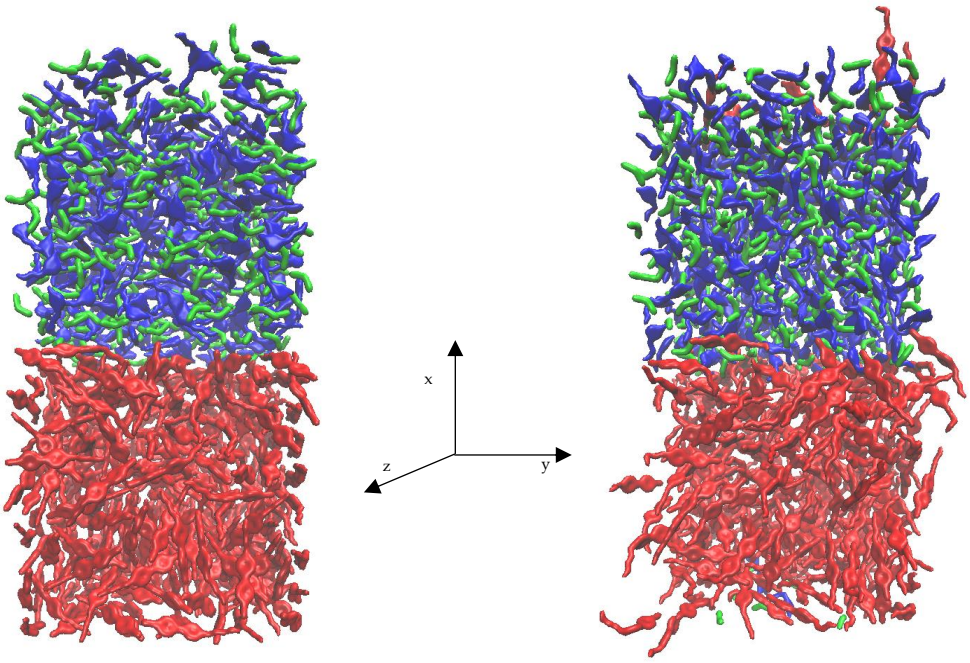

Figure 38 a) Snapshot of the first frame of the simulation where the interface was forced **b**) Snapshot of the last frame of the forced interface simulation, for 100 ns, at 300 K, at 1 atm, with a box with the following axis dimensions X =10 nm, y,z = 5 nm, with 312 5CB molecules and 384 IL molecules, with the colour code is the same as Figure 36

The simulation undertook 100 ns and outputted the following state portrayed in Figure 38 b).

Analyzing Figure 39 b) it is possible to see a clear interface, as confirmed by the calculation of density along the X axis. Confirmed in Plot 11.

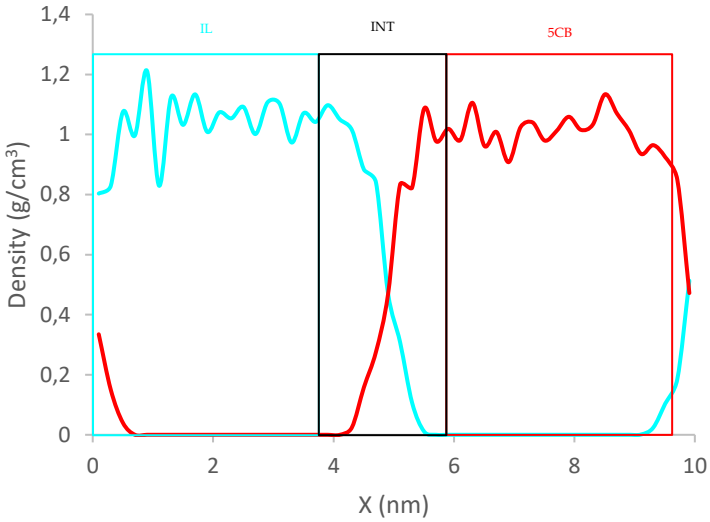

Plot 11 Calculation of the density of 5CB (red line) and the IL cation (cyan line) along the X axis

Through the review of Plot 13 it is possible to see a clear phase separation in the middle of the at 5 nm, and having LC density of 1,02 g/cm^3, being in accordance with the density obtained in previous simulations, being in accordance to the experimental value of 1,02 g/cm^3. And the IL presents a density value of 1,05 g/cm^3.

So, an interface between the two phases was achieved, however through visual inspection a nematic phase still hasn't been achieved. Confirmed by the calculation of the P2 order value that is very similar to the value obtained in the simulation without an interface, reaching only a maximum value of 0,16. The P2 order parameter evolution trough time is depicted in Plot 12.

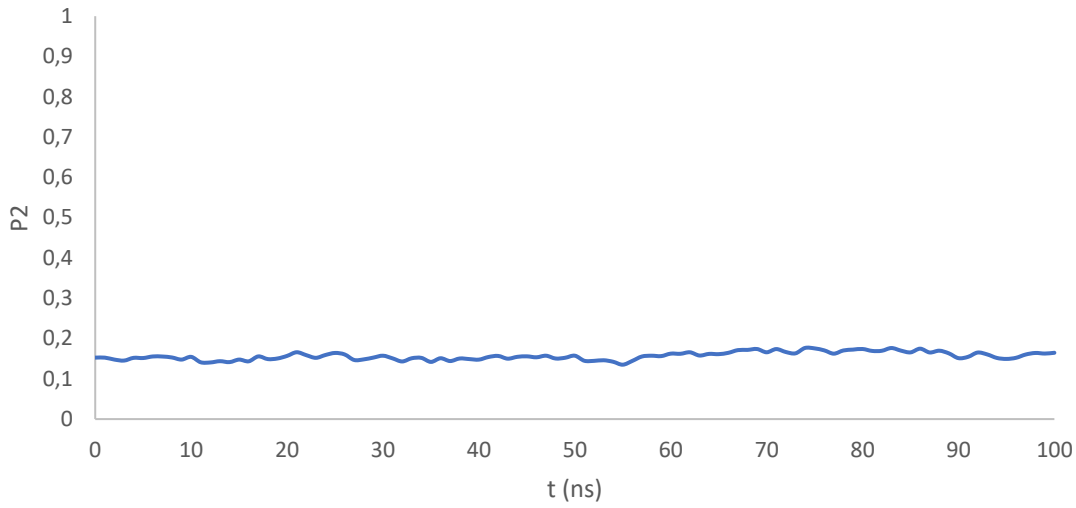

Plot 12 P2 evolution along time of the forced interface simulation

As seen in Plot 12, it is possible to conclude that the system does not achieve a nematic phase.

However, the lack of order could be due to the fact that the LC was having influence by both layers of IL (as depicted in Figure 38) with both the layers forcing the LC to align to them and ending up in a disordering made by the LC bilayer. So, to avoid turning off the periodic boundary conditions, since to turn them off, the thermostat and barostat would have to be changed, the method for searching neighboring molecules would have to be changed as well. And since time was a valuable asset, repetition of all the work developed so far would be impossible to perform.

In order to mitigate the effect of both the layers of IL messing up the order in the system, a longer LC compartment was arranged, maintaining the amount of IL in the system, the 382 molecules, the amount of size available for the LC was now 10 nm and 610 molecules were now in the system, so now it would be expected for the system to achieve some kind of ordering in the bulk of the system, where the effects of the anchoring to the IL would now diminish giving the increased distance. So, the final parallelepipedal box has the X axis with 20 nm, Y and Z axis with 5 nm sides.

All the parameters in the simulation would remain the same being the only change the ones mentioned above. Leading to a system configuration as the one depicted in Figure 39 a).

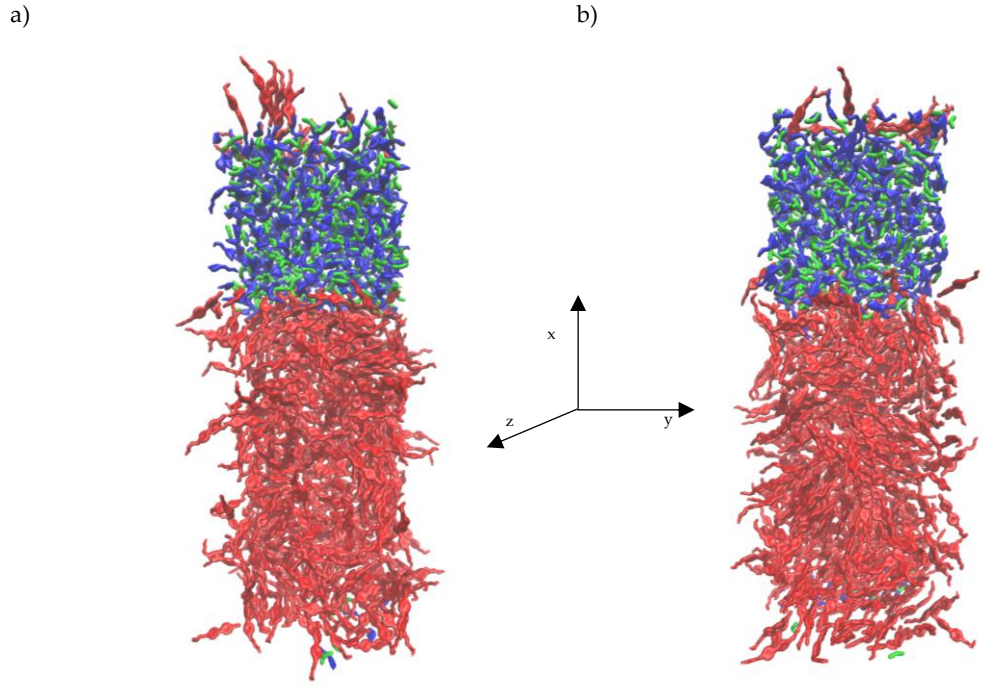

Figure 39 a) Initial frame of the simulation with 610 molecules of 5CB and 386 molecules of IL, with the colour code the same as Figure 37 **b)** final frame of 100 ns of simulation, at 300K, at 1atm, box with X =15 nm, y,z = 5 nm, with 610 molecules of 5CB and 386 moelcules of IL

The initial frame demonstrates a starting point of the simulation with an isotropic distribution of the LC and random distribution of the cation and anion inside the compartment.

The result of 100 ns of simulation is represented in Figure 39 b).

Through the analysis of Figure 41 b) it is possible to unveil that as the last simulation, phase separation is achieved as proven in calculation of density along the X axis, the density is Plotted against the X axis variation in Plot 13.

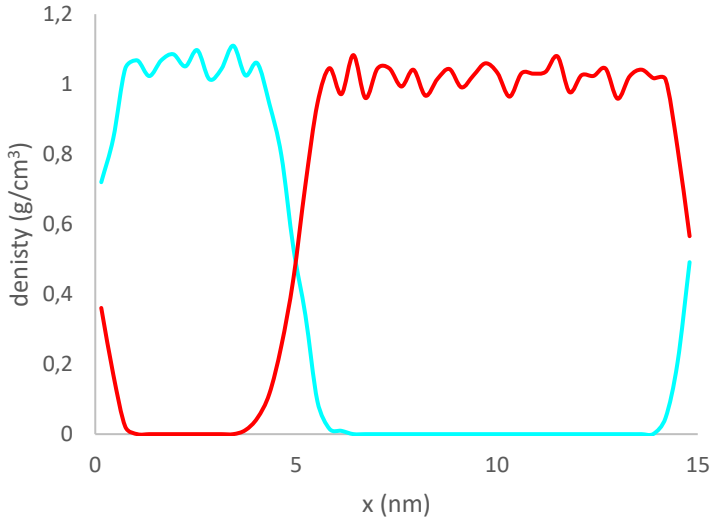

Plot 13 Density values for 5CB (orange line) and IL (blue line) along the X axis

The density along the X axis allows for the confirmation of the phase separation. The density value of 5CB in the bulk is 1,02 g/cm^3, is in accordance with the experimental value described in the literature, and the density value for the IL is 1,06 g/cm^3 and the value is in accordance with the value reported in the literature.

Regarding the P2 value along time, is Plot ted in Plot 14. The overall P2 value reached is 0,12, translating in an isotropic phase.

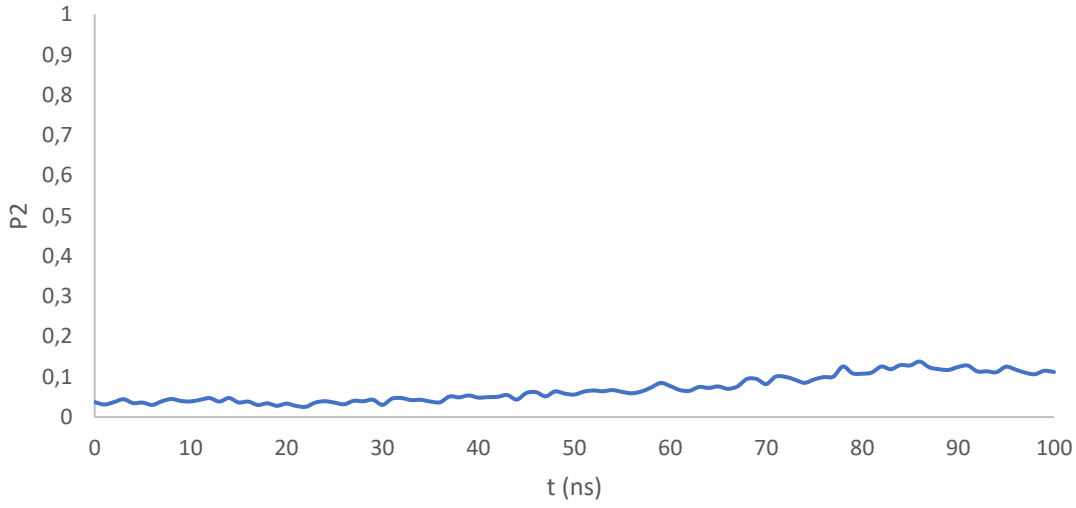

Plot 14 P2 evolution along time

The overall P2 translates in a disorganized phase of LC, so a change in protocol needs to be done, and there are two options for the disorganization either the 5CB molecules don't have enough space to move freely and therefore organize themselves given the conditions. One possibility to rectify this lack of freedom is to add a layer of vacuum underneath the 5CB layer, giving space for the 5CB to more freely move and needing less energy to organize. The other option is that water (that is present in the protocol for the sensing-gel) plays a crucial role in the organization of the LC layer.

In order on easiness of reading the first option approached, is the addition of a vacuum layer, as water adds another layer of complexity to the discussion of results.

The system containing vacuum, had the same parameters as all the previous simulations, changing only the number of molecules, the number of LC molecules remained the same, and the amount of IL was lowered in order to diminish the anchoring effects in the LC phase, the initial phase before MD simulation is shown in Figure 40.

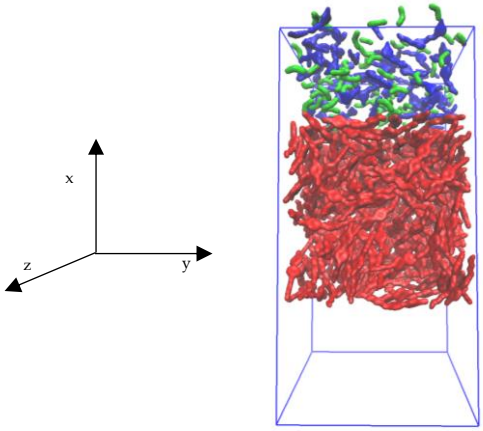

Figure 40 Depiction of the vacuum in the starting structure before the energy minimization

As seen in Figure 40 it is possible to see the amount of vacuum, shown as blank space, after energy minimization and equilibrations, outputs the structure shown in Figure 41.

a) b)

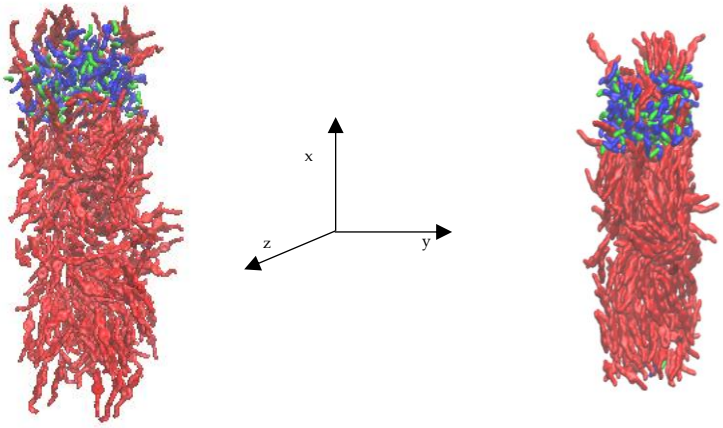

Figure 41 a) Stage of Simulation after equilibration and energy minimization **b)** Last frame pf the simulation ran for 120 ns, in a box dimensions of X = 13 nm, Y,Z = 5 nm with 311 molecules of 5CB (red), 83 molecules of [BMIM] (blue) [DCA] (green) at 300 K in 1 atm of pressure

By direct analysis of Figure 41 a) it is possible to understand that the empty space was occupied by the LC since it is energetically favorable for it to occupy as much space as possible given there is less repulsion between the molecules, leading to a more stable energetic level. However, the effect wanted from the

extra space was still achieved because, just by equilibration is possible to see major improvements comparing to previous simulations as LC molecules are starting to order themselves, at the end of equilibration a P2 order value of 0,2.

The final stage after 120 ns of simulation (extra simulation steps were added to this simulation since what is trying to be seen is the diffusion of order along time, and diffusion is very slow, because every molecule depends on the movement of each molecule) it was then reasonable to conclude that maybe molecules don't have enough time to reach their most stable conformation. The rest of the parameters are equal to the previous simulations.

By the inspection of Figure 41 b) it is possible to see the start of ordering to rise in the system, as can be confirmed by the evaluation of the P2 order value along time, resulting in Plot 15.

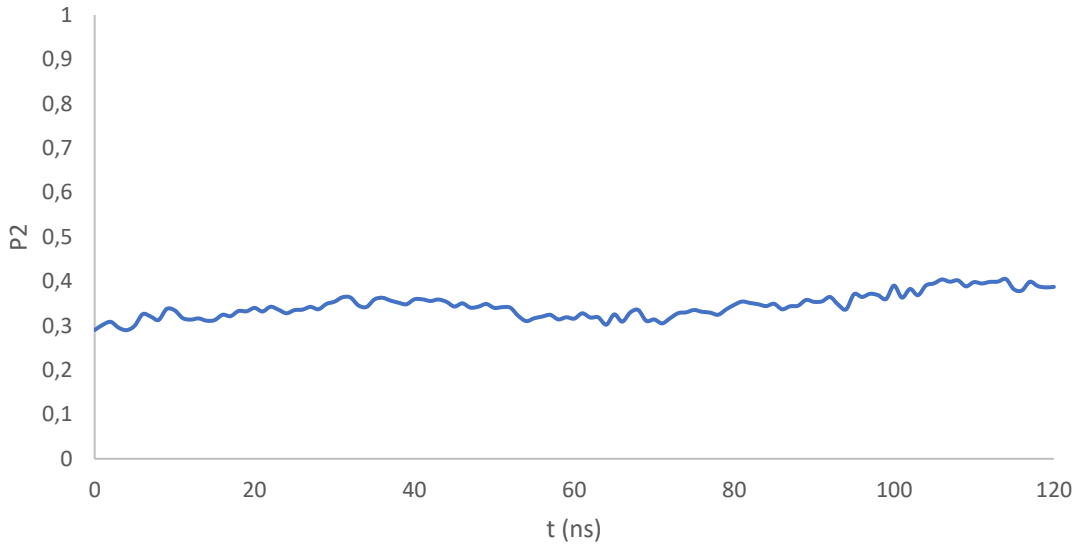

Plot 15 P2 evolution along time of the simulation that contained vacuum added to the simulation box

Although the variation on the P2 may not be large it reaches an overall value of 0,4 near 100 ns of simulation, indicating that a nematic phase was achieved, indicating that it is possible to simulate a nematic phase in a mixture with Ionic Liquid, so the alignment is expected to be homeotropic so it can be in accordance with the results obtained experimentally. To see what the alignment

of the LC is, the P2 value is going to be calculated along a plane and an axis. Resulting in Plot 16.

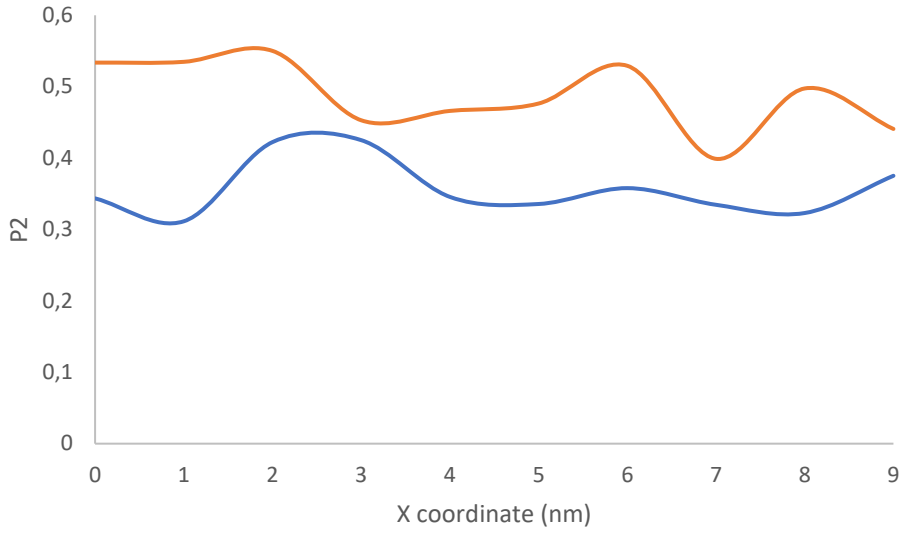

Plot 16 P2 order value to the YZ plane (blue) and to the X axis (blue line) through the X coordinates of the box

Through the analysis of Plot 16 it is possible to conclude that near the interface at about 7 nm it is possible to see the interface of the system, and analyzing the value it is possible to conclude that there isn't a preferred orientation of the molecules long axis according to the plane or the vector however there are slightly more molecules aligned to the X axis than the YZ plane, leading to a partial homeotropic alignment. This result indicates that the geometry retrieved from such a system in an experimental work, an intermediate configuration would be obtained in the droplet, however this is not the result expected as to have a radial droplet, the simulations must have a major homeotropic alignment and not a residual advantage over the planar alignment.

Having had regarded the P2 order part of the simulation, density is now to be studied, and for that density was calculated along the X axis, outputting the following Plot 17.

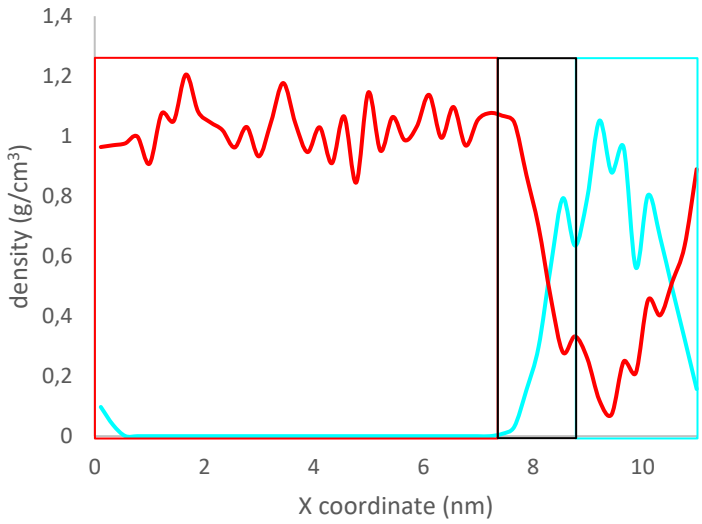

Plot 17 Density calculations of 5CB in orange and the IL in blue along the time

Calculating the density of the bulk 5CB a value of 1,03 g/cm^3 is achieved that is in accordance with the literature value, however when studying the value for the IL a value of 0,964 g/cm^3, being very far apart from the value found in the literature having an error of 9 %, indicating that the number of the IL present in the simulation is crucial to the correct simulation of the IL inside the system.

Having then discarded the possibility of adding vacuum without turning off the periodic boundary conditions, the path chosen to be followed was by adding water randomly in all empty spaces to the simulation containing both a considerable amount of LC and IL, this is the simulation that contained double the amount of 5CB compared to IL. And besides the vacuum it was added a layer of 3 nm of water.

The initial frame for this simulation is depicted in Figure 42 a).

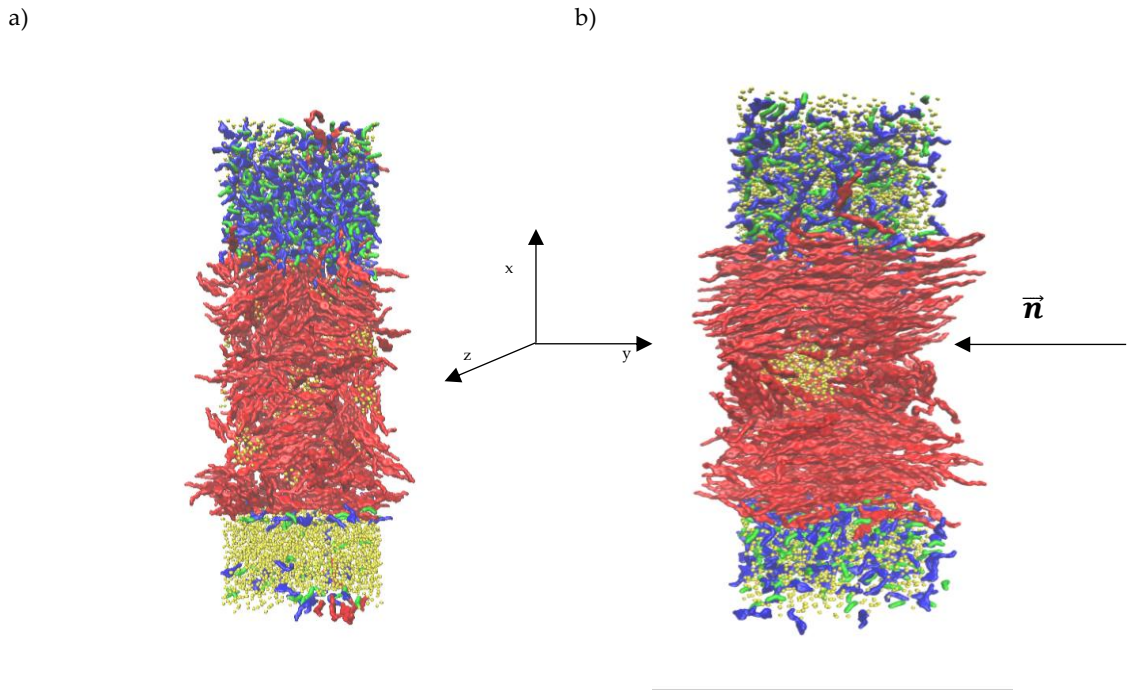

Figure 42 a) Snapshot of the initial state of the simulation with water and 610 LC molecules and 386 IL molecules **b)** last frame of the simulation (on the right), during 200 ns, at 300 K, at 1 atm, with box dimensions of: X =18 nm; Y,Z = 5nm, with 610 molecules of 5CB (red) 386 molecules of IL ([BMIM] blue; [DCA] green) and 3217 water molecules (yellow), where $\vec{n}$ is the nematic phase director

By the analysis of Figure 42 a) it is possible to say that water, filled empty spaces inside the 5CB layer, however that may be a problem since it is known that water forces planar anchoring to 5CB, however it may still work since all the water is on the top part of the simulation and box, leaving the bottom part empty for homeotropic alignment.

As can be seen in Figure 42 b), indeed a nematic phase was obtained, as can be confirmed by the calculation of the P2 order value, obtaining a maximum value of 0,37 after the first 100 ns, however after another 100 ns of simulation a value of 0,58 was achieved.

Whoever by visual analysis it is seen that the molecules tend to assume a planar anchoring, which is in accordance with the literature, that states that the interaction between an amphiphilic molecule and LC is not strong enough to overcome the anchoring force of water and 5CB and, so near the amphiphile a quasi-isotropic phase is notice near the interface and a nematic phase is observed in the rest of the system, as seen by the calculation of P2 order values to the YZ plane and to the X axis. As seen in Plot 18.

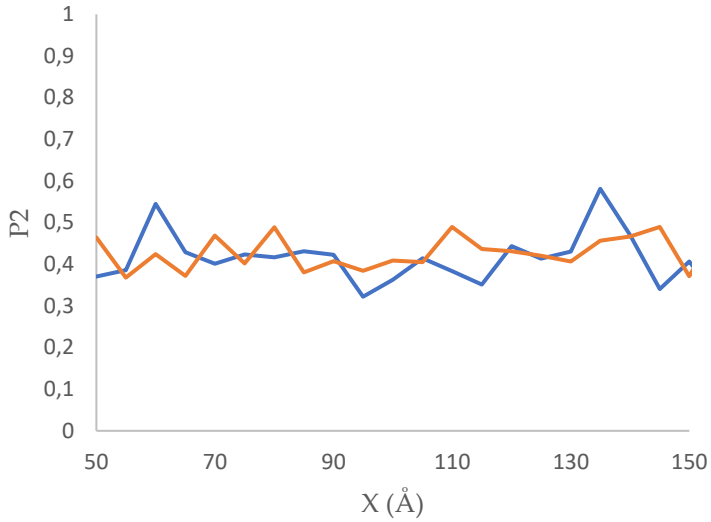

Plot 18 P2 order value along the X axis in (blue) and along the YZ plane (orange)

As expected the system near the interface at 50 Å presented a quasi-isotropic behavior not having well defined arrangement, however the planar alignment was more likely to happen than the homeotropic one, given the difference between the P2, the tendency to remain nematic maintained along the box with the director being somewhere in between the YZ plane and X axis.

The second part of scrutiny of this simulation is by studying the density values along the X axis, outputting the Plot 19.

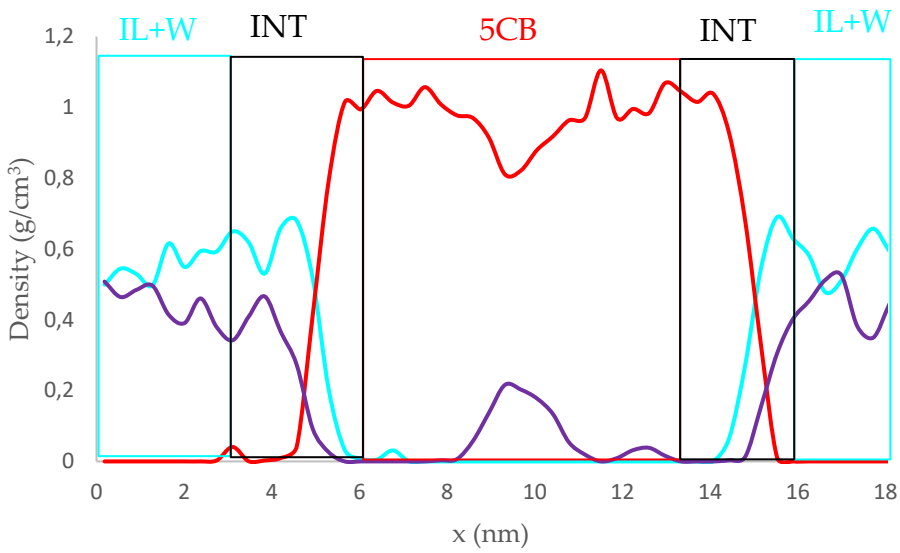

Plot 19 Density values of 5CB (orange), IL (blue) and water (gray) along the X axis

The values of density of 5CB in the bulk is 0,975 g/cm³ this distance to the real value is due to the fact that the molecules besides having water in the middle of the layer, as seen in Plot 19, by adding a 3nm layer of water the IL and water fully mixed as seen in the Plot above, created more space for the 5CB to freely move and diminishing the density value, lowering more than expected in the simulation. This freedom associated with the force of the water forcing the planar arrangement lead to the build of the nematic phase observed.

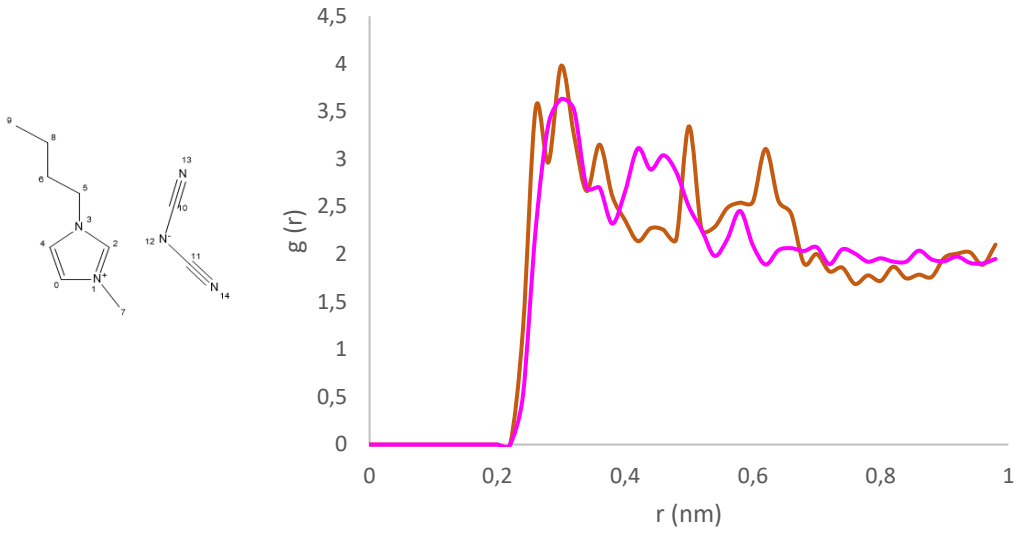

Plot 20 RDF performed in the 5CB-IL-water simulation, with the orange line representing the RDF between IL hydrogen bonded to carbon number 2, and the blue line representing the IL hydrogens linked to carbon number 7, both were calculated having as a reference

To assess the simulation of the IL, since water and Ionic Liquid fully mixed it is necessary to scrutinize the RDF and compare them with the RDF obtained from the simulations of IL alone.

Comparing Plot 20 to Plot 8 is possible to see various changes in the sharpness of the peaks, this is suggestive that the presence of water is pushing the anion and cation to more defined positions. As it is possible to see in the scale of the Y axis of the plot reaching maximum values of 4, whilst in Plot 10 only a maximum value of 3. However, the maximum peaks of both the lines stayed in the same position in length indicating that the distribution of the cation and anion is the same as in bulk.

In order to assess the major type of interactions between the IL and 5CB, RDF's concerning both the molecules were executed in order to see which part of the molecules were interacting more. There were three possibilities of interaction, hydrophobic interactions between the hydrophobic parts of the cation and 5CB, π-π stacking between the 5CB biphenyl moiety and the cation imidazolium ring and electrostatic interactions between the 5CB polar cyano moiety and the imidazolium positively charged nitrogens. The results are depicted in Plot 21.

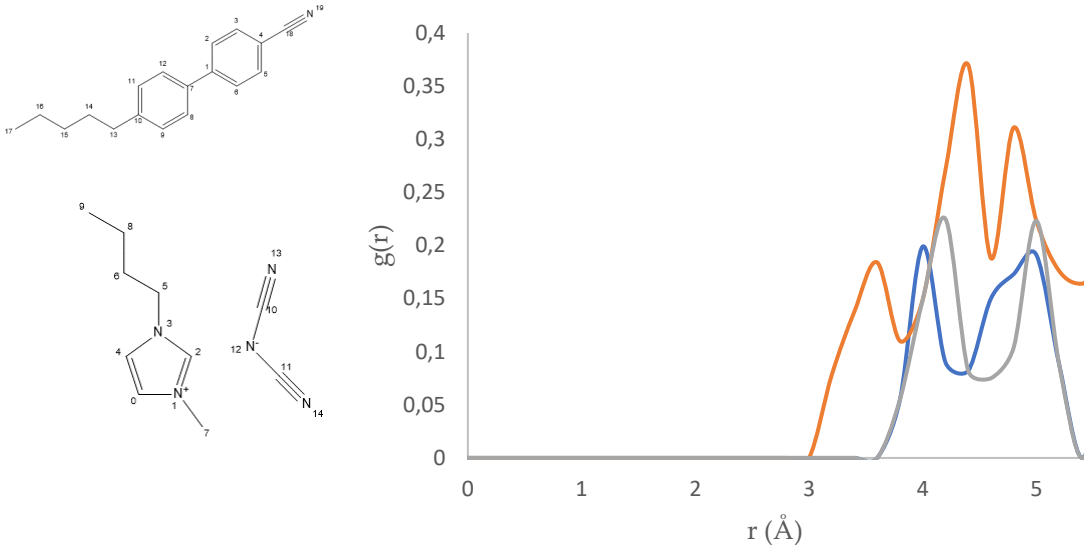

Plot 21 RDF between 5CB and the IL cation, with the blue line representing between the Centre of mass of each of the aromatic moieties (5CB - biphenyl ; [BMIM - imidazolium ring); orange between the nitrogen in the cyano moiety and the nitrogens in the imidazolium ring; and the gray line represents the RDF between the cyano moiety and the center of mass of the imidazolium ring

By analyzing Plot 21 it is possible to see that a *quasi-isotropic* phase is obtained in the interface between the IL and the 5CB since there is no preferred anchoring of the 5CB molecules (as it can be seen in the RDF as the intensity of the values of g(r) are very small). Instead what is seen is a mixture of the anchoring present in the interface of the following cases:

- **π-π stacking between the aromatic rings**

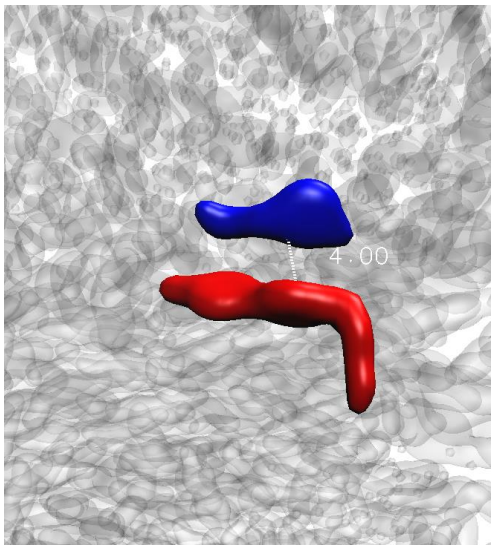

Figure 43 π-π stacking between the imidazolium moiety of [BMIM] and the biphenyl moiety of 5CB, with a distance between each other of 4 Å

As seen in the former Figure there is a clear π-π stacking of both the molecules, these interactions are the main reason for the planar anchoring in this system

- **Electrostatic interactions between cyano dipole and the imidazolium ring**

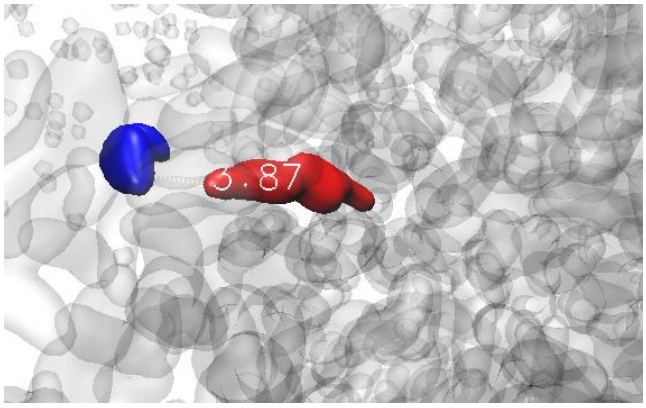

Figure 44 Interaction between the imidazolium moiety of [BMIM] and the cyano moiety of 5CB, with a distance between each other of 3,87 Å

As seen in the former Figure there is an interaction between the cyano moiety of the LC and the imidazolium ring of the IL, these interactions are the reason for the distortion of the nematic phase in the interface of this system.

Given that the homeotropic alignment wasn't reached, the hypothesis that the initial shape of the system would determine the anchoring of the system, maybe a spherical core of 5CB would be determinant to reach the homeotropic alignment.

So, a system considering the amounts used in the protocol of the development of the gas-sensing gel was used.

The system consisted of a spherical core of 5CB and a box filled with [BMIM][DCA], as depicted in Figure 46 a) and the frame after a simulation time of 130 ns, at 300 K in 1 atm of pressure is shown in Figure 45 b).

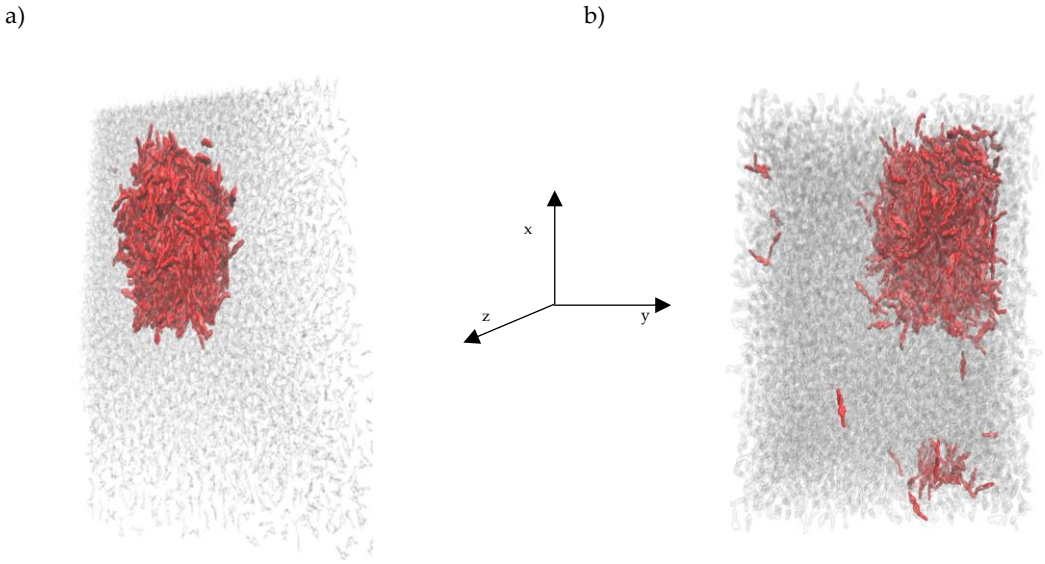

Figure 45 a) Initial frame of simulation in a box containing 931 molecules of IL, 7517 molecules of IL and 28 molecules of water inside a cubic box of 16 nm side **b)** final frame of simulation after 130 ns, at 300 K, at 1 atm.

The analysis procedure was the same for this simulation as it was for the previous, so the first step was to calculate the P2 order value for the whole system, the plot obtained is depicted in Plot 24.

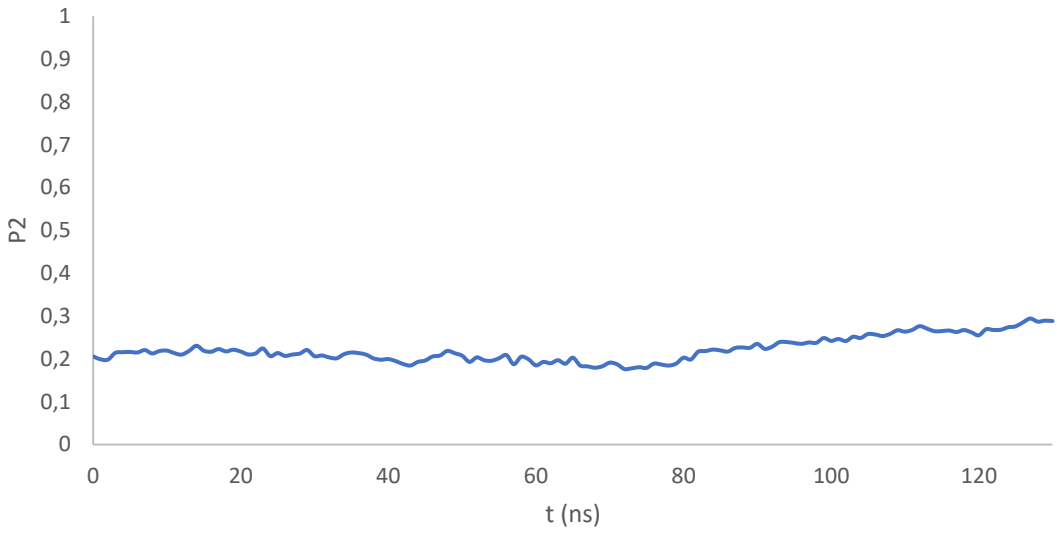

Plot 22 P2 evolution of nano-scale simulation of droplet

As it is possible to confirm by analyzing the previous plot it is possible to confirm that a nematic phase was not achieved. This could be caused by the great number of molecules that are present in the simulation, leading to 130 ns not being enough to have an impact on the organization of the system. However, it is possible to see a small rise of order towards the end, indicating if the simulation time was bigger a possible nematic phase would be achieved.

Not having a nematic phase led to the decision of not calculating RDF's to see the anchoring of the LC molecules to the IL layer, however there are visual indications that the molecules are tending to have a planar arrangement in the IL layer. In order to proceed with these studies, a CG approach is necessary, since in order to simulate 130 ns, one full month of calculation was necessary and, given that the phase obtained is not a nematic phase, this indicates that further extend of the simulation is required.

The next step in order to assess the trustworthiness of the simulation the calculation of 5CB and IL were undertaken, being displayed in Plot 23.

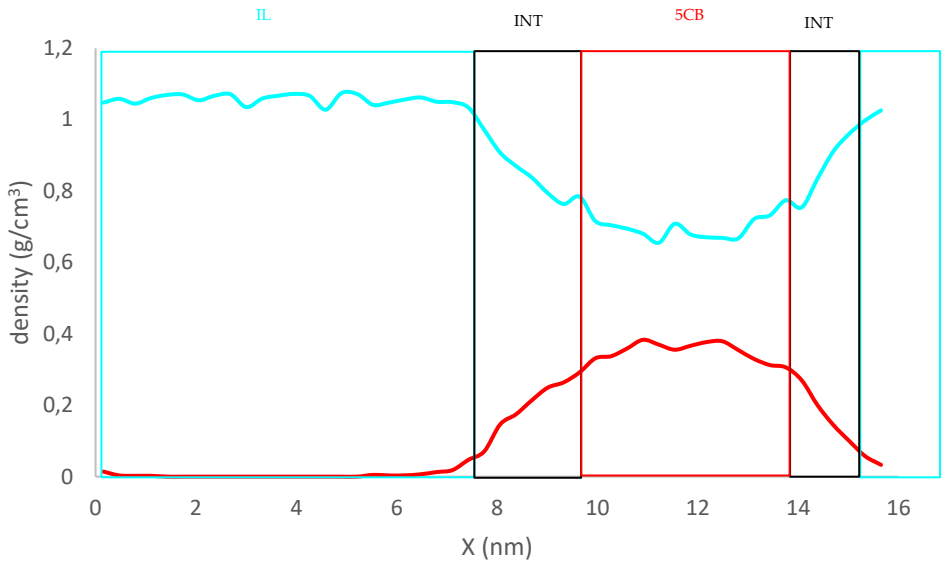

Plot 23 Partial densities of 5CB (red) and IL (cyan) of the simulation concerned with ratios of IL and 5CB.

The density calculation for the IL molecules is direct since there is a clear phase in the X axis where only molecules of IL are located, allowing for a simple average of the partial densities, outputting a density value of 1,06 g/cm³, being in accordance with values represented in the literature. However, since there is not a coordinate in the X axis which is full of 5CB a correction is necessary in order to obtain the real density of 5CB and not just over a complete layer. So a correction over the sphere of 5CB was done, considered the bulk as a cuboid, using the following equation.

$$density_{real} = \langle densities_{partial_{m,n}} \rangle * \frac{L}{m-n} \qquad \text{Equation 8}$$

Where $density_{real}$ is the value of the 5CB bulk effective density, $\langle densities_{partial_{m,n}} \rangle$ denotes the average of the values of density outputted in Plot 25, L is the side of the box, and m and n are the X coordinates in which droplet is located. Applying Equation 8 to this system, the value of 5CB obtained is of 1,04 g/cm³ having an associated error of 2,82%, being well inside the error range.

However, there is an inherent error in this simulation, this is, while the ratios of the protocol are in accordance with the literature [20], a crucial factor is not being taken into account, the amount of humidity in the air, and as discussed

before water plays an important role in the ordering of the LC phase, so in the future the amount of water present in the sensing chamber should be taken into account.

3.4 – 8CB

In other to study the effect of the change in the alkyl chain, and the effect of a different liquid crystal phase, 8CB simulations, as depicted in Figure 46.

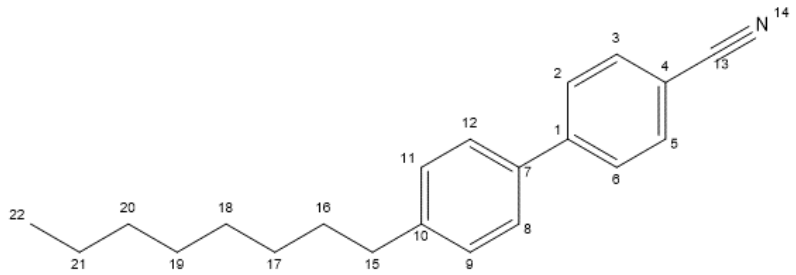

Figure 46 Structure of 8CB with arbitrary numeration to ease RDF analysis

So, the changes when considering 5CB and 8CB, is the size of the alkyl chain, where 5CB has a pentyl moiety and 8CB has an octyl moiety. Another difference between 5CB and 8CB presents a smectic-A phase [79].

Regarding 8CB order parameter, the P2 order value have been calculated for the nematic phase using OPLS forcefield, being reported values as high as 0,8 and that they are temperature dependent [80, 81].

The method to unveil if the phase obtained is smectic-A or nematic is through the performance of RDF either perpendicular or parallel to the director of the phase in order to calculate the spacing between each layer of molecules. So if 8CB molecules have a smectic-A phase, the RDF (between the molecules center of mass) parallel to the phase director should have well defined peaks, indicating that the centers of mass have a well-defined layer spacing, however if the RDF doesn't show any defined peak, it means that there is no positional ordering implicating that the phase obtained is indeed nematic [79]. However, during the process of this work a script that performed such RDF's was not found.

The density of 8CB at 300 K was found to be 1,028 g/cm^3, at 320 K was found to be 1.005 g/cm^3 [82].

All the simulations used the same input parameters as the 5CB simulations, using OPLS forcefield and LigParGen molecular parametrization. All simulations went according to the procedure described in the methods sub-chapter.

The first simulations were undertaken at 300 K, for 100 ns at 1 atm, the initial stage of the simulation is depicted in Figure 47 a), and the final simulation after 100 ns is depicted in Figure 47 b) with 141 molecules of 8CB in a 5 nm sided cubic box.

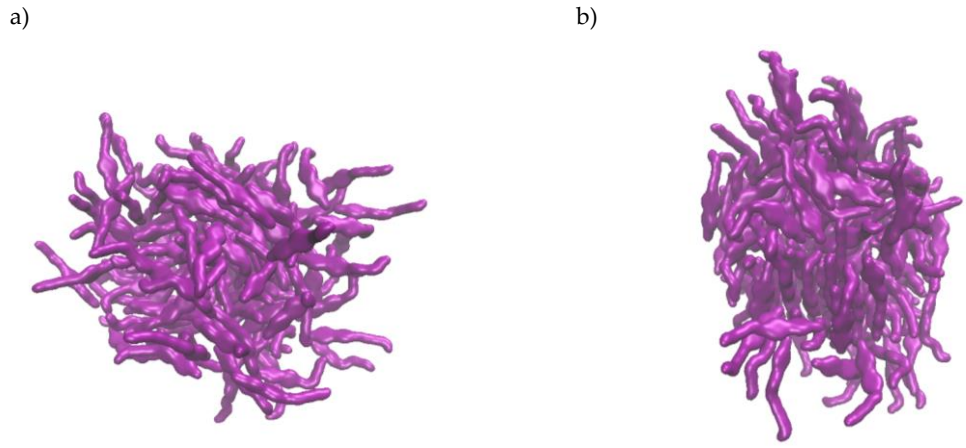

Figure 47 a) Initial frame of the MD simulation of a box containing 141 molecules of 8CB (purple) inside a 5 nm sided cubic box **b)** final frame of simulation after 100 ns of simulation at 300 K in 1 atm of pressure.

By the analysis of Figure 52 b) it is possible to see the lack of ordering arising from the simulation, however this is in accordance with the literature [74] that states that at 300 K some crystallization starts to occur. This leads to a lack of ordering inside the system, to prove such thing the P2 order parameter was calculated.

The P2 order parameter over time is depicted in Plot 26.

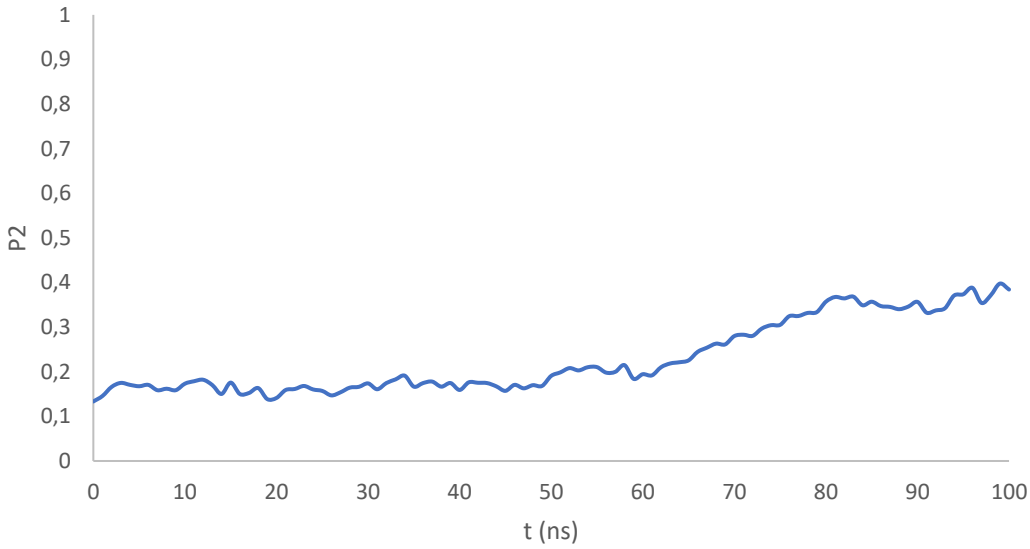

Plot 24 P2 evolution over time of the 8CB simulation at 300 K.

Studying Plot 24 it is possible to conclude that the P2 order value at 100 ns is 0,38 indicating that a nematic phase wasn't achieved, as was expected.

The density values of 8CB of this simulation is of 0,989 g/cm^3 having an error of 3,79% of the value represented in the literature [82].

Assuming there were traces of crystallization, the temperature of the simulations was risen to 320 K as it was reported as a transition temperature of 8CB using OPLs forcefield [78]. All the conditions remained the same except for the Temperature. This simulation is depicted in Figure 48 (initial frame with 141 8CB molecules inside a 5 nm sided cubic box (a) and the final frame after 100 ns of simulation at 320 K with 1 atm of pressure (b)).

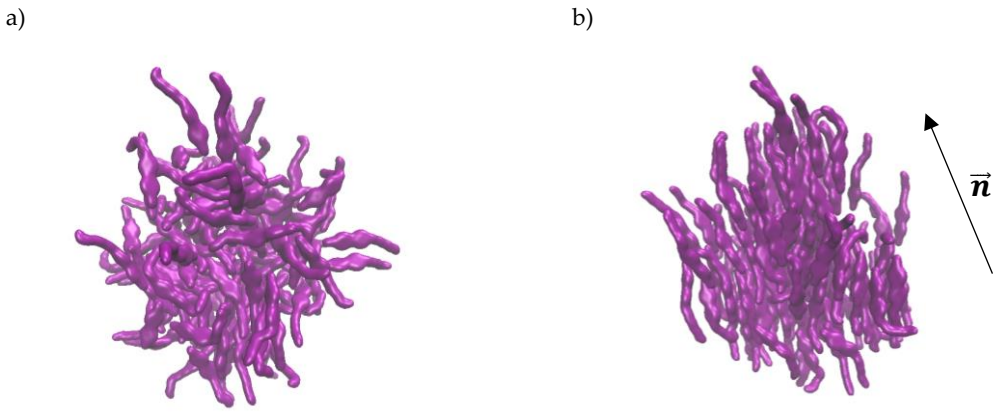

Figure 48 a) Initial frame of simulation of a 5nm side cubic box containing 141 molecules of 8CB (purple). **b)** Final frame of simulation during 100 ns, at 320 K in 1 atm of pressure.

By the analysis of Figure 48 a) it is possible to see that a full isotropic phase was the starting point for the simulation of 8CB, and that after 100 ns of simulation a clear nematic phase was achieved having then obtained a P2 order value of 0,85 in the last frame (plotted in Plot 27).

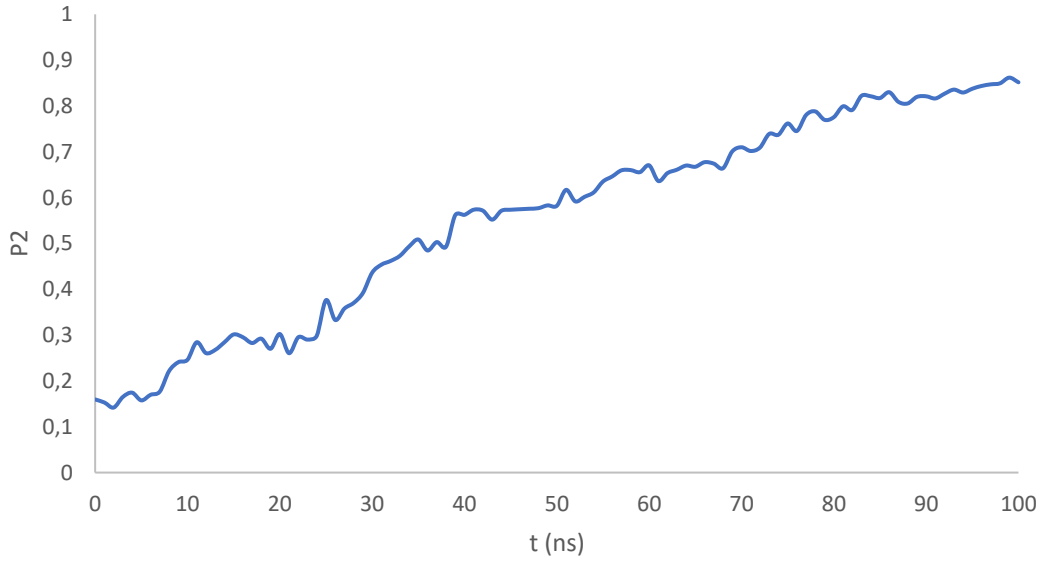

Plot 25 P2 evolution over time of the simulation containing 141 molecules of 8CB for 100 ns at 320 K

Analyzing Plot 25 it is possible to confirm the orientational ordering present in the system. However, at 320 K, it was described that a smectic-A phase should be obtained [78], but this was not observed, since no layering was present in this simulation. This could be because there were not enough molecules in order to make a second layer of molecules.

So to rectify this, a new simulation was done, doubling the size of the box that was outputted by the previous simulation along the Z axis, and randomly adding molecules in the empty space created by the elongation of the box, creating the system represented in Figure 49 a) the final system ended up with 280 molecules of 8CB dispersed along 10 nm of the Z axis and 5 nm of the X and Y axis. In Figure 49 b) is represented the final frame of simulation after 200 ns at 320 K at 1 atm of pressure.

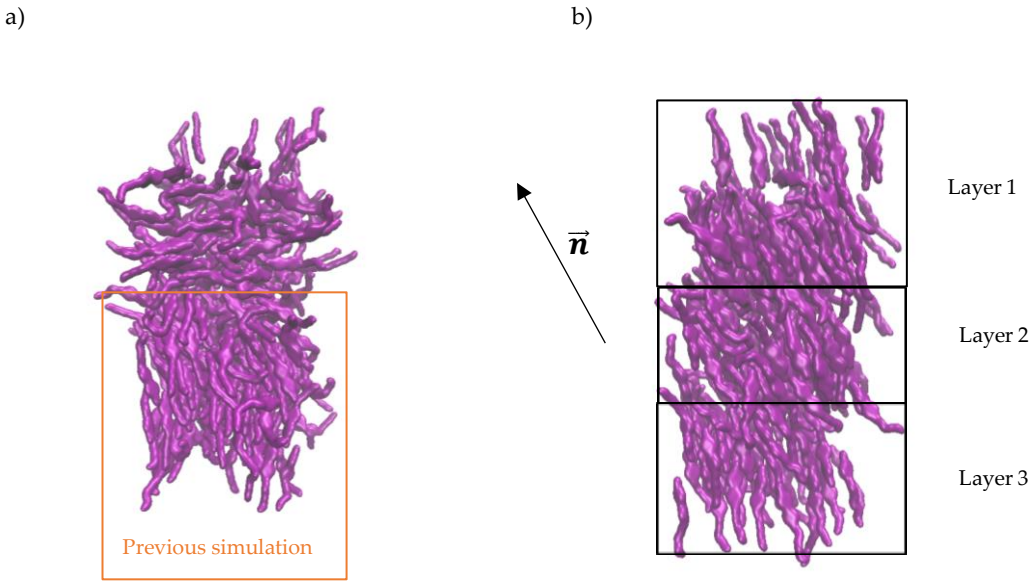

Figure 48 a) Initial frame of the simulation after inserting randomly the molecules on the blank space created by the elongation of the Z axis now 10 nm, the X and Y axis a 5 nm length, and having 280 molecules. **b)** final frame of simulation after 200 ns, at 320 K and in 1 atm of pressure.

By the analysis of Figure 48 a) it is possible to see that the highlighted in orange it is possible to see already some orientational order inside the system from the previous simulation.

Studying Figure 48 b) it is possible to see clearly orientational order of the system, being proven by the calculation of the P2 order value, depicted in Plot 26.

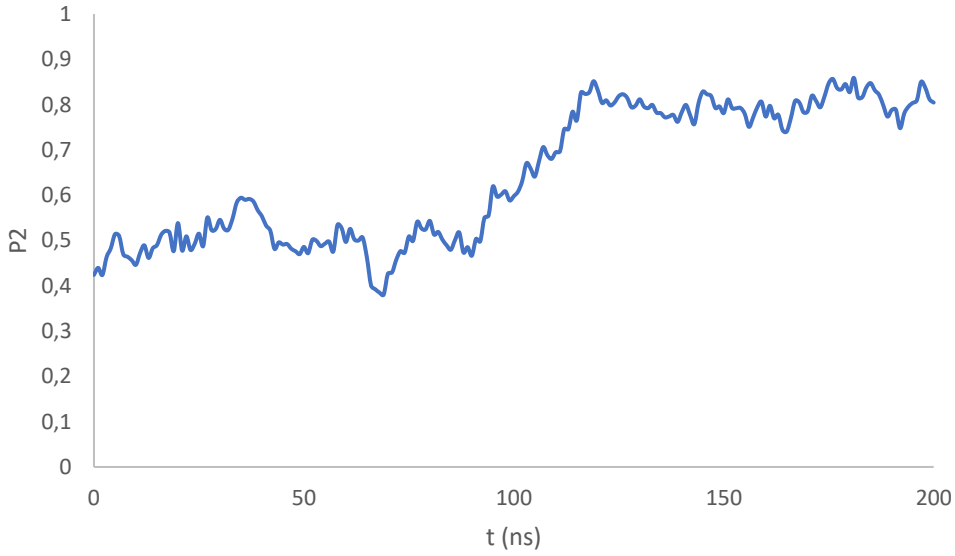

Plot 26 P2 over time of the 300 ns of simulation of the system containing 280 8CB molecules inside a box with 10 nm length of the Z axis and X and Y axis with 5 nm length, at 320 K and at 1 atm.

As it was previously stated the system started with an ordered layer, as can be seen from the initial value of the P2 order value of 0,4, and after 200 ns of simulations it is possible to see that there is a clear orientational ordering of the system. However, to calculate the positional ordering of the system in order to assess if the system was indeed smectic, the RDF in an axis would need to be performed. Since the RDF was not performed only a visual inspection was done, and by the visual inspection partial layering was found, depicted by the black rectangles in Figure 54 b) as each rectangle is a possible layer of 8CB.

The density of the simulation was found to be, 0,975 g/cm^3 which has an error of 2,98% with the value in the literature [82].

The last step in this simulation is to study packing of the molecules in the LC phase (since it is the first to present layering) in order to study this various RDF's were performed.

The RDF's are going to be performed between the atoms number 10 of every molecule, between the atoms 14 of every molecule. The RDF are present in Plot 27.

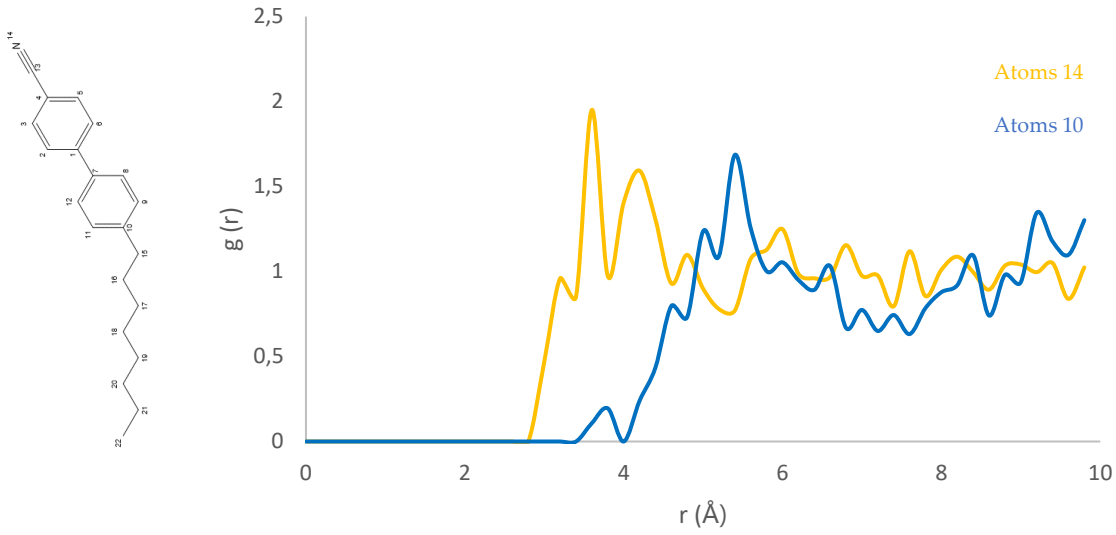

Plot 27 RDF studies of 8CB simulation with the yellow line representing the RDF between atoms 14, gray line represents between atoms 10 and 14 and the blue line represents between the atoms number 10.

Analysing the RDF is possible to see that the first peak in the yellow line represents the interaction between neighbours cyano moieties as depicted in Figure 55 a), being responsible the parallel arrangement of the 8CB molecules, and that the blue line presents a peak at around 5,4 Å representing the π-π stacking occurring in the system as represented in Figure 55 b), responsible by the anti-parallel packing of molecules.

a) cyano moieties interaction

b) π-π stacking

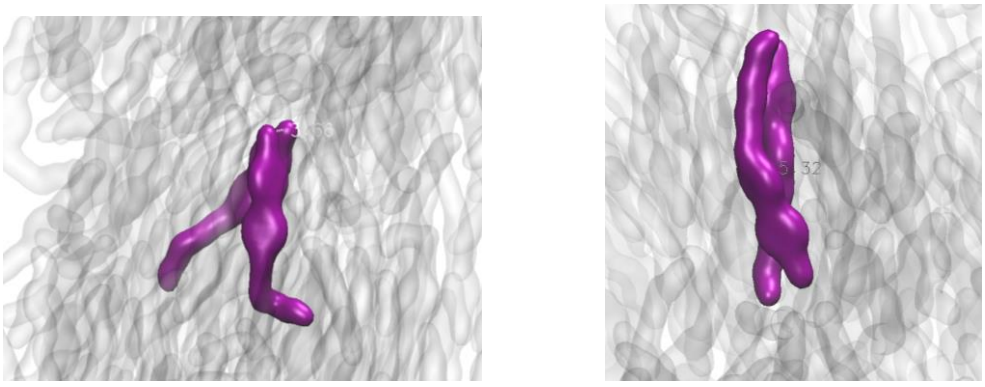

Figure 49 a) Interaction between the dipole present in the cyano moieties of 8CB responsible for the parallel arrangement of the 8CB molecules. **b)** Interaction between the biphenyl moieties responsible of the anti-parallel arrangement.

The next step in this work was to make a system containing 8CB and [BMIM][DCA] and study the effects of the longer aliphatic tail in the system. And the effect of a smectic mesomorph instead of a nematic mesomorph as it is 5CB.

4

Conclusion & Future Remarks

With this work it was able to conclude that effectively 5CB can be well simulated using MD to unveil packing, ordering effect of other liquids in the anchoring, by a simple submission of a molecule to an online server a complete and very reliable topology was retrieved allowing for very accurate simulations. And very clear depictions of chemical and physical aspects that allow for Liquid Crystal to have the physical and chemical properties they have, such as ordering and density, and how the molecules packing effect the either the interaction with other as well as how it impacts the order of the nematic phase itself.

The same can be concluded to ionic liquids it is possible to have a very reliable outcome that takes into account all the electrostatic potentials behind the correct parametrization of each molecules, especially those that contain highly polar moieties, that have a crucial role in how the molecule behaves in the bulk phase or in the interface with other liquids.

Despite not being able to reproduce truthfully the homeotropic anchoring for radial droplets given various factors, as not turning off the periodic boundary conditions, not using the correct stoichiometric ratios to more truthfully depict the real sensing gel, or even by simply not allowing the system to simulate enough time to reach the homeotropic alignment.

With this work a first step inside the simulation this kind of complex system, containing IL and LC mixed together opened doors to someone who wants to continue to simulate and work on such.

However, some conclusions could be withdrawn from this work:

- Without the right amount of IL and water no kind of organization can be achieved;
- Water is very important to maintain a clear phase separation between IL and 5CB, since IL is very hygroscopic, they tend mix with water, leaving a polar surface that the 5CB doesn't tend to mix with, this leads to the last conclusion of this work;

- Time of simulation is very important to the development of the ordering in the system, since diffusion is very slow, the bigger the system the slower the diffusion becomes.

In order to reach the goal of homeotropic alignment of the system, crucial steps need to be taken, they are going to be stated, however any kind of importance is implicit in the order they appear written.

- Convert the forcefield from fully atomistic, to Coarse-Grained, OPLS is a forcefield that allows for this transferability of simulation type, however some changes would needed to be made in order to truthfully in Coarse Grained, one of them being the need to favor parallel and antiparallel interactions and penalize perpendicular interactions, and maintain the anion at a constant distance from the cation, all of this needs to be done, based on the fully atomistic simulations;

- The change of simulation leads to the second point, with it being letting the simulations run for longer times, as with the bigger systems, bigger diffusion times are needed for the effects on ordering to start to have effects on the system;

- Turn off Periodic Boundary Conditions along an axis in simulations were water or other kind of molecules is interacting with LC since most commonly water anchoring is strong enough to diminish the effect of other kind of homeotropic alignment inducing agents;

- Finally, to get the values for each component right inside the simulations, for example, don't forget that the water in the protocol is not the only water present in the system as the gel is hygroscopic and the presence of water.

Regarding the simulations containing 8CB it was possible to reproduce a nematic phase of 8CB and upon visual inspection, partial layering was starting to happen. However, to confirm the presence of a smectic layer, RDF's parallel to the director of the system need to be performed.

The next step in the 8CB simulations is to simulate the mixture between it and an IL, like [BMIM][DCA] and study the conformational changes inside the 8CB layer.

And after the change in LC the next step is to study different IL in the system, with different cations, like changing the aliphatic tail of $[BMIM]^+$ from a nutyl to an octyl, for example. Or change the anion from an $[DCA]^-$ to a $[Cl]^-$.

References

[1] - Singh, S. and Dunmur, D. (2002). Liquid crystals. 1st ed. New Jersey: World Scientific, pp.1, 3.

[2] - Gennes, P. and Prost, J. (1993). The physics of liquid crystals. 2nd ed. Oxford: Clarendon Press, pp.1,2.

[3 a] - Figure withdrawn from: https://chem.libretexts.org/Bookshelves/Physical_and_Theoretical_Chemistry_Textbook_Maps/Supplemental_Modules_(Physical_and_Theoretical_Chemistry)/Physical_Properties_of_Matter/States_of_Matter/Phase_Transitions/Phase_Diagrams (visited at 15:01 23/09/2019)

[3 b] – Figure withdrawn from: https://www.cleanpng.com/png-state-of-matter-sublimation-gas-phase-transition-l-6504112/ (visited at 15:50 20/09/2019)

[4] - Reinitzer, F. (1888). Beitr ge zur Kenntniss des Gholesterins. Monatshefte Für Chemie, 9(1), 421–441.

[5] - H. Kelker (1973) History of Liquid Crystals, Molecular Crystals and Liquid Crystals, 21:1-2, 1-48, DOI: 10.1080/15421407308083312

[6] - D. Andrienko, Introduction to liquid crystals, Journal of Molecular Liquids (2018), https://doi.org/10.1016/j.molliq.2018.01.175

[7] - Demus, D. (1998). Handbook of liquid crystals. 2nd ed. Weinheim: Wiley-VCH, p.3.

[8] - Priestley, E., Wojtowicz, P. and Sheng, P. (2013). Introduction to liquid crystals. 1st ed. [S.l.]: Springer, pp.3,4.

[9] - Nanomaterials 2017, 7, 305; doi:10.3390/nano7100305

[10] - Wang, X. and Zhou, Q. (2006). Liquid crystalline polymers. New Jersey [etc.]: World Scientific, pp.197,198.

[11] - Demus, D. (1998). Handbook of liquid crystals. 2nd ed. Weinheim: Wiley-VCH, p.6.

[12] -Zhang, J., Su, J., & Guo, H. (2011). An Atomistic Simulation for 4-Cyano-4′-pentylbiphenyl and Its Homologue with a Reoptimized Force Field. The Journal of Physical Chemistry B, 115(10), 2214–2227. doi: 10.1021/jp111408n

[13] - Bruce, D. W., Deschenaux, R., Donnio, B., & Guillon, D. (2007). Metallomesogens. In Comprehensive Organometallic Chemistry III (pp. 195–293). Elsevier. https://doi.org/10.1016/b0-08-045047-4/00170-9

[14] - Zakharov, A. V., Tsvetkova, M. N., & Korsakov, V. G. (2002). Elastic properties of liquid crystals. Physics of the Solid State, 44(9), 1795–1801. https://doi.org/10.1134/1.1507268

[15] - Vertogen, G. and Jeu, W. (1988). Thermotropic Liquid Crystals, Fundamentals. 1st ed. Berlin, Heidelberg: Springer Berlin Heidelberg, p.92.

[16] - Chandrasekhar, S., & Krishnamurti, D. (1966). Birefringence of nematic liquid crystals. Physics Letters, 23(7), 459–460. https://doi.org/10.1016/0031-9163(66)91094-8

[17] - Issaq, H.J., Janini, G.M., Poehland, B. et al. ChromatoGraphia (1981) 14: 655. https://doi.org/10.1007/BF02291107

[18] - Ding, X., & Yang, K.-L. (2012). Liquid crystal based optical sensor for detection of vaporous butylamine in air. Sensors and Actuators B: Chemical, 173, 607–613. https://doi.org/10.1016/j.snb.2012.07.067

[19] - An, S. S., Nguyen, T. T., Han, G.-R., Jang, C.-H., & Ju, H. (2015). Optical birefringence of liquid crystals for label-free optical biosensing diagnosis. International Journal of Nanomedicine, 25. https://doi.org/10.2147/ijn.s88286

[20] - Hussain, A., Semeano, A. T. S., Palma, S. I. C. J., Pina, A. S., Almeida, J., Medrado, B. F., … Roque, A. C. A. (2017). Tunable Gas Sensing Gels by Cooperative Assembly. Advanced Functional Materials, 27(27), 1700809, https://doi.org/10.1002/adfm.201700803

[21] - Vertogen, G. and Jeu, W. (1988). Thermotropic Liquid Crystals, Fundamentals. Berlin, Heidelberg: Springer Berlin Heidelberg, pp.25,28.

[22] - Lee, S. S., Seo, H. J., Kim, Y. H., & Kim, S.-H. (2017). Structural Color Palettes of Core-Shell Photonic Ink Capsules Containing Cholesteric Liquid Crystals. Advanced Materials, 29(23), 1606894. https://doi.org/10.1002/adma.201606894

[23] - hilaya, G. (n.d.). Cholesteric Liquid Crystals: Optics, Electro-optics, and Photo-optics. In Partially Ordered Systems (pp. 159–185). Springer-Verlag. https://doi.org/10.1007/0-387-21642-1_6

[24] - Li, Y., Liu, Y., & Luo, D. (2017). Optical thermal sensor based on cholesteric film refilled with mixture of toluene and ethanol. Optics Express, 25(21), 26349. https://doi.org/10.1364/oe.25.026349

[25] - West, J., Yang, D-K.(1995) United States Patent No. USOO5453863A. Retrieved from https://patentimages.storage.googleapis.com/a4/77/90/7ee773c9fc1931b/US5453863.pdf

[26] -Farjon, J., & Giraud, N. (2018). 1H NMR analyses of enantiomeric mixtures using chiral liquid crystals. Current Opinion in Colloid & Interface Science, 33, 1–8. https://doi.org/10.1016/j.cocis.2017.11.001

[27] - Goh, M., Matsushita, S., & Akagi, K. (2010). From helical polyacetylene to helical graphite: synthesis in the chiral nematic liquid crystal field and morphology-retaining carbonisation. Chemical Society Reviews, 39(7), 2466. https://doi.org/10.1039/b907990b

[28] - Singh, S. and Dunmur, D. (2002). Liquid crystals. 1st ed. New Jersey: World Scientific, pp. 221-225

[29] - Demus, D. (1998). Handbook of liquid crystals. 2nd ed. Weinheim: Wiley-VCH, p.7-17.

[30] - Pasini, P., Žumer, S. and Zannoni, C. (2005). Computer simulations of liquid crystals and polymers. Dordrecht: Kluwer Academic Publishers, pp.7-8.

[31] - Jones, S. A., Bailey, J., Walker, D. R. E., Bryan-Brown, G. P., & Jones, J. C. (2018). Method for Tuneable Homeotropic Anchoring at Microstructures in Liquid Crystal Devices. Langmuir, 34(37), 10865–10873. https://doi.org/10.1021/acs.langmuir.8b01951

[32] - Mormile, P., Petti, L., Abbate, M., Musto, P., Ragosta, G., & Villano, P. (1998). Temperature switch and thermally induced optical bistability in a PDLC. Optics Communications, 147(4–6), 269–273. https://doi.org/10.1016/s0030-4018(97)00551-8

[33] - Lai, Y.-T., Kuo, J.-C., & Yang, Y.-J. (2014). A novel gas sensor using polymer-dispersed liquid crystal doped with carbon nanotubes. Sensors and Actuators A: Physical, 215, 83–88. https://doi.org/10.1016/j.sna.2013.12.021

[34] - Scherschener, E., Perciante, C. D., Dalchiele, E. A., Frins, E. M., Korn, M., & Ferrari, J. A. (2006). Polymer-dispersed liquid-crystal voltage sensor. Applied Optics, 45(15), 3482. https://doi.org/10.1364/ao.45.003482

[35] - Lampert, C. M. (2003). Large-area smart glass and integrated photovoltaics. Solar Energy Materials and Solar Cells, 76(4), 489–499. https://doi.org/10.1016/s0927-0248(02)00259-3

[36] - Patnaik, S. S., & Pachter, R. (1999). Anchoring characteristics and interfacial interactions in a polymer dispersed liquid crystal: a molecular dynamics study. Polymer, 40(23), 6507–6519. https://doi.org/10.1016/s0032-3861(98)00851-9

[37] - WANG, L., MENG, F., SUN, Y., & YANG, H. (2013). EFFECT OF SURFACTANT-MODIFIED ZNS:MN NANOPARTICLES ON THE ELECTRO-OPTICAL PROPERTIES OF COMPOSITE POLYMER-DISPERSED LIQUID CRYSTAL FILMS. COMPOSITES PART B: ENGINEERING, 45(1), 780–784. HTTPS://DOI.ORG/10.1016/J.COMPOSITESB.2012.05.055

[38] - RAMEZANI-DAKHEL, H., RAHIMI, M., PENDERY, J., KIM, Y.-K., THAYUMANAVAN, S., ROUX, B., … DE PABLO, J. J. (2018). AMPHIPHILE-INDUCED PHASE TRANSITION OF LIQUID CRYSTALS AT AQUEOUS INTERFACES. ACS APPLIED MATERIALS & INTERFACES, 10(43), 37618–37624. HTTPS://DOI.ORG/10.1021/ACSAMI.8B09639

[39] - MACFARLANE, D., KAR, M., & PRINGLE, J. (2017). FUNDAMENTALS OF IONIC LIQUIDS (P. 2). WEINHEIM: WILEY-VCH.

[40] - PAULECHKA, Y. U., ZAITSAU, D. H., KABO, G. J., & STRECHAN, A. A. (2005). VAPOR PRESSURE AND THERMAL STABILITY OF IONIC LIQUID 1-BUTYL-3-METHYLIMIDAZOLIUM BIS(TRIFLUOROMETHYLSULFONYL)AMIDE. THERMOCHIMICA ACTA, 439(1–2), 158–160. HTTPS://DOI.ORG/10.1016/J.TCA.2005.08.035

[41] - GHANDI, K. (2014). A REVIEW OF IONIC LIQUIDS, THEIR LIMITS AND APPLICATIONS. GREEN AND SUSTAINABLE CHEMISTRY, 4(1), 44–53. HTTPS://DOI.ORG/10.4236/GSC.2014.41008

[42] - WANG, P., ZAKEERUDDIN, S. M., COMTE, P., EXNAR, I., & GRÄTZEL, M. (2003). GELATION OF IONIC LIQUID-BASED ELECTROLYTES WITH SILICA NANOPARTICLES FOR QUASI-SOLID-STATE DYE-SENSITIZED SOLAR CELLS. JOURNAL OF THE AMERICAN CHEMICAL SOCIETY, 125(5), 1166–1167. DOI: 10.1021/JA029294

[43] - FIRESTONE, M., DZIELAWA, J., ZAPOL, P., CURTISS, L., SEIFERT, S., & DIETZ, M. (2002). LYOTROPIC LIQUID-CRYSTALLINE GEL FORMATION IN A ROOM-TEMPERATURE IONIC LIQUID. LANGMUIR, 18(20), 7258-7260. DOI: 10.1021/LA0259499

[44] - LEACH, A. (2001). MOLECULAR MODELLING (P. 1). HARLOW, ENGLAND: PRENTICE HALL.

[45] – LEACH, A. (2001). MOLECULAR MODELLING (PP. 26 - 34). HARLOW, ENGLAND: PRENTICE HALL.

[46] – LEACH, A. (2001). MOLECULAR MODELLING (PP. 35 - 36). HARLOW, ENGLAND: PRENTICE HALL.

[47] - ONCHOKE, K. K. (2011). DFT/TD-DFT INVESTIGATION OF OPTICAL ABSORPTION SPECTRA, ELECTRON AFFINITIES, AND IONIZATION POTENTIALS OF MONO-NITRATED BENZANTHRONES. COMPUTATIONAL AND THEORETICAL CHEMISTRY, 963(1), 40–50. DOI: 10.1016/J.COMPTC.2010.09.007

[48] - SUNDARAGANESAN, N., SALEEM, H., MOHAN, S., RAMALINGAM, M., & SETHURAMAN, V. (2005). FTIR, FT-RAMAN SPECTRA AND AB INITIO DFT VIBRATIONAL ANALYSIS OF 2-BROMO-4-

METHYL-PHENYLAMINE. SPECTROCHIMICA ACTA PART A: MOLECULAR AND BIOMOLECULAR SPECTROSCOPY, 62(1-3), 740–751. DOI: 10.1016/J.SAA.2005.02.043

[49] - ZHANG, G., & MUSGRAVE, C. B. (2007). COMPARISON OF DFT METHODS FOR MOLECULAR ORBITAL EIGENVALUE CALCULATIONS. THE JOURNAL OF PHYSICAL CHEMISTRY A, 111(8), 1554–1561. DOI:10.1021/JP061633O

[50] - CIOBÎCAˇ I. M., FRECHARD, F., SANTEN, R. A. V., KLEYN, A. W., & HAFNER, J. (2000). A DFT STUDY OF TRANSITION STATES FOR C−H ACTIVATION ON THE RU(0001) SURFACE†. THE JOURNAL OF PHYSICAL CHEMISTRY B, 104(14), 3364–3369. DOI: 10.1021/JP993314L

[51] - THAPA, B., & SCHLEGEL, H. B. (2016). DENSITY FUNCTIONAL THEORY CALCULATION OF PKA'S OF THIOLS IN AQUEOUS SOLUTION USING EXPLICIT WATER MOLECULES AND THE POLARIZABLE CONTINUUM MODEL. THE JOURNAL OF PHYSICAL CHEMISTRY A, 120(28), 5726–5735. DOI: 10.1021/ACS.JPCA.6B05040

[52] - BÜYÜKÖZTÜRK, O., BUEHLER, M. J., LAU, D., & TUAKTA, C. (2011). STRUCTURAL SOLUTION USING MOLECULAR DYNAMICS: FUNDAMENTALS AND A CASE STUDY OF EPOXY-SILICA INTERFACE. INTERNATIONAL JOURNAL OF SOLIDS AND STRUCTURES, 48(14-15), 2131–2140. DOI: 10.1016/J.IJSOLSTR.2011.03.018

[53] - LAMBERTI, V. E., FOSDICK, L. D., JESSUP, E. R., & SCHAUBLE, C. J. C. (2002). A HANDS-ON INTRODUCTION TO MOLECULAR DYNAMICS. JOURNAL OF CHEMICAL EDUCATION, 79(5), 601. HTTPS://DOI.ORG/10.1021/ED079P601

[54] - DAGGETT, V. (2003). ADVANCES IN PROTEIN CHEMISTRY (1ST ED., P. 29). AMSTERDAM: ELSEVIER ACADEMIC PRESS.

[55] - JORGENSEN, W. L., MAXWELL, D. S., & TIRADO-RIVES, J. (1996). DEVELOPMENT AND TESTING OF THE OPLS ALL-ATOM FORCE FIELD ON CONFORMATIONAL ENERGETICS AND PROPERTIES OF ORGANIC LIQUIDS. JOURNAL OF THE AMERICAN CHEMICAL SOCIETY, 118(45), 11225–11236. HTTPS://DOI.ORG/10.1021/JA9621760

[56] – JENSEN, F. (2007). INTRODUCTION TO COMPUTATIONAL CHEMISTRY (2ND ED., PP. 383 - 384). CHICHESTER [U.A.]: WILEY.

[57] - LEACH, A. (2001). MOLECULAR MODELLING (2ND ED., PP. 264 - 267). HARLOW, ENGLAND: PRENTICE HALL.

[58] - CUENDET, M. A., & VAN GUNSTEREN, W. F. (2007). ON THE CALCULATION OF VELOCITY-DEPENDENT PROPERTIES IN MOLECULAR DYNAMICS SIMULATIONS USING THE LEAPFROG INTEGRATION ALGORITHM. THE JOURNAL OF CHEMICAL PHYSICS, 127(18), 184102. DOI:10.1063/1.2779878

[59] – HUMMER, G., SCHOTTE, F., & ANFINRUD, P. A. (2004). UNVEILING FUNCTIONAL PROTEIN MOTIONS WITH PICOSECOND X-RAY CRYSTALLOGRAPHY AND MOLECULAR DYNAMICS SIMULATIONS.

Proceedings of the National Academy of Sciences, 101(43), 15330–15334. doi: 10.1073/pnas.0405295101

[60] – Ferruz, N., Harvey, M. J., Mestres, J., & Fabritiis, G. D. (2015). Insights from Fragment Hit Binding Assays by Molecular Simulations. Journal of Chemical Information and Modeling, 55(10), 2200–2205. doi: 10.1021/acs.jcim.5b00453

[61] - Vidossich, P., & Magistrato, A. (2014). QM/MM Molecular Dynamics Studies of Metal Binding Proteins. Biomolecules, 4(3), 616–645. doi: 10.3390/biom4030616

[62] - Sidky, H., de Pablo, J. J., & Whitmer, J. K. (2018). In Silico Measurement of Elastic Moduli of Nematic Liquid Crystals. Physical Review Letters, 120(10). https://doi.org/10.1103/physrevlett.120.107801

[63] - Ramezani-Dakhel, H., Sadati, M., Rahimi, M., Ramirez-Hernandez, A., Roux, B., & de Pablo, J. J. (2016). Understanding Atomic-Scale Behavior of Liquid Crystals at Aqueous Interfaces. Journal of Chemical Theory and Computation, 13(1), 237–244. https://doi.org/10.1021/acs.jctc.6b00844

[64] - Abraham, M. J., Murtola, T., Schulz, R., Páll, S., Smith, J. C., Hess, B., & Lindahl, E. (2015). GROMACS: High performance molecular simulations through multi-level parallelism from laptops to supercomputers. SoftwareX, 1–2, 19–25. https://doi.org/10.1016/j.softx.2015.06.001

[65] - Martínez, L., Andrade, R., Birgin, E. G., & Martínez, J. M. (2009). PACKMOL: A package for building initial configurations for molecular dynamics simulations. Journal of Computational Chemistry, 30(13), 2157–2164. https://doi.org/10.1002/jcc.21224

[66] - Oostenbrink, C., Villa, A., Mark, A. E., & Van Gunsteren, W. F. (2004). A biomolecular force field based on the free enthalpy of hydration and solvation: The GROMOS force-field parameter sets 53A5 and 53A6. Journal of Computational Chemistry, 25(13), 1656–1676. https://doi.org/10.1002/jcc.20090

[67] - Stroet, M., Caron, B., Visscher, K. M., Geerke, D. P., Malde, A. K., & Mark, A. E. (2018). Automated Topology Builder Version 3.0: Prediction of Solvation Free Enthalpies in Water and Hexane. Journal of Chemical Theory and Computation, 14(11), 5834–5845. https://doi.org/10.1021/acs.jctc.8b00768

[68] - van Aalten, D. M. F., Bywater, R., Findlay, J. B. C., Hendlich, M., Hooft, R. W. W., & Vriend, G. (1996). PRODRG, a program for generating molecular topologies and unique molecular descriptors from coordinates of small molecules. Journal of Computer-Aided Molecular Design, 10(3), 255–262. https://doi.org/10.1007/bf00355047

[69] - Dodda, L. S., Cabeza de Vaca, I., Tirado-Rives, J., & Jorgensen, W. L. (2017). LigParGen web server: an automatic OPLS-AA parameter generator for organic ligands. Nucleic Acids Research, 45(W1), W331–W336. https://doi.org/10.1093/nar/gkx312

[70] - Doherty, B., Zhong, X., & Acevedo, O. (2018). Virtual Site OPLS Force Field for Imidazolium-Based Ionic Liquids. The Journal of Physical Chemistry B, 122(11), 2962–2974. https://doi.org/10.1021/acs.jpcb.7b11996

[71] – Kuprusevicius, E., Edge, R., Gopee, H., Cammidge, A., McInnes, E., Wilson, M. and Oganesyan, V. (2010). Prediction of EPR Spectra of Liquid Crystals with Doped Spin Probes from Fully Atomistic Molecular Dynamics Simulations: Exploring Molecular Order and Dynamics at the Phase Transition. Chemistry - A European Journal, 16(38), pp.11558-11562.

[72] - McGibbon, R. T., Beauchamp, K. A., Harrigan, M. P., Klein, C., Swails, J. M., Hernández, C. X., … Pande, V. S. (2015). MDTraj: A Modern Open Library for the Analysis of Molecular Dynamics Trajectories. Biophysical Journal, 109(8), 1528–1532. https://doi.org/10.1016/j.bpj.2015.08.015

[73] - Gowers, R., Linke, M., Barnoud, J., Reddy, T., Melo, M., Seyler, S., … Beckstein, O. (2016). MDAnalysis: A Python Package for the Rapid Analysis of Molecular Dynamics Simulations. In Proceedings of the 15th Python in Science Conference. SciPy. https://doi.org/10.25080/majora-629e541a-00e

[74] - Jorgensen, W. L., Maxwell, D. S., & Tirado-Rives, J. (1996). Development and Testing of the OPLS All-Atom Force Field on Conformational Energetics and Properties of Organic Liquids. Journal of the American Chemical Society, 118(45), 11225–11236. https://doi.org/10.1021/ja9621760

[75] - Amovilli, C., Cacelli, I., Campanile, S., & Prampolini, G. (2002). Calculation of the intermolecular energy of large molecules by a fragmentation scheme: Application to the 4-n-pentyl-4′- cyanobiphenyl (5CB) dimer. The Journal of Chemical Physics, 117(7), 3003–3012. https://doi.org/10.1063/1.1494799

[76] - Ju, S.-P., Huang, S.-C., Lin, K.-H., Chen, H.-Y., & Shen, T.-K. (2016). Prediction of Optical and Dielectric Properties of 4-Cyano-4-pentylbiphenyl Liquid Crystals by Molecular Dynamics Simulation, Coarse-Grained Dynamics Simulation, and Density Functional Theory Calculation. The Journal of Physical Chemistry C, 120(26), 14277–14288. https://doi.org/10.1021/acs.jpcc.5b12222

[77] - Engineering ToolBox, (2003). Water - Density, Specific Weight and Thermal Expansion Coefficient. [online] Available at: https://www.engineeringtoolbox.com/water-density-specific-weight-d_595.html [Accessed 01 10 2019].

[78] – Batista, M. L. S., Kurnia, K. A., Pinho, S. P., Gomes, J. R. B., & Coutinho, J. A. P. (2015). Computational and Experimental Study of the Behavior of Cyano-Based Ionic Liquids in Aqueous Solution. The Journal of Physical Chemistry B, 119(4), 1567–1578. doi: 10.1021/jp510125x

[79] - Gürbulak, O., & Cebe, E. (2017). Molecular dynamics simulations on the adsorption of 4-n-octyl-4′-cyanobiphenyl (8CB) at the air/water interface. Journal of Dispersion Science and Technology, 39(5), 655–664.

https://doi.org/10.1080/01932691.2017.1380530

[80] - Chami, F., Wilson, M. R., & Oganesyan, V. S. (2012). Molecular dynamics and EPR spectroscopic studies of 8CB liquid crystal. Soft Matter, 8(25), 6823. https://doi.org/10.1039/c2sm25429h

[81] – Matsuhashi N., Kimura M, Akahane T. & Yoshida M. (2007). Structure Analysis Of 4Octyl4′Cyanobiphenyl Liquid-Crystalline Free-Standing Film By Molecular Dynamics Simulation. AZojomo, 3, 1-13. https://doi.org/10.2240/azojomo0234

[82] - Leadbetter, A. J., Durrant, J. L. A., & Rugman, M. (1976). The Density Of 4 n-Octyl-4-Cyano-Biphenyl (8CB). Molecular Crystals and Liquid Crystals, 34(10), 231–235. https://doi.org/10.1080/15421407708083712

Supporting Info

S1 - STANDARD INPUT PARAMETERS

INPUT PARAMETERS:

INTEGRATOR = MD

TINIT = 0

DT = 0.002

NSTEPS = 500000000

INIT-STEP = 0

SIMULATION-PART = 1

COMM-MODE = LINEAR

NSTCOMM = 100

BD-FRIC = 0

LD-SEED = 2428728329

EMTOL = 10

EMSTEP = 0.01

NITER = 20

FCSTEP = 0

NSTCGSTEEP = 1000

NBFGSCORR = 10

RTPI = 0.05

NSTXOUT = 1000

NSTVOUT = 1000

NSTFOUT = 0

NSTLOG = 1000

NSTCALCENERGY = 100

NSTENERGY = 1000

NSTXOUT-COMPRESSED = 0

COMPRESSED-X-PRECISION = 1000

CUTOFF-SCHEME = VERLET

NSTLIST = 1

NS-TYPE = GRID

PBC = XYZ

PERIODIC-MOLECULES = FALSE

VERLET-BUFFER-TOLERANCE = 0.005

RLIST = 1

RLISTLONG = 1

NSTCALCLR = 1

COULOMBTYPE = PME

COULOMB-MODIFIER = POTENTIAL-SHIFT

RCOULOMB-SWITCH = 0

RCOULOMB = 1

EPSILON-R = 1

EPSILON-RF = INF

VDW-TYPE = CUT-OFF

VDW-MODIFIER = POTENTIAL-SHIFT

RVDW-SWITCH = 0

RVDW = 1

DISPCORR = ENERPRES

TABLE-EXTENSION = 1

FOURIERSPACING = 0.12

FOURIER-NX = 72

FOURIER-NY = 72

FOURIER-NZ = 72

PME-ORDER = 4

EWALD-RTOL = 1E-05

EWALD-RTOL-LJ = 0.001

LJ-PME-COMB-RULE = GEOMETRIC

EWALD-GEOMETRY = 0

EPSILON-SURFACE = 0

IMPLICIT-SOLVENT = NO

GB-ALGORITHM = STILL

NSTGBRADII = 1

RGBRADII = 1

GB-EPSILON-SOLVENT = 80

GB-SALTCONC = 0

GB-OBC-ALPHA = 1

GB-OBC-BETA = 0.8

GB-OBC-GAMMA = 4.85

GB-DIELECTRIC-OFFSET = 0.009

SA-ALGORITHM = ACE-APPROXIMATION

SA-SURFACE-TENSION = 2.05016

TCOUPL = V-RESCALE

NSTTCOUPLE = 1

NH-CHAIN-LENGTH = 0

PRINT-NOSE-HOOVER-CHAIN-VARIABLES = FALSE

PCOUPL = BERENDSEN

PCOUPLTYPE = ISOTROPIC

NSTPCOUPLE = 1

TAU-P = 0.6

COMPRESSIBILITY (3X3):

COMPRESSIBILITY[0]={ 4.50000E-05, 0.00000E+00, 0.00000E+00}

COMPRESSIBILITY[1]={ 0.00000E+00, 4.50000E-05, 0.00000E+00}

COMPRESSIBILITY[2]={ 0.00000E+00, 0.00000E+00, 4.50000E-05}

REF-P (3X3):

REF-P[0]={ 1.00000E+00, 0.00000E+00, 0.00000E+00}

REF-P[1]={ 0.00000E+00, 1.00000E+00, 0.00000E+00}

REF-P[2]={ 0.00000E+00, 0.00000E+00, 1.00000E+00}

REFCOORD-SCALING = NO

POSRES-COM (3):

POSRES-COM[0]= 0.00000E+00

POSRES-COM[1]= 0.00000E+00

POSRES-COM[2]= 0.00000E+00

POSRES-COMB (3):

POSRES-COMB[0]= 0.00000E+00

POSRES-COMB[1]= 0.00000E+00

POSRES-COMB[2]= 0.00000E+00

QMMM = FALSE

QMCONSTRAINTS = 0

QMMMSCHEME = 0

MMCHARGESCALEFACTOR = 1

QM-OPTS:

NGQM = 0

CONSTRAINT-ALGORITHM = LINCS

CONTINUATION = TRUE

SHAKE-SOR = FALSE

SHAKE-TOL = 0.0001

LINCS-ORDER = 4

LINCS-ITER = 1

LINCS-WARNANGLE = 30

NWALL = 0

WALL-TYPE = 9-3

WALL-R-LINPOT = -1

WALL-ATOMTYPE[0] = -1

WALL-ATOMTYPE[1] = -1

WALL-DENSITY[0] = 0

WALL-DENSITY[1] = 0

WALL-EWALD-ZFAC = 3

PULL = FALSE

ROTATION = FALSE

INTERACTIVEMD = FALSE

DISRE = NO

DISRE-WEIGHTING = CONSERVATIVE

DISRE-MIXED = FALSE

DR-FC = 1000

DR-TAU = 0

NSTDISREOUT = 100

ORIRE-FC = 0

ORIRE-TAU = 0

NSTORIREOUT = 100

FREE-ENERGY = NO

COS-ACCELERATION = 0

DEFORM (3X3):

DEFORM[0]={ 0.00000E+00, 0.00000E+00, 0.00000E+00}

DEFORM[1]={ 0.00000E+00, 0.00000E+00, 0.00000E+00}

DEFORM[2]={ 0.00000E+00, 0.00000E+00, 0.00000E+00}

SIMULATED-TEMPERING = FALSE

E-X:

N = 0

E-XT:

N = 0

E-Y:

N = 0

E-YT:

N = 0

E-Z:

N = 0

E-ZT:

N = 0

SWAPCOORDS = NO

ADRESS = FALSE

USERINT1 = 0

USERINT2 = 0

USERINT3 = 0

USERINT4 = 0

USERREAL1 = 0

USERREAL2 = 0

USERREAL3 = 0

USERREAL4 = 0

GRPOPTS:

NRDF: 122927

REF-T: 300

TAU-T: 0.1

ANNEALING: NO

ANNEALING-NPOINTS: 0

ACC: 0 0 0

NFREEZE: N N N

ENERGYGRP-FLAGS[0]: 0

STANDARD INPUT PARAMETERS OF GROMACS

S2

MODIFIED INPUT PARAMETERS OF GROMACS

INPUT PARAMETERS:

INTEGRATOR = MD

TINIT = 0

DT = 0.002

NSTEPS = 50000000

INIT-STEP = 0

SIMULATION-PART = 1

COMM-MODE = LINEAR

NSTCOMM = 100

BD-FRIC = 0

LD-SEED = 310865856

EMTOL = 10

EMSTEP = 0.01

NITER = 20

FCSTEP = 0

NSTCGSTEEP = 1000

NBFGSCORR = 10

RTPI = 0.05

NSTXOUT = 1000

NSTVOUT = 1000

NSTFOUT = 0

NSTLOG = 1000

NSTCALCENERGY = 100

NSTENERGY = 1000

NSTXOUT-COMPRESSED = 0

COMPRESSED-X-PRECISION = 1000

CUTOFF-SCHEME = VERLET

NSTLIST = 1

NS-TYPE = GRID

PBC = XYZ

PERIODIC-MOLECULES = FALSE

VERLET-BUFFER-TOLERANCE = 0.005

RLIST = 1.4

RLISTLONG = 1.4

NSTCALCLR = 1

COULOMBTYPE = PME

COULOMB-MODIFIER = POTENTIAL-SHIFT

RCOULOMB-SWITCH = 0

RCOULOMB = 1.4

EPSILON-R = 1

EPSILON-RF = INF

VDW-TYPE = CUT-OFF

VDW-MODIFIER = POTENTIAL-SHIFT

RVDW-SWITCH = 0

RVDW = 1.4

DISPCORR = ENERPRES

TABLE-EXTENSION = 1

FOURIERSPACING = 0.12

FOURIER-NX = 36

FOURIER-NY = 36

FOURIER-NZ = 36

PME-ORDER = 4

EWALD-RTOL = 1E-05

EWALD-RTOL-LJ = 0.001

LJ-PME-COMB-RULE = GEOMETRIC

EWALD-GEOMETRY = 0

EPSILON-SURFACE = 0

IMPLICIT-SOLVENT = NO

GB-ALGORITHM = STILL

NSTGBRADII = 1

RGBRADII = 1

GB-EPSILON-SOLVENT = 80

GB-SALTCONC = 0

GB-OBC-ALPHA = 1

GB-OBC-BETA = 0.8

GB-OBC-GAMMA = 4.85

GB-DIELECTRIC-OFFSET = 0.009

SA-ALGORITHM = ACE-APPROXIMATION

SA-SURFACE-TENSION = 2.05016

TCOUPL = V-RESCALE

NSTTCOUPLE = 1

NH-CHAIN-LENGTH = 0

PRINT-NOSE-HOOVER-CHAIN-VARIABLES = FALSE

PCOUPL = BERENDSEN

PCOUPLTYPE = ISOTROPIC

NSTPCOUPLE = 1

TAU-P = 1

COMPRESSIBILITY (3X3):

COMPRESSIBILITY[0]={ 4.50000E-05, 0.00000E+00, 0.00000E+00}

COMPRESSIBILITY[1]={ 0.00000E+00, 4.50000E-05, 0.00000E+00}

COMPRESSIBILITY[2]={ 0.00000E+00, 0.00000E+00, 4.50000E-05}

REF-P (3X3):

REF-P[0]={ 1.03000E+00, 0.00000E+00, 0.00000E+00}

REF-P[1]={ 0.00000E+00, 1.03000E+00, 0.00000E+00}

REF-P[2]={ 0.00000E+00, 0.00000E+00, 1.03000E+00}

REFCOORD-SCALING = NO

POSRES-COM (3):

POSRES-COM[0]= 0.00000E+00

POSRES-COM[1]= 0.00000E+00

POSRES-COM[2]= 0.00000E+00

POSRES-COMB (3):

POSRES-COMB[0]= 0.00000E+00

POSRES-COMB[1]= 0.00000E+00

POSRES-COMB[2]= 0.00000E+00

QMMM = FALSE

QMCONSTRAINTS = 0

QMMMSCHEME = 0

MMCHARGESCALEFACTOR = 1

QM-OPTS:

NGQM = 0

CONSTRAINT-ALGORITHM = LINCS

CONTINUATION = TRUE

SHAKE-SOR = FALSE

SHAKE-TOL = 0.0001

LINCS-ORDER = 4

LINCS-ITER = 1

LINCS-WARNANGLE = 30

NWALL = 0

WALL-TYPE = 9-3

WALL-R-LINPOT = -1

WALL-ATOMTYPE[0] = -1

WALL-ATOMTYPE[1] = -1

WALL-DENSITY[0] = 0

WALL-DENSITY[1] = 0

WALL-EWALD-ZFAC = 3

PULL = FALSE

ROTATION = FALSE

INTERACTIVEMD = FALSE

DISRE = NO

DISRE-WEIGHTING = CONSERVATIVE

DISRE-MIXED = FALSE

DR-FC = 1000

DR-TAU = 0

NSTDISREOUT = 100

ORIRE-FC = 0

ORIRE-TAU = 0

NSTORIREOUT = 100

FREE-ENERGY = NO

COS-ACCELERATION = 0

DEFORM (3x3):

DEFORM[0]={ 0.00000E+00, 0.00000E+00, 0.00000E+00}

DEFORM[1]={ 0.00000E+00, 0.00000E+00, 0.00000E+00}

DEFORM[2]={ 0.00000E+00, 0.00000E+00, 0.00000E+00}

SIMULATED-TEMPERING = FALSE

E-X:

N = 0

E-XT:

N = 0

E-Y:

N = 0

E-YT:

N = 0

E-Z:

N = 0

E-ZT:

N = 0

SWAPCOORDS = NO

ADRESS = FALSE

USERINT1 = 0

USERINT2 = 0

USERINT3 = 0

USERINT4 = 0

USERREAL1 = 0

USERREAL2 = 0

USERREAL3 = 0

USERREAL4 = 0

GRPOPTS:

NRDF: 16353

REF-T: 320

TAU-T: 0.1

ANNEALING: NO

ANNEALING-NPOINTS: 0

ACC: 0 0 0

NFREEZE: N N N

ENERGYGRP-FLAGS[0]: 0

S3 - MDTRAJ SCRIPT

```
IMPORT MDTRAJ AS MD
TRAJ = MD.LOAD("TRAJOUT.XTC", TOP = "TOPOLOGY.GRO")
INDICES = [[N+X FOR X IN RANGE(NUMBER OF ATOMS IN A SINGLE MOLECULES)] FOR N IN RANGE(0, TOTAL NUMBER OF ATOMS IN THE SYSTEM, NUMBER OF ATOMS IN A MOLECULE)]
P2 = MD.COMPUTE_NEMATIC_ORDER(TRAJ, INDICES)
TIMESTEP = RANGE(NUMBER OF FRAMES)
IMPORT CSV
WITH OPEN('ORDET.CSV', 'W', NEWLINE = '') AS F:
    THEWRITER = CSV.WRITER(F)
    FOR L IN RANGE(0,LEN(TIMESTEP)):
        THEWRITER.WRITEROW([TIMESTEP[L], P2[L]])
```

S4 – MDANALYSIS SCRIPT

```
IMPORT MDANALYSIS AS MDA
IMPORT CSV
IMPORT NUMPY AS NP
IMPORT NUMPY
U = MDA.UNIVERSE("TOPOLOGY.GRO", "TRAJECTORY.XTC")
A_TEMP= U.SELECT_ATOMS("RESNAME DCAA") #EMPTY ATOMS GROUP
VECTOR = [0, 1 , 1]
VECTOR1 = [1, 0 , 0]
#ATOM_GROUPS=[]
#ATOM1_GROUPS=[]
P2_LIST = []
P2_AVG_LIST = []
COS_XY_LIST = []
INDEXES=[]
FOR I IN REVERSED(RANGE(50,160,5)):
    PRINT(I)
    INDEXES.APPEND(I)
    TEMP_STR="NAME N00 AND RESNAME RY1Q AND PROP ABS " + STR(I) + " <= X" #CHOOSE ATOMS ALONG THE AXIS
    G2 = U.SELECT_ATOMS(TEMP_STR)
    #ATOM_GROUPS.APPEND(G2)
```

```
            DIFF_ = G2 - A_TEMP

            RESIDS= DIFF_.RESIDS

            PRINT(BACALHAU)
TEST=STR(RESIDS).REPLACE("\N","").REPLACE("[","").REPLACE("]","")
TEMP_RES=U.SELECT_ATOMS("NAME C0D AND RESID" + TEST)
#ATOM1_GROUPS.APPEND(TEMP_RES)

            VA=DIFF_.POSITIONS - TEMP_RES.POSITIONS

            COS_XY =NP.ASARRAY([NP.ARRAY(NUMPY.DOT(X, VECTOR) / (NUMPY.LINALG.NORM(X) *
NUMPY.LINALG.NORM(VECTOR))) FOR X IN VA])

            P2=3/2 * NP.RESHAPE(COS_XY, (LEN(COS_XY),1))**2 - 0.5

            P2_AVG = NP.AVERAGE(NP.ABS(P2))

            P2_LIST.APPEND(P2)

            P2_AVG_LIST.APPEND(P2_AVG)

            COS_XY_LIST.APPEND(COS_XY)

            A_TEMP=G2

        WITH OPEN('P2_ALONG_AXIS.CSV','W', NEWLINE='') AS G:

            WRITER = CSV.WRITER(G)

            WRITER.WRITEROW(['T(NS)', 'S2'])

            FOR L IN RANGE(0,LEN(INDEXES)):

                WRITER.WRITEROW([INDEXES[L],P2_AVG_LIST[L]])
```